# Design and Control of Robotic Systems Using Bio-Inspired Artificial Muscle Recruitment Strategy

*MATTHEW P. BOWERS*


A Dissertation
Submitted to the Faculty
of the
WORCESTER POLYTECHNIC INSTITUTE
in partial fulfillment of the requirements for the
Degree of Doctor of Philosophy
in
Robotics Engineering

February 2021

APPROVED:

_____
Professor Marko B. Popovic, Primary Advisor
Worcester Polytechnic Institute

_____
Professor William R. Michalson, Committee Member
Worcester Polytechnic Institute

_____
Professor Germano S. Iannacchione, Committee Member
Worcester Polytechnic Institute

_____
Professor Lenore Rasmussen, Committee Member
Ras Labs, Inc.

# ACKNOWLEDGMENTS

I would like to thank my advisor, Prof. Marko B. Popovic, who provided knowledge, guidance, and support to me during my PhD candidacy. His insight and direction were invaluable in exploring the world of bio-inspired actuation. He has provided me with a foundation that shaped my research and beyond.

I would like to thank those whose insight and collaboration over the years aided my research: Dr. Lenore Rasmussen, Dr. Germano S. Iannacchione, Dr. William R. Michalson Dr. Karen Troy, Dr. Michael Gennert, and Dr. Hideyuki Kimpara.

I would also like to thank the many people I have worked with in Popovic Labs, their collaboration and friendship was both essential and enjoyable: Saivimal Sridar, Chinmay V. Harmalkar, Ananth Jonnavittula, Phillip Schaffer, Seiichiro Ueda, R. Matthew Rafferty, Amaid Zia, Varun V. Verlencar, John D. Kelly, Lynn R. Koesterman, Juan-Diego Florez-Castillo, Felix Sanchez, Thane R. Hunt, Julia D'Agostino, Ellie Clarrissimeaux, Shannon M. Moffat, Michael Pickett, Yunda Li, Ankur Agrawal, Abhishek Kashyap, Jonathan Tai, and many more.

Finally, I would like to thank my family. They have provided so much more than I could ever express. They have given me so much support and love and I would not be here without them.

# ABSTRACT

Even before the word “robot” was formally introduced the goal has been to create a synthetic system in our image. Clearly, human-like or biologically more realistic robots have a much better chance for safer, easier, and more universal interaction with humans. Hence, in order to move robots from factory lanes that prohibit human presence into our homes it is necessary to create that huge leap from the 20th century senseless, zero intelligence, high-gain, position controlled rigid machine to more human-like robots. This is also critical for the advancement of prosthetics and assistive devices.

In nature, the actuator that is used across species is the familiar biological muscle. Perhaps it is less known that each muscle in the human body consists of more than a hundred motor units that can be selectively recruited. As form and function are naturally intertwined, what are the mechanical and control advantages of this dominant actuation architecture? How can this architecture help us create more human-like robots?

To address these and other questions a biologically inspired leg will be designed with multiple independently controlled artificial muscles acting in parallel, allowing the use of a bio-inspired recruitment control strategy. More specifically this actuation architecture will be explored in the development and testing a variety of robotic legs.

Control of compliant artificial muscles is clearly challenging, but through the design and use of novel hydraulic system elements, modeling, as well as the implementation of bio-inspired control strategies, successful, human-like performance, can be achieved.

## TABLE OF CONTENTS

Page

## LIST OF TABLES

Table Page

## LIST OF FIGURES

Figure Page

# CHAPTER 1

# INTRODUCTION

## 1.1 Motivations

Compliant actuation is essential for inherently safe human robotic interactions and interfaces. While advances in control-based compliance push ever forward, this approach cannot guarantee safety when something goes wrong. In environments where compliance is required at all times, actuators with inherent compliance are required. Over the last few decades, many compliant actuators have been developed. While these actuators are useful in a variety of scenarios, they often necessitate new control strategies to maximize their potential. These actuators often have properties unlike those of traditional actuators. This means that there is generally not of the shelf control solutions available. Rubber based actuators provide the compliance desired, however they are often difficult to control precisely and have outputs that are constrained by their elastic properties. In order to solve these current limitations new control strategies and systems must be developed.

In summary the Motivations for this dissertation work are:

- Increasing need for compliant actuation due to increased human robot interaction

- Some of these compliant actuators, including the Hydro Muscle, are made of rubber causing their force and stiffness to be a property of the material itself.
- Low cost off the shelf solutions for control of these novel actuators often do not exist.

## 1.2 Related Work

### 1.2.1 Hydro Muscle

Hydro Muscles [1], a new type of hydraulically actuated muscles, originally developed at WPI, and its pneumatic counterpart the Air Muscles, are linear actuators resembling ordinary biological muscles in terms of active dynamic output, passive material properties and appearance [2], [3].

The Hydro Muscle has a single water flow opening and is comprised of an inner and an outer structural element. The inner element is a smooth tubing made of an elastic material such as latex (performs better than silicon, see Section 2.2). An added non-stretchable sleeve, outer element, is made of a soft, inelastic material, such as polyester, to limit radial expansion while promoting lengthwise expansion when pressurized.

The muscle architecture with the most similarities to the Hydro Muscle is the Pneumatic Rubber Artificial Muscle (PRAM) [4], originally developed at Okayama University, which is silicon based pneumatic actuator with polyester bellow system, with inner and outer below radius tightly limiting radial expansion of silicon tube and possibly

reinforced with tape on one side such that actuator naturally bends in that direction when pressurized. PRAM has been used in context of upper [4] as well as lower [5] extremities power assist devices. Hydro Muscle and PRAM differ in terms of actuating fluid (water vs air), materials used for elastic tubing (latex vs silicon) and different outer elements (sheathing vs bellows).

More distant designs still similar to the Hydro Muscle are PneuFlex [6], originally developed at TU Berlin, and Fiber Reinforced Actuator (FRA) [7], and originally developed at the Harvard Wyss Institute. Both PneuFlex and FRA utilize air, are silicon based, and have typically helix-like fibers either bonded to the surface (PneuFlex) or embedded deeper within silicon (FRA). Hydro Muscle's outer layer is connected to elastic tubing only at the muscle ends.

Even more distant design is that of popular pneumatic McKibben artificial muscles [8], [9], & [10] in use since the 1950s. Biological muscles and McKibben muscle soften radially while elongating axially and they bulge and stiffen radially while contracting axially. In difference, Hydro Muscles elongate axially and stiffen radially without bulging when pressurized and they contract axially and soften radially when depressurized. Substantial radial expansion and deflation of McKibben's elastomer introduces substantial energy that is lost as it is not transferred from source to actuated load. Hence, one expects lower energy conversion efficiency.

Efficiency is one of the most critical performance metrics for an actuator. Hypothesis tested here is that Hydro Muscles have better efficiency than McKibben muscles when both muscles utilize water as incompressible fluid. Previous studies of Pneumatic McKibben muscles obtained an efficiency of 0.22 [11] under quasi-stationary isotonic shortening conditions.

Biological muscles and cord driven muscles (Bowden cable based muscles are the exception here [12], [13]) can effectively apply only pulling force. Similarly, Hydro Muscle, like other types of soft muscles is prone to bowing when exerting a pushing force. This problem can be eliminated in several ways. For example, Hydro Muscle can be embedded with small rigid telescoping component or soft non-stretchable sheathing can be placed on the external actuated frame. Another approach is to embed and pressurize granular media (elastic or rigid) between muscle's inner and outer member in order to increase critical bending force that could cause Hydro Muscle buckling.

### 1.2.2 Walking Chair Utilizing an Uncoupled Synthetic Muscle Joint System

Legged vehicles intended for the transport of a human in a seated position have been addressed in the past. The first man-carrying computer controlled walking machine was the "six-legged hydraulic walker" [14], [15]. A variable structure quadruped/biped human-carrying walking chair anticipated to transition between two and four-legged configurations, depending on task, was recently considered [16]. However most of the research has been centered around bipedal platforms including,

the early work on the statically balanced ”My Agent” [17] locomotion module, the human arm powered, statically balanced, ”Walking Chair” [18], [19], the 2 *m* (78.7 *in*) tall (including cockpit) ”HUBO FX-1” [20] which uses a real-time balance control strategy for walking composed of a damping controller, a ZMP compensator, landing controllers, and a vibration reduction controller, also the 2.3 *m* (90.6 *in*) tall (including cockpit) dynamically balanced ”i-foot” [21] which is capable of ascending and descending stairs, and finally the dynamically balanced ”Waseda Leg” [22], [23] which utilizes Stewart platform type legs with a typical gait speed of 0.1 *m step/s* (3.94 *in step/s*) while taking about 6 *s* for stair climbing/descending step negotiating up to a step height of 250 *mm* (9.8 *in*).

### 1.2.3 Multi-fiber Hydro Muscle Ankle

It is broadly anticipated that humanoid robots and other advanced robots will “live” among us and perform numerous everyday tasks becoming an integral part of society in the near future, often times in close proximity with humans. The need for safe interaction drives a requirement for robots to utilize actuators with inherent compliance, such as the Hydro Muscle [1] - [3], [24], [25], originally developed at WPI. Furthermore, it is expected that Biomechatronics will substantially advance the ability to interface the human body with prostheses, improving the quality of life and potentially extending human lifespan. However, current assistive robotics are still unaffordable to the average person. As of now, even the leading economies have only a few government funded functional

humanoid robots [26], [27]. Nearly all state-of-the-art robotic prostheses are confined to research labs. Those that are out in the market are unaffordable for the ordinary citizen regardless of how economically advanced the country is. It appears that current technologies are neither robust nor lucrative enough for large-scale markets even if some designs can provide the required functionality to a certain degree. Hydro Muscles are inexpensive relative to other actuators which could lead to affordable, safe, and effective robots and prostheses.

### 1.2.4 Variable stiffness leg for soft landing

According to Sung [28], early work on robotic landing used the simplified model of a mass spring system. This approach however is over simplified and does not accurately represent human movement. In order to compensate for this, they developed overly complicated control techniques that often-required predetermined center of gravity paths. Sung developed a landing controller that utilized stiffness and damping because in landing we first behave as a spring, but then as the landing continues, we become more like a damper. This allows for a simplified control that alters the stiffness and damping based only on the center of gravity height. Research in variable stiffness of artificial muscles for locomotion has been explored by Lei [28], [29] who showed that they could achieve this variation with McKibben artificial muscles. While Tisujita [30] studied the stability of a PAM driven bipedal robot, in particular they looked at how oscillation of joint

stiffness during the contact phase could improve stability. Calderon [31] looked to reduce the forces a robot sees upon impact when they fall by varying the stiffness of the robot.

### 1.3 Contributions

The goal of this research work is to advance the capabilities of the Hydro Muscle, a compliant artificial muscle, this is done through improving hydraulic control options as well as developing bio inspired control methods that can increase the utility of the actuator. Several innovative designs were developed including quick release reservoirs, a coupling/decoupling mechanism, various valve and pump designs, as well as utilization of the bio inspired multi-fiber approach to antagonistic control of rotational joints using artificial muscles.

### 1.4 Dissertation Outline

The next chapter will introduce the Hydro Muscle and some implementations of controlling it as well as an approach to variable stiffness. In the following chapter a new method of uncoupling the artificial muscle is developed in order to provide a given torque at all possible angles. Next, the concept of multiple individually actuated artificial muscles is explored in order to make force output, position, and joint stiffness independent of each other. In the final chapter a novel servo valve is developed to provide control of a leg that can vary its stiffness for soft landings.

# CHAPTER 2

# HYDRO MUSCLE –A NOVEL SOFT FLUIDIC ACTUATOR

This chapter contains the preliminary work on artificial muscles and variable stiffness. The chapter covers the early utilization, modelling, and testing of the hydro muscle as well as the variable stiffness hydro bone. Additionally, several proof of concept systems are explored.

---

The material in this chapter is adopted from the self-authored publication: [25]
S. Sridar, C.J. Majeika, P. Schaffer, M. Bowers, S. Ueda, A. J. Barth, J. L. Sorrells, J. T. Wu, T. R. Hunt, and M. Popovic. "Hydro Muscle - a novel soft fluidic actuator," IEEE International Conference on Robotics and Automation (ICRA), pp. 4014-4021. IEEE, 2016.

## 2.1 Introduction

A basic fluid muscle model is introduced in Section 2.2. Passive material properties of frequently used latex tubing-based muscles were experimentally investigated; test procedures and results are presented in Section 2.3. Physical realization of modular Hydro Muscles embedded with pressure and in house-built length sensors and fine flow control valve are described in Section 2.4. Position and force control tests were performed to characterize inexpensive modular muscles; experimental procedures and test results are presented in Section 2.5. Efficiency of the Hydro Muscle is determined and compared to a hydraulically actuated McKibben in Section 2.6. Fluid based muscles are discussed in Section 2.7 in the context of conventional hydraulic and pneumatic systems; and a range of potential application are addressed by various currently undergoing projects within WPI Popovic Labs. Summary and future work are addressed in Section 2.8.

## 2.2 Muscle Model

When the elastic contractile force due to the elongation of inner tubing is larger than the force produced by the pressure of the actuating fluid, the Hydro Muscle will exert a pulling force. When the force produced by the pressure of the actuating fluid is larger than the elastic contractile force due to elongation of inner tubing, the Hydro Muscle will produce a pushing force. If the buckling problem is remedied, then this removes the necessity for an antagonistic pairing. This allows one joint to be fully actuated by a single muscle, thus providing a distinct advantage.

The relaxed wall area of latex rubber, $\boldsymbol{A_{W0}}$ shrinks under strain, ε, by a factor $\boldsymbol{c(\varepsilon)} = \left[\mathbf{1} - (\mathbf{1} + \boldsymbol{\varepsilon})^{-\mathbf{0.5}}\right]^{\mathbf{2}}$, roughly independent of fluid pressure, Section 2.3. As the outer diameter is constant due to the non-stretchable sleeve, the net muscle force in terms of pressure, p, and strain, is

$$F(p, \varepsilon) = p[A_M - c(\varepsilon)A_{W0}] - E_{RW}c(\varepsilon)A_{W0}\varepsilon \quad , \tag{1}$$

with constant muscle area, $A_M$, defined by the outer maximal diameter (for fully radially pressurized state) and elastic tube wall's Young modulus, $E_{RW}$, discussed next.

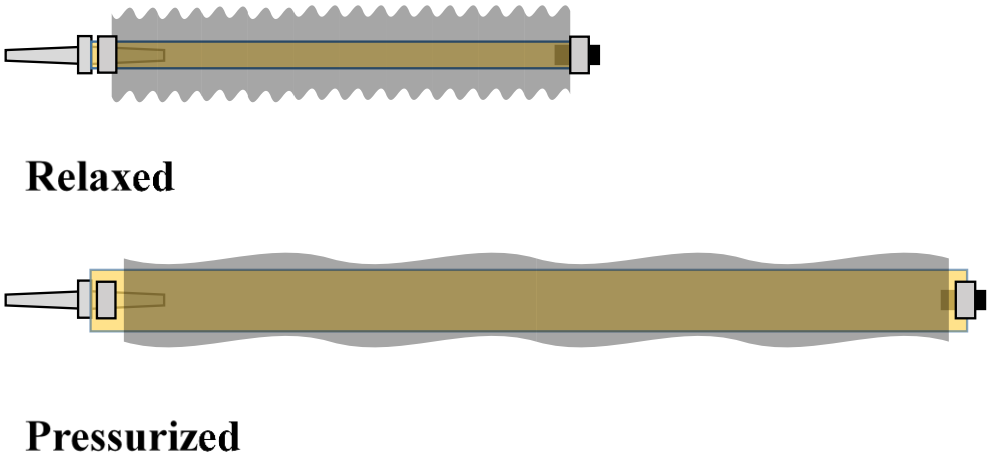


**Figure 1: Sketch of Relaxed and Pressurized Fluidic Muscle.**

### 2.3 Muscle Passive Property Characterization

Testing was carried out to characterize the Young's modulus, hence relating hydraulic pressure and muscle length with net muscle force, Eq. 1.

A sample of the rubber tubing, with length L = 16 cm (6.3 in), was stretched to a value of 100% strain and then returned to its original length. During this cycle force and position data was collected. The rubber tubing was first stretched by applying mechanical force on its end points (dry condition) and then by pressurizing the fluid (wet condition), Figure 2.

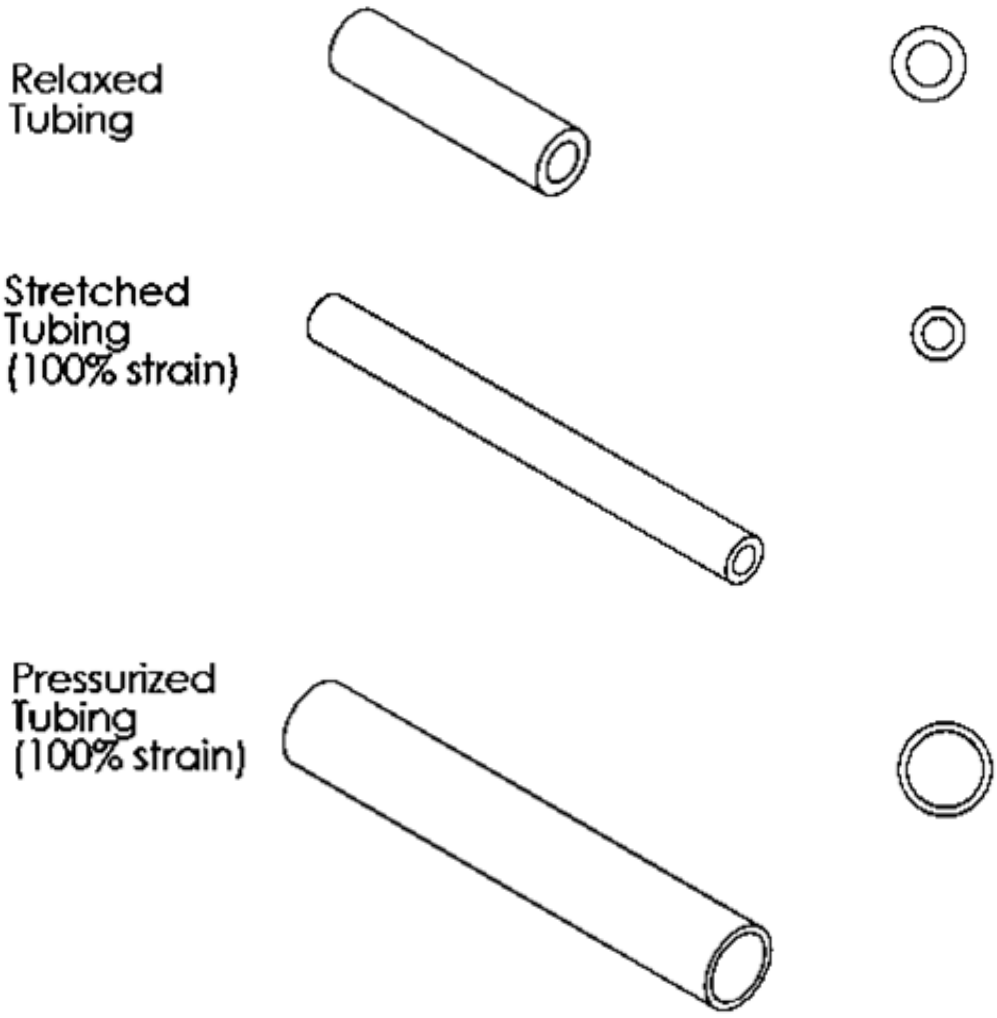


**Figure 2: Scaled representation of tubing length and cross-sectional area. Pressurized tubing (bottom) expands due to internal fluid pressure compared to the stretched tubing (middle) without fluid.**

The testing was completed using the Vernier Software & Technology LabPro system [32] in conjunction with a Dual-range Force Sensor, Motion Detector device, and the LoggerPro Software (ver. 3.8.6.2).

One end of the sample was affixed to the force sensor, which was attached to the lab frame; the sensor was oriented such that the force prong was directed

downwards. The other end of the sample was strained vertically and sensed by the motion detector. The samples were strained at a rate of approximately 1 cm/s (6.25% L/s).

The strain was obtained as ratio of the change in length, ΔL, over the original relaxed length of the sample, L. The stress was calculated as force over the cross-sectional area of the tubing wall. The cross-sectional area was adjusted based upon the Poisson ratio of rubber, v=0.5 [33], [34], and the decrease in tubing diameter d, defined [35] as

$$\Delta d = (-d)\left(1 - \left(1 + \frac{\Delta L}{L}\right)^{-v}\right). \quad (2)$$

From the stress-strain data, Figure 3, the Young's modulus of the tubing was found to be 1.34 MPa at 100% strain, which can be compared to an expected value of 1 to 5 MPa for latex rubber [36].

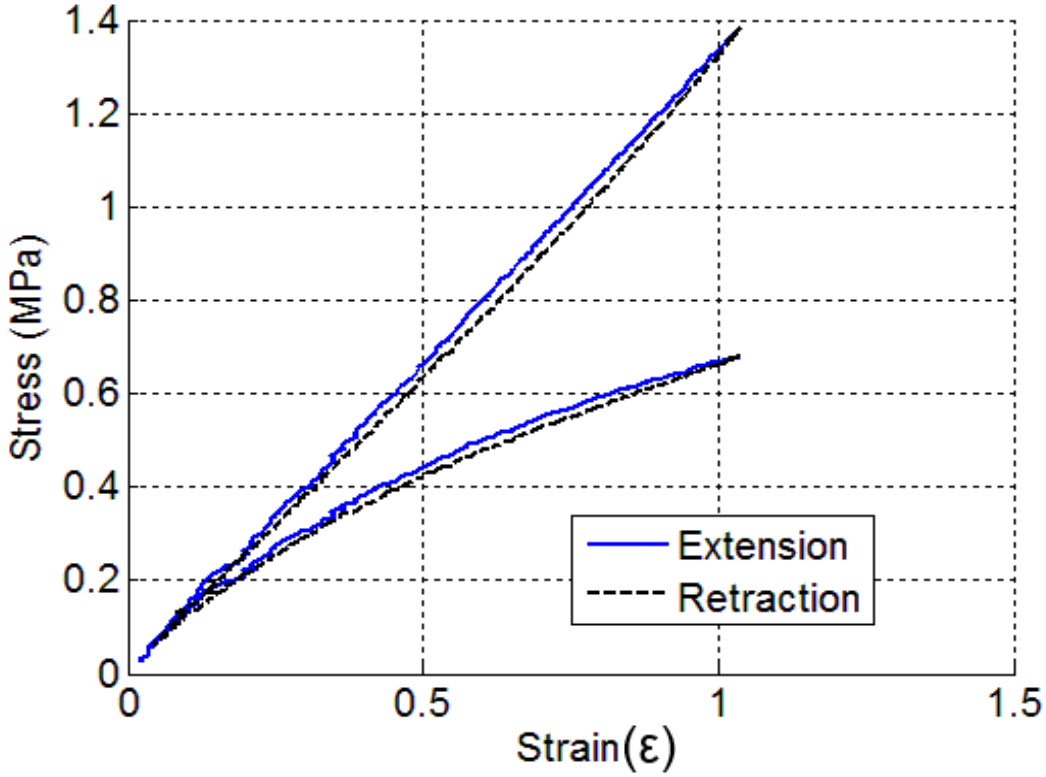


**Figure 3: Extension and retraction of stretched rubber tubing, with (top) and without (bottom) stretch-corrected tube wall area, Eq. 1.**

These tests were also performed for a sample of silicone tubing, which was being considered as a potential material for the muscle. The silicone tubing was rejected based upon the large amounts of hysteresis seen during the extension and retraction stress-strain curve, with about 30% of the input energy being lost.

Next, the cross-sectional wall area was measured of the water filled latex tubing stretched by fluid pressure. The mass of the dry tube was subtracted from the mass of the pressurized tube. The difference attributed to water was utilized to obtain inner diameter of tube whereas the outer diameter of tube was directly measured. For the range of

pressures up to 1MPa (150 psi), it was verified that difference of wall area as function of strain between dry and wet condition was within experimental error.

The 100% strain testing was then repeated for the latex tubing in extension (no retraction) using an Instron 5567A system running the Blue Hill 2 software [37]. A dry rubber tubing sample approximately 6.35 cm (2.5 in.) long was secured in the machine's grips and pulled to a strain of 100% at three rates; 0.25, 0.5, and 1 cm/s. Three extension curves were collected for each of the three different strain rates, and then averaged within their speeds. The spring constant (K) values for the three speeds were found to be 331.9, 330.9, and 325.3 N/m, respectively. A paired t-test showed that there was no statistical difference between any of the data sets for the three speeds, suggesting that the material properties are minimally dependent on the time/strain rate of extension. For natural muscles the passive force increases with small lengthening speed [38].

The stress-strain data collected using Instron machine was then fit to the Standard Linear Solid (SLS) model [38], [39] which accounts for viscosity, and is similar to the Hill's muscle model [40]. The SLS model utilizes both the strain (ε) and stress (σ) of the material, as well as their changes with time (t). The material properties are the two moduli, $E_1$ and $E_2$, and the viscosity coefficient, η,

$$\frac{\partial \varepsilon(t)}{\partial t} = \frac{\frac{\partial \sigma(t)}{\partial t} + \frac{E_2}{\eta}\sigma(t) - \frac{E_1 E_2}{\eta}\varepsilon(t)}{E_1 + E_2} \quad . \tag{3}$$

A first-degree polynomial was fit to each of the collected stress-strain data sets to represent the change in stress over time for use in the SLS model. Nonlinear regression

[41] was then used to evaluate the best fit values of the material properties ($E_1$, $E_2$, η), Table 1. The average coefficient of determination ($R^2$) of the SLS fit was found to be 0.9996.

**Table 1: Calculated properties of 6.35 cm (2.5 inch) long sample**

| Strain Rate (m/s) | $E_1$ (MPa) | $E_2$ (MPa) | η (MPa s) |
|---|---|---|---|
| 0.01<br>(N = 3) | 1.359<br>± 0.029 | 30,500<br>± 1,050 | 0.0038<br>± 2.3E-4 |
| 0.005<br>(N = 3) | 1.356<br>± 0.0033 | 30,700<br>± 160 | 0.0039<br>± 5.31E-19 |
| 0.0025<br>(N = 3) | 1.339<br>± 0.0052 | 30,500<br>± 350 | 0.0039<br>± 5.77E-5 |

These results agree with outcome of initial experiments that the elastic modulus of the latex rubber is approximately 1.3 MPa. They also show a tendency of having higher stiffness for faster lengthening speed, hence resembling biological muscles.

Finally, two more experiments were performed to evaluate the effect of stress relaxation and creep on the latex tubing. For stress relaxation, a 16 cm (6.3 in.) sample was strained to 80% (17.02 N), and the force was seen to decrease to a minimum value of 16.1 N (5.9% reduction) over the course of two hours. For the creep experiments, a mass of 950 g was attached to the 16 cm sample, and was suspended for a period of 12 hours, straining along the length of the tubing. No significant change in the length of the sample was seen over that period of time.

For comparison to the calculated Young's modulus of rubber tubing, it was seen that the human soleus muscle has a modulus of approximately 0.655 MPA. This is based upon maximum measurements of 38 MPa [42] and 58% strain [43] in the soleus during experiments. The tensile strength may vary across muscles, as the stress values have been seen to range from 0.2 to 1 MPa [38].

It is worth noticing that the fluid muscle's effective Young's modulus, $E_M$ is much smaller than latex rubber wall's Young's modulus, $E_{RW}$. The two are related via area of the fluid muscle, $A_M$, and area of the rubber wall, $A_{RW} = c(\varepsilon)A_{w0}$,

$$E_M = E_{RW}\frac{A_{RW}}{A_M} = E_{RW}\frac{c(\varepsilon)A_{w0}}{A_M} \quad . \tag{4}$$

If the fluid muscle operates in a fully radially pressurized state, the $A_M$ may be treated as constant whereas $A_{RW}$ depends on the strain.

### 2.4 Integrated Modular Hydro Muscle

The current realization of the Hydro Muscle was somewhat inspired by the commercially available X-Hose [44] comprising of an elastic inner material surrounded by an inelastic material that limits the expansion of the elastic material in the radial direction, but not the longitudinal direction. Similar to the Hydro Muscle, the X-Hose retracts to its original size when the pressure is released. X-Hose closely relates to a class of systems [45]-[51] with corrugated walls that expand under fluid pressure. Other relevant systems include borescopes and endoscopes [52].

The Hydro Muscle differs from the X-Hose in that it has a single opening and utilizes smooth elastic walls for its tubing, rather than the corrugated elastic material. An additional non-stretchable sleeve is made of a soft, inelastic material, such as polyester, to limit radial expansion while promoting lengthwise expansion when pressurized. The Hydro Muscle is inexpensive and convenient to manufacture and operate. In comparison with conventional actuators with similar dynamic properties, Hydro Muscles are drastically (roughly two orders of magnitude) more cost effective [1], [2].

The muscles were constructed by inserting a section of latex tubing [53] into nylon tubular webbing [54], constraining the radius of the latex during expansion. Lengthwise, the inelastic tubular webbing, if completely stretched, defines the maximal muscle elongation. A plastic hose-barb to thread adapter was then inserted into each end of the tubing and secured with an adjustable hose tie.

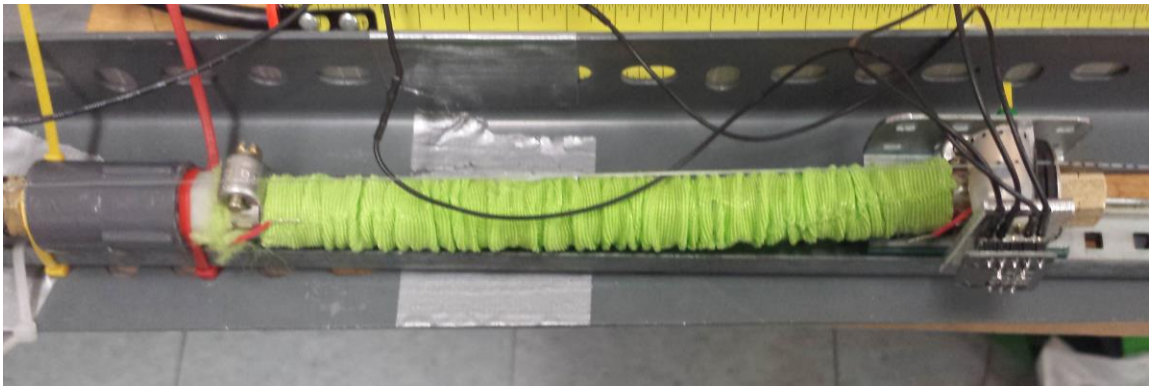

**Figure 4: Hydro Muscle during control tests.**

In order to monitor the elongation and internal pressure of the muscles, length and pressure sensors were added to the muscles. The inexpensive pressure sensor [55] was

inserted through a small hole drilled through the endcap and secured using epoxy. Several length sensing techniques were tested including those utilizing stretching of conductive elastic cord [56], water resistance measurements, and a small rotary encoder. The best length sensing was obtained with the rotary encoder [57].

The stretching method utilized the inexpensive Conductive Elastic Cord from Adafruit [56]. The conductive elastic material was anchored to muscle endpoints. The resistance of the elastic element increases as it is stretched so the length of the muscle can be calculated by using a voltage divider. However, due to hysteresis, creep, etc., readouts had a lot of noise and were not repetitive even with the noise filtered out. A similar problem was encountered with the measurement of water resistance. Replacing the metal endcaps and fittings with plastic parts greatly reduced these inconsistencies, but not enough to provide adequately robust sensing. Finally, the most successful length sensing method implemented the KY040 Rotary Encoder [57] with small return spring. The small rotary encoder was attached to one end of the muscle. Fishing line was looped around the shaft of the encoder, threaded through the muscle's sheathing, and attached to the other end. When the muscle extended and contracted the line would spin the encoder. This length sensing method was the most reliable.

### 2.5 Position and Force control tests

The muscles were controlled by an Arduino Uno [58] that read input from the sensors and controlled valves. The flow control system consisted of two on/off solenoid

valves [59] to control the inlet and outlet of water, as well as an adjustable ball valve [60] actuated by a servo [61] for fine flow control. The servo is capable of turning the ball valve from fully closed to fully open in less than half a second. The response time of the system is about 50 ms, Figure 5.

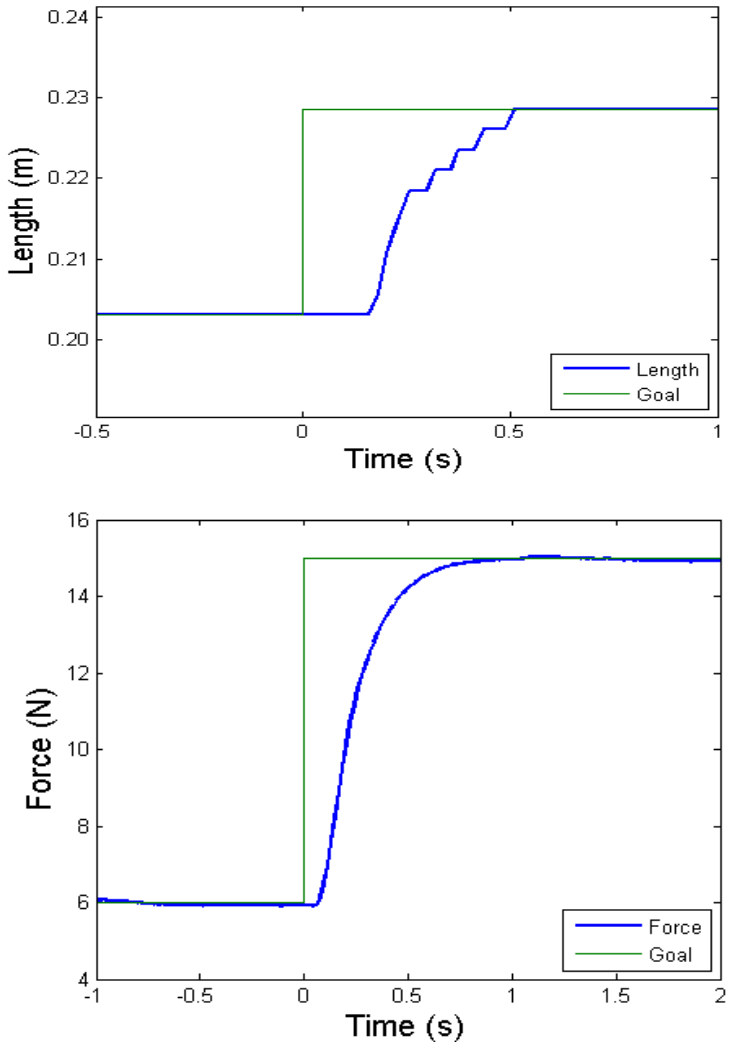


**Figure 5: Position (top) and force (bottom) control test results.**

The system used PD control to control the position or force of the muscle. The output of the PD control was the angle to turn the ball valve to, with 0 degrees being fully closed, and 90 degrees being fully open. To prevent the muscle from jittering back and forth around the setpoint, a small deadband was introduced. The system also reduced the flow rate if it was repeatedly crossing the setpoint. This helped to reduce the amplitude of the overshoot if the system was underdamped. The flow rate would be decreased by 17.7% each time it crossed the same setpoint again, resulting in much lower overshoot. This decrease would be reset each time the setpoint changed. This was in order to allow the system to quickly reach the new setpoint, even if it was oscillating around the previous one.

For length control, a P value of 17.7 deg/cm and a D value of 0.11 deg s/cm were used. The muscle would stop moving when it got within 0.38 cm of the target position. For force control, a P value of 4.5 deg/N and a D value of 0.84 deg s/N were used. The muscle would stop pressurizing when it got within 0.25 N of the target force. When measuring the force, our readings were noisy, due to the inertial properties of the water, when the valves were opened or closed. To compensate for this, the signal was passed through a low pass filter with a cutoff frequency of approximately 1.5 Hz before the error to use in the PD control was computed.

For position test, Figure 5, one end of the muscle was secured to the table. The other end was affixed to a slide, constraining the muscle to only extend linearly. The length was measured by the encoder and verified with a ruler.

For force test, Figure 5, the muscle was stretched to 38.5% strain, i.e. 22.86cm (9in), and affixed to prohibit further changes in length. The force was obtained from pressure and strain, Eq. 1 and recorded using a Vernier Dual Range Force Sensor [32].

### 2.6 Efficiency Tests

A hanging mass $m$, was connected to the muscle by a cord that passes without sliding over a small pulley. Hydraulic work was obtained by integrating the product of the measured pressure $p$ and the incremental changes in fluid volume, $dV$.

Efficiency of the Hydro Muscle *without* considering return fluid work, is obtained as positive work performed by the muscle on mass, $mg(z_{max} - z_{min})$, over the sum of the positive work performed by gravity, $mg(z_p - z_{min})$, and the positive work done by the hydraulic system during pressurization of the muscle,

$$W_+(z_{max} \rightarrow z_p) = W_+^{F\neq 0}(z = z_{max}) + W_+^{F=0}(z_{max} \rightarrow z_p). \quad (5)$$

Here $z_p$ is the height of load when it first engages the muscle during the work cycle (and then drops to $z_{min}$ while stretching the muscle) and $z_{max}$ is the maximal height of the load when the fluid pressure is lowered to atmospheric pressure. The weight is then removed and the muscle length is kept constant while the hydraulic system performs positive work, $W_+^{F\neq 0}(z = z_{max})$, by adding fluid until the muscle force, $F$, becomes zero. Subsequently the hydraulic system performs positive work, $W_+^{F=0}(z_{max} \rightarrow z_p)$ with $F = 0$

in quasi-static regime until $z_p$ is again reached. For reference this is compared with the efficiency of the McKibben muscle *without* considering return fluid work, obtained as $mg(z_{max} - z_{min})$ over positive work performed by the hydraulic system, $W_+(z_{min} \rightarrow z_{max})$.

Finally, efficiency of the Hydro Muscle *with* considering return fluid work, is obtained as

$$\varepsilon = \frac{mg(z_{max} - z_{min}) + |W_-(z_{min} \rightarrow z_{max})|}{mg(z_p - z_{min}) + W_+(z_{max} \rightarrow z_p)}. \quad (6)$$

$W_-(z_{min} \rightarrow z_{max})$ being the negative work performed by the hydraulic system, i.e. positive work performed by the muscle on the hydraulic system. Again, the denominator is the total energy added to the muscle over the work cycle.

### 2.7 Discussion: Comparison and Applications

Fluidic Muscles, i.e. Hydro Muscle and Air Muscle, have several practical advantages over standard hydraulic and pneumatic actuators. These muscles are soft, lightweight, inexpensive, easy to manufacture from commercially available materials, easy to modify both in terms of mechanical properties and in the way they interface with supporting “skeletal” structure. Moreover, they have inherent elasticity which in turn make them suitable for power augmentation paradigm; release of muscle’s stored energy onto load can be much faster than transferring a pump’s energy into the muscle.

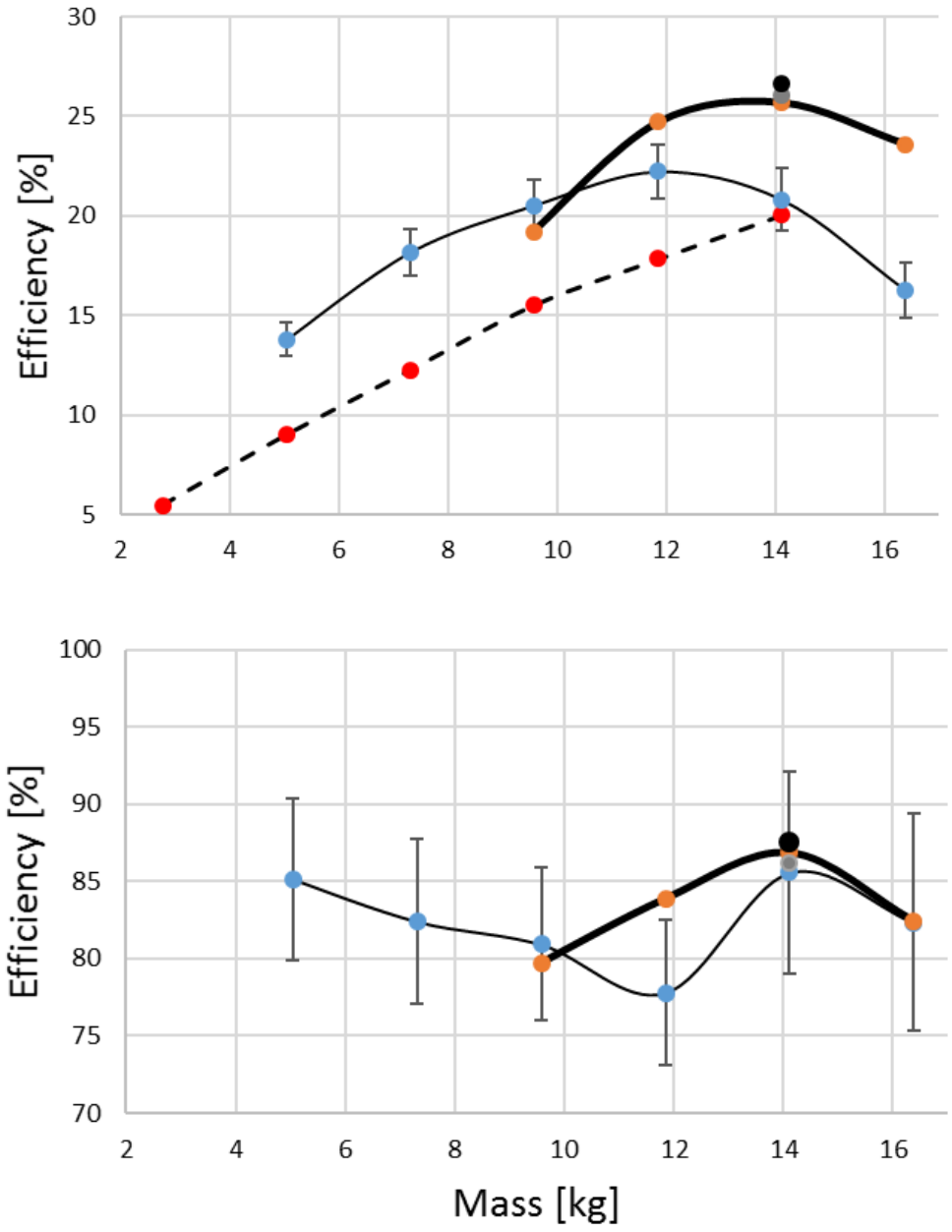


**Figure 6: Efficiency without (top) and with (bottom) return flow work: Hydro muscle without lubricant stretched with 100 ml (thin line with Standard Deviation error bars) and 150 ml (thick line) fluid input. Hydro muscle with lubricant (gray and black dots). McKibben muscle with 200 ml fluid input without return flow work consideration (dash line). Both muscles utilized 1.91 cm inner diameter, 2.86 cm outer diameter, 18.3 cm long latex tube in a relaxed state.**

Hydro Muscles are highly efficient actuators; there are almost no losses due to heating of working fluid, and latex within 100% strain range performs almost as an ideal spring, Figure 3. The hypothesis that the Hydro Muscle has a greater efficiency than the McKibben muscle is also confirmed. According to Figure 6, the Hydro Muscle maximal efficiency is 33% greater than that of the McKibben muscle maximal efficiency despite the latter having larger fluid input volume. This is as expected due to fact that a large portion of the McKibben's hydraulic energy is not transferred onto the load as it is instead used for radial expansion of the muscle. This loss is significantly less in the case of the Hydro Muscle due to the non-stretchable sheathing preventing elastic tubing from substantial radial expansion. The standard deviation of the 100 ml test gives us an idea of the error in our experimental data. It has a standard deviation that is approximately 6.8% of the mean. While in our tests the McKibben was tested with liquid to make a more direct comparison, the efficiency of the pneumatic McKibben muscle is even smaller due to air being compressible and thermodynamic heating losses. As discussed silicon based designs [3], [4], & [5] have additional losses on the order of 30%. In comparison dielectric electroactive polymer based muscles [62] have energy conversion efficiency of about 18% [63].

A notable feature that the Hydro Muscles have in common with conventional hydraulic and pneumatic actuators are that a single motor unit (i.e. a pump) can power many actuated degrees of freedom while electrical motors with non-fluidic actuation can typically only actuate a single degree of freedom. Moreover, in case of a wearable system, a conventional pump can be easily positioned more proximally to the center of mass

without adding distal masses close to the joints. Finally, hydraulic based transmissions are often more easily implemented than gearing mechanisms for pure mechanical transmissions.

The presented type of fluidic muscle has not been pressurized in excess of 1MPa (145 psi), hence limiting the maximum loading force to approximately 100N per $cm^2$. If more force is needed several muscles can be aligned in parallel or one could operate a single muscle with very large cross-sectional area. However, for applications where fast muscle "charging" is necessary, high flow could present a challenge for the pump's flow-pressure performance.

Fluidic muscles' operation is also limited by the quality of valves used. The least expensive, off-the-shelve, active valves are typically bulky and operate in an on/off regime with substantial time delays on the order of a few 100ms. Somewhat more advanced, off-the-shelf, active valves can be smaller, lighter, and operate with continuous pressure or flow control. These valves typically operate with time delays on the order of 10 ms but they tend to be more expensive. A possible solution to compensate for the difference in the quality of the valves can be addressed by using an in-house-built valve as presented here with a small motor operating an otherwise passive flow control valve.

Possible drawbacks of fluidic muscles compared to conventional hydraulic and pneumatic systems are related to their inherent mechanical compliance. They are more

ideal in performing pulling vs pushing tasks; a pressurized muscle could bow when subject to a constant distance between attachment points (e.g. due to heavy load).

Bowing can be remedied with a rigid telescoping element or non-stretchable sheathing i.e. “skin” enclosing the “skeletal” structure and muscle. The later approach can be used to improve the muscle force-joint torque profile by increasing the angle between the muscle and the supporting structure, Figure 7.

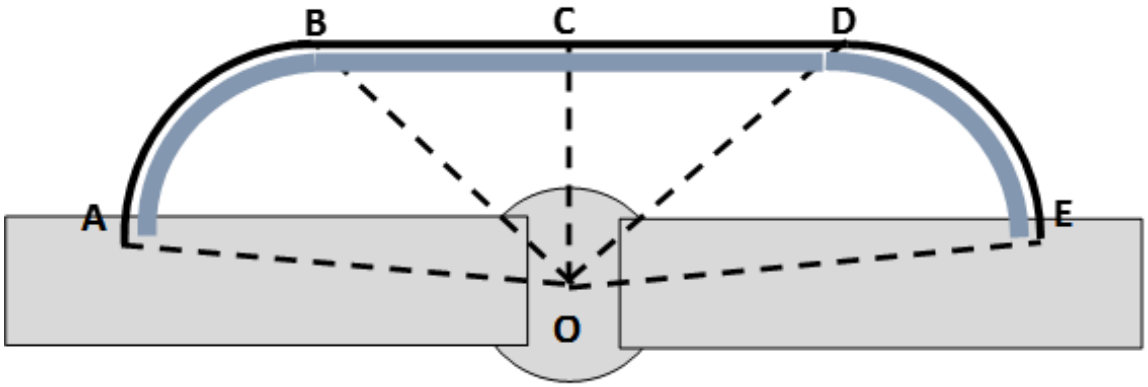


**Figure 7: Sketch of guiding “skin” (curve ABCDE) improving force vs. joint (O) torque profile for bowing Hydro Muscle.**

If some bowing is desirable the inner member wall can have variable elastic properties and a different cross section along the muscle length. Furthermore, the inner member wall can have variable elastic properties and thickness as a function of the azimuthal angle; for example one side of the inner member wall can be reinforced such that pressurizing actuating fluid will cause the Hydro Muscle to curve toward opposite side, Figure 8.

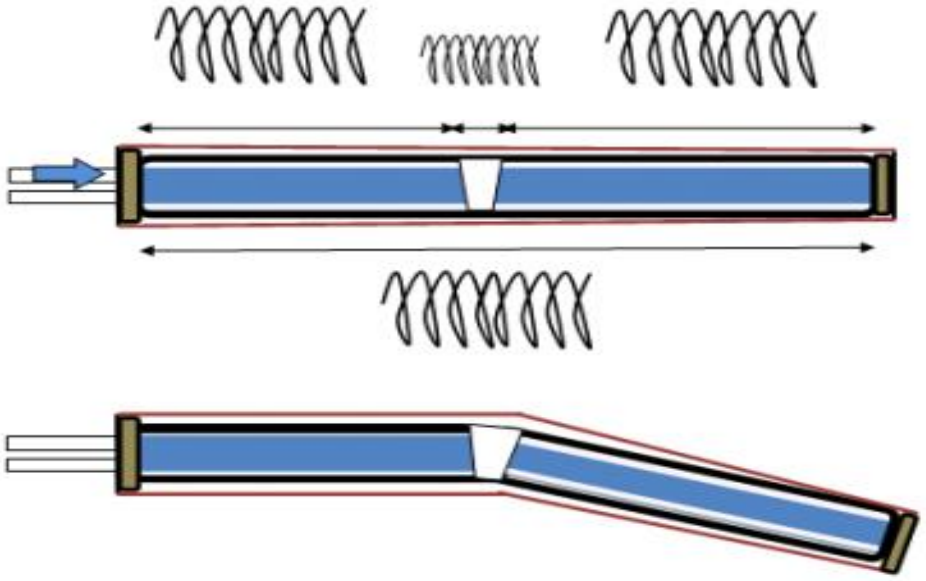

**Figure 8: Example of "stiffness" modulation for desired bowing.**

Another way to address the bowing problem is to modify the muscle by adding granular media (elastic or rigid) between the latex tube and the muscle's outer layer, Figure 9.

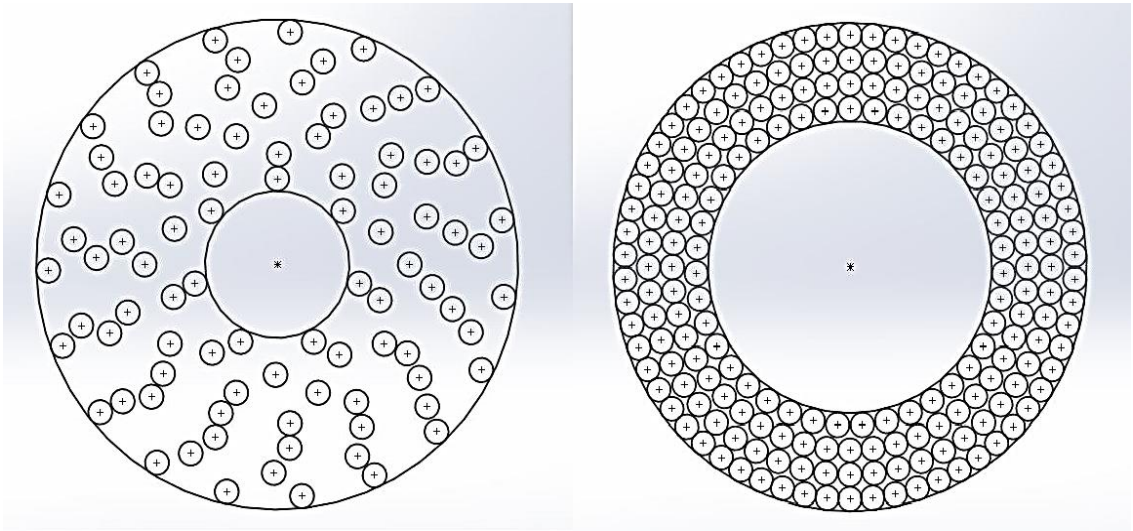

**Figure 9: Granular media jamming concept with Hydro Muscle; cross section with non-jammed (left) and jammed (right) granules.**

When the muscle is pressurized, the granular media is compressed uniformly, thus stiffening the interior support of the muscle, which decreases or completely eliminates bowing, Figure 9.

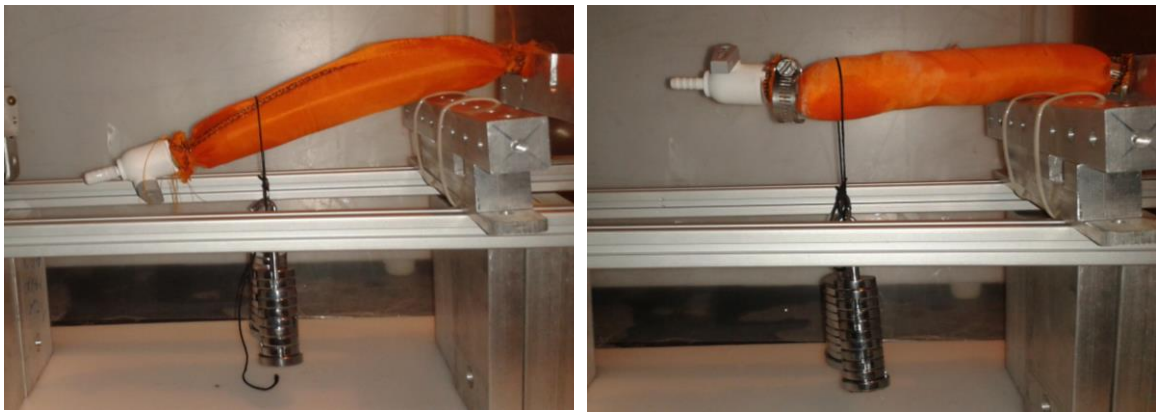

**Figure 10: Deflections of Hydro Muscle without (left) and with (right) granular media for approximately same torque and pressure.**

The fluidic muscle type presented here is currently used for several robotic systems under development including wearable systems like our Arm and Leg Exo-musculatures, and various independent systems: flapping wings, hopping biped, and bounding gait quadruped.

Elbow Exo-musculatures with teleoperation capability [3], Figure 11, utilizes two Hydro Muscles along both sides of a conventional hinged elbow brace combined with 80/20 extrusions extending toward the bicep and forearm to ease fine-tuning of the attachment points. Two braces built using this design work as a master and slave system. Muscles attached to the slave brace extend or contract to match the length of the muscles on the master brace. Simultaneously, muscles on the master brace pressurize or

depressurize in order to apply the same force that the muscles on the slave brace are applying. Goal is to provide a force feedback allowing the wearer to feel the forces being applied to the slave brace. Similarly, Knee Exo-musculature, Figure 11, utilizes two Hydro Muscles along both sides of a conventional hinged elbow brace added with 80/20 extrusions extending away from the joint to ease fine-tuning of attachment points. Goal is to add extra force to knee for either physical therapy, daily assistance, or an augmentation system.

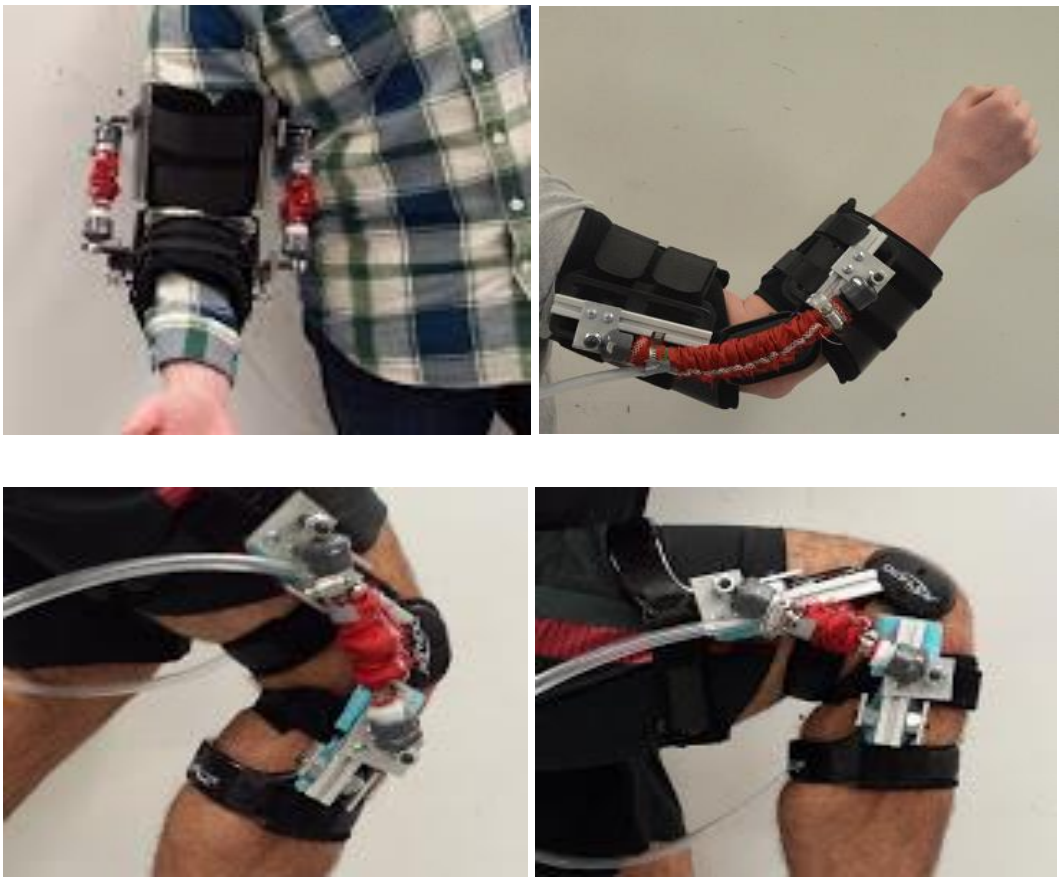

**Figure 11: Hydro Muscle pair fitted onto conventional elbow (top) and knee (bottom) brace; each muscle generates up to 500N force.**

A flapping wing system utilizes pneumatics for a fluidic muscle powered ornithopter [64]. Using 0.53 MPa (80 Psi) of compressed air, one muscle per wing is lengthened while wings are pulled up by an additional passive spring on top. The muscle taking the place of the pectoral muscle then depressurizes to create a powerful down flap. The use of pneumatics allows for an open system that uses fewer heavy components and eliminates the need to store any fluid onboard further reducing the system weight. Testing has been conducted with up to 1Hz flapping frequency and preliminary results show substantial lifting forces.

A hopping biped system, kangaroo robot [65] has six air muscles used in parallel for each leg joint, Figure 12. The stronger ankle muscles are attached via the Achilles tendon, onto the posterior surface of the Calcaneus, or heel bone. Energy is first slowly stored by pressurizing the muscles and then quickly released by depressurizing the muscles. This allows the muscles to contract and perform similarly to the Gastrocnemius and Soleus muscles. During the aerial phase, an accumulator is used to quickly pressurize the muscles again to reposition the legs in preparation of ground foot contact.

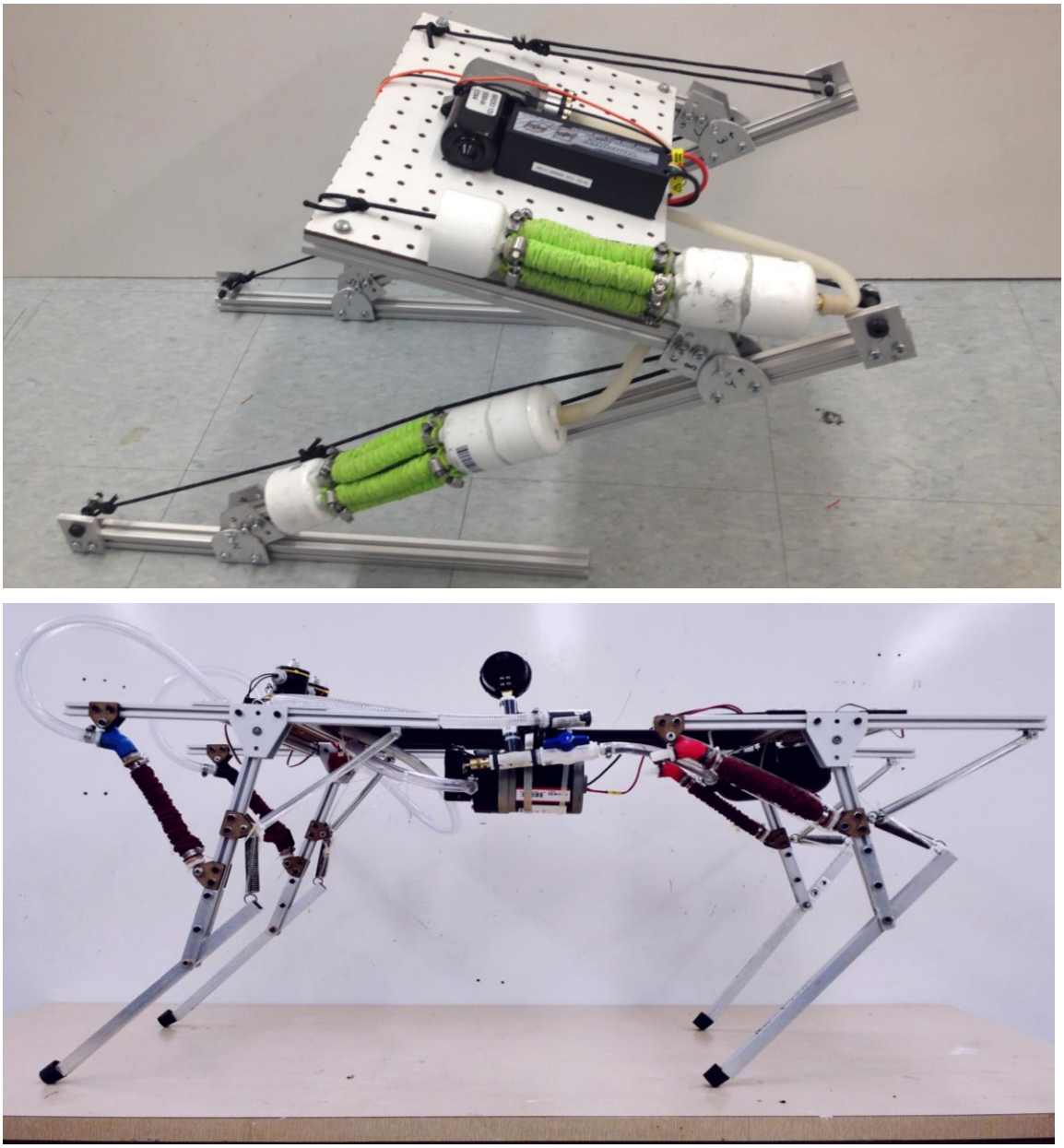

**Figure 12: Kangaroo robot with 6 strong muscles in parallel per joint (top) and a lightweight quadruped, Hydro Dog robot (bottom).**

A bounding gait quadruped, Hydro Dog design and realization [65] was simplified through the use of large Hydro-muscles, Figure 12. The bounding gait requires sudden and repetitive large forces. The control approach is one where an impulse force is

introduced to the elastically constrained legs such that the natural frequency of the system is activated. This results in an efficient, dynamic, and life-life gait. A similarly-sized system actuated with hydraulic cylinders or McKibben muscles would have to rely on a large and powerful pump to create the large periodic forces required for this bounding gait, whereas the quadruped presented here takes advantage of the Hydro-muscle's power augmentation characteristic. The robot is in the aerial phase (with the muscles being pressurized) for at least half of the gait cycle, such that the legs can output a power of twice what the pump could provide continuously. The pump used here is 375 W, therefore the robot has approximately 750 W (~1 HP) jumping power resulting in a lightweight, energetic biologically inspired legged machine.

### 2.8 Conclusions and Recommendations

Actuators which are lightweight, small, efficient, fluid, fast, muscle-like, and cost-effective are critical for advancement of robot actuation. The fluidic muscles, Hydro Muscles and Air Muscles, presented here are simple novel actuators that meet these requirements. These may be utilized as modular building blocks for robots that can be rapidly assembled and utilized as either perform-alone or wearable, human body-symbiotic systems. Clearly, they can be also an excellent educational tool for moderate-budget robotics classrooms and labs. They can utilize ordinary tap water and effectively operate even at standard household pressures of about 0.59 MPa (85 psi). A single source can actuate many muscles by flow and/or pressure control.

There are many attractive avenues for future work, development, and application for this technology. For example, in the medical field these muscles can be used as soft actuators for everyday assistance or for rehabilitation and physical therapy, they can be used in both labor and the military as method of augmenting strength, and they can be used as a soft-robotics alternative to virtually all rigid robotic motors and actuators. Further research and development can potentially advance these muscles into commercially attractive soft robotics actuators.

# CHAPTER 3

# SYNTHETIC MUSCLE JOINT SYSTEM WITH SELECTIVE MUSCLE ENGAGEMENT, FOR HUMANOID ROBOTIC APPLICATIONS

In this chapter the next step in the advancement of Hydro Muscle control is explored. A robotic leg was developed. In order to gain better control of the Hydro Muscle this leg implemented several new ideas. Instead of a large reservoir near the pump we used several smaller reservoirs implemented closer to each hydro muscle to decrease water evacuation time. We implemented multiple low-cost valves in series to try and implement better control in different scenarios including both fast actuation and finer muscle movements. One of our most innovative approaches was to develop a coupling/decoupling mechanism that would allow the Hydro Muscle to implement a given force at any angle instead of being limited by the geometry of the leg's structure and the elastic properties of the Hydro Muscle.

## 3.1 Introduction

The Joint System is proposed as a synthetic muscle actuated robotic joint with the ability for different actuation modes based on the selective engagement of its muscles, which may benefit applications that require high moments but also cases of unrestricted movement, such as powered exoskeletons and humanoid robots. This is similar in construction to the antagonistic muscle pair muscle structure, a typical muscle structure seen in biology and other synthetic actuators. Here, two multiple muscle

groups are fixed to each side of the joint which is actuated when one muscle is released while the other is being charged. While the Joint System uses more components in it to actuate a joint, it can prevent muscle groups from interfering with each other's movements.

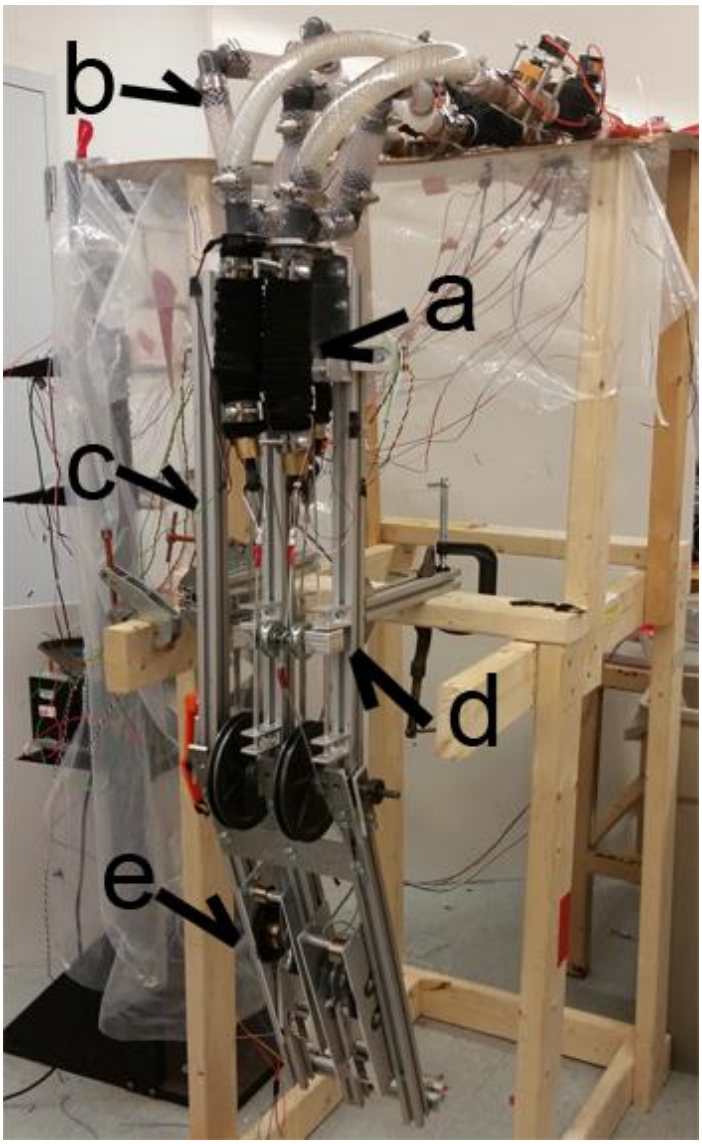


**Figure 13: Legchair Knee System. a) Hydro Muscle Pair, b) Hydraulics c) Joint System Support Architecture d) Force Augmentation e) Coupler/Decoupler**

An instance of the Joint System was designed and manufactured based on the requirements of an in-development humanoid robot called the Legchair. The Legchair robot is proposed as an assistive bipedal transportation device that could be beneficial to the large population of wheelchair users. The instance of the Joint System was designed as a knee joint scaled to meet the expected moment needs of the Legchair and user. Between 2.2 million [67] and 2.7 million [68] people use wheelchairs in the US alone and about 1% of the population worldwide [69] (~74 million) require a wheelchair on a daily basis. Unfortunately, standard wheelchairs have a number of deficiencies including an inability to cross large obstacles, ineffectiveness in traversing less rigid terrain (e.g. mud, sand, etc.), and an incapacity to ascend or descend stairs. While more advanced wheelchairs like iBOT [70] can address staircase locomotion they still fail to satisfy other basic tasks requiring more substantial separation between disjointed ground supports. For environments characteristic of human habitats, the two-legged walker seems to be the most appropriate choice. Although more challenging in terms of postural stability, e.g. dynamically balanced human gait [10], the bipedal robot carrying a seated person is anticipated to perform better than a quadruped particularly in the context of staircase tasks.

The design and physical realization of a biologically inspired knee joint instance of the Joint System which could lift the combined mass of a person and the Legchair of 150 *kg* (331 *lbm*) is presented in Figure 13. In contrast to previous research on human carrying walkers, the Legchair knee joint is closely modeled after human leg

proportions, whereas its dynamics are based on a biomimetic mode of muscle-tendon inspired actuation with human-like peak joint torque and power requirements scaled up to match the combined mass. Hydro Muscle [1], [25] artificial muscles in series with tendon-like cabling structures are utilized to actuate the legs. Hydro Muscles are linear actuators similar to ordinary biological muscles in terms of active dynamic output, passive material properties, and appearance. Hydro Muscles have a greater efficiency than McKibben Muscles. Hydro Muscle peak efficiency with (without) back flow consideration is 88% (27%) [25]. The muscles are inexpensive (on the order of standard latex tubes of comparable size), made of off-the-shelf elements in less than 10 minutes, easily customizable, lightweight, biologically inspired, efficient, compliant soft linear actuators that are adept for power-augmentation. Moreover, a single source can actuate many muscles by utilizing control of flow and/or pressure.

To address the large joint moment requirement of the Legchair, the force from Hydro Muscle groups is further augmented by utilizing a pulley-based Force Multiplier subsystem, Section 3.2.

In a biological system, the increased frequency of action potential for a specific motor unit results in an increased motor unit force until the maximal tetanus condition is met. Here, the depressurization of Hydro Muscle increases the muscle force and maximal force is met when fluid pressure in the muscle is approximately equal to the low hydraulic pressure (e.g. atmospheric pressure). Furthermore, in a biological system,

the increased synaptic activity results in a gradual increase of force corresponding to gradual, likely same order, motor units recruitment within the muscle, often referred to as the size principle [71]. Here, a similar but binary mechanism is accomplished in the form of the novel Coupler/Decoupler subsystem, Section 3.2. The controlled presence or absence of a constant force spring in between the Hydro Muscle and the actuated joint defines the decoupled or coupled states. This in turn provides approximately equal, maximally attainable muscle force across the entire range of joint angles.

In section 3.2, Methods, the biomechanical data is used to set the requirements on the Joint System dynamics for the knee joint of the combined Legchair and user. Furthermore, the numerical simulation of Hydro Muscle pressurization and depressurization depicts artificial muscle dynamics. The overall hydraulics subsystem of the Joint System is also described. Finally, the remaining subsystems of the Joint System are presented in the context of the actuation mechanism, Coupler/Decoupler selective engagement, sensory, and control subsystems. In Section 3.3, Experiment, the position and force control tests of the Legchair knee instance of the Joint System physical prototype are described. In Section 3.4, the main experimental results are presented. Finally, Section 3.5 provides a discussion of results and presents future work.

## 3.2 Methods

### 3.2.1 Biologically Inspired Performance Requirements

Central to achieving robust Legchair mobility are power and moment capabilities of individual joints. The combined Legchair and user system is anticipated to resemble a scaled up human model. Hence the knee power and moment requirements of this instance of the Joint System are obtained from scaled up human biomechanics data. For stair ascent (descent), knee joint peak moment is in the range of 0.6 ± 0.2 *N • m/kg* (0.4 ± 0.2 *N • m/kg*) [72] and knee joint peak power is in the range of 1.25 ± 0.32 *W/kg* (0.20 ± 0.21 W */kg*) [73]. The moment data suggest that the Legchair and user 150 *kg* (200 *kg*) combined mass requires 90 *N • m* (120 *N • m*).

The Hydro Muscle is adept at power augmentation through elastic energy storage and subsequent quick release. Hence a brief burst of energy characterized with high power output is readily achievable. More constraining is the average power output for repetitive tasks like walking at a self-selected speed estimated for both legs in the range between 1 *W/kg* (1,500 $in^2/s^3$) [74] and 2.5 *W/kg* (3,875 $in^2/s^3$) [75]. Recent study of the Hydro Muscle [25] revealed that its peak energy efficiency, without (with) considering return flow, is 27% (88%). This can then be related to the hydraulic system power requirement. For example if only 22% of the initial 1000 *W* (1.34 *hp*) the pump produces is transferred as useful power and if one assumes that the mass normalized average power of both legs for walking at a self-selected speed is 1.75 *W/kg* (2,713 $in^2/s^3$), then the combined system mass must be smaller than 126 *kg* (278 *lbm*). If 1000

*W* (1.34 *hp*) is used only for a single knee and the worst case scenario of 1.25 *W/kg* (1,938 $in^2/s^3$) of continuous normalized power (instead of just a short burst) is assumed, then the limit on the combined mass is 176 *kg* (388 *lbm*).

### 3.2.2 Hydro Muscle Dynamics

The dynamics of the Hydro Muscle have been formulated using Newton's laws and Bernoulli's equation. The results give an approximate simulation of the state of the Hydro Muscle while it is subjected to contraction. The state of the Hydro Muscle is specified by the pressure, acceleration, velocity, and the extension at the mobile end of the entire Muscle. The dynamics are modeled for muscle contraction, i.e. a single Hydro Muscle, initially extended to a known length and then allowed to contract by releasing the pressure in the muscle. The Hydro Muscle has a mass of 10 *kg* (22 *lbm*) suspended by a string at its tip. The initial elongation of the muscle is taken to be 0.15 *m* (5.9 *in*). A valve is then opened, subjecting the muscle to atmospheric pressure.

The relaxed length of the hydro muscle is taken to be 0.165 *m* (6.5 *in*). The spring constant k=5,885 *N/m* (33.6 *lbs/in*) of the hollow tube of the hydro muscle is experimentally obtained. The inner 2.54 *cm* (1 in) and outer 3.81 cm *(*1.5 *in*) diameters of the hydro muscle are measured. The maximum radial expansion of the hydro muscle will be equal to the inner diameter of the sheathing which is measured to be 5.59 *cm* (2.2 *in*). This makes the cross-section area of the muscle to be 0.0014 $m^3$ (85.4 $in^3$).

The inner diameter of the valve is 2 *cm* (0.8 *in*). This makes the cross-sectional area of the valve to be $3.017 \times 10^{-4}$ $m^3$ (18.4 $in^3$).

The stopping condition for the model is considered to be the point at which the Muscle reaches its relaxed length. The dynamic model assumes water to be a non-viscous, incompressible fluid, and that the Hydro Muscles do not have a damping factor. The simulation is conducted for two different arrangements, one in which the valve is completely opened, the second in which the area of the valve is increased at 1% per millisecond.

Figure 14 shows the results obtained from the simulation of the muscle. The initial pressure in the muscle is 749 *kPa* (109 *PSI*) and drops to 101 *kPa* (14.6 *PSI*). The time taken to reach a state of static equilibrium is greater if the area of the valve is increased at 1% per millisecond. The Hydro Muscle experiences high initial pressure if the valve is opened at a lower rate. The pressure obtained varies due to the presence of the velocity of the Hydro Muscle.

### 3.2.3 Hydraulics

The hydraulic subsystem is composed of a reservoir that feeds the pump [76], which is powered by a 1000 *W* (1.34 *hp*) BLDC motor [77]. The pump is connected to a pressure relief valve that regulates the maximum gauge pressure at 793 *kPa* (115 *PSI*). The flow is directed through the artery, see Figure 15 and into a muscle pair if the entrance valves are open. The solenoid valves are used for rapid on/off control,

while the servo-controlled butterfly valves are used for finer control of the flow. With the entrance valves open, the muscle pair can be pressurized pair by closing the exit valves. When the desired muscle state is achieved, the entrance valves can be closed to maintain that state. Depressurization of the muscles occurs when the exit valves are open. The quick release bag allows for a greater exit flow rate, and therefore a more rapid actuation of the muscle pair. A check valve is placed between the quick release bag and the vein in order to prevent backflow. The vein is then connected back to the reservoir.

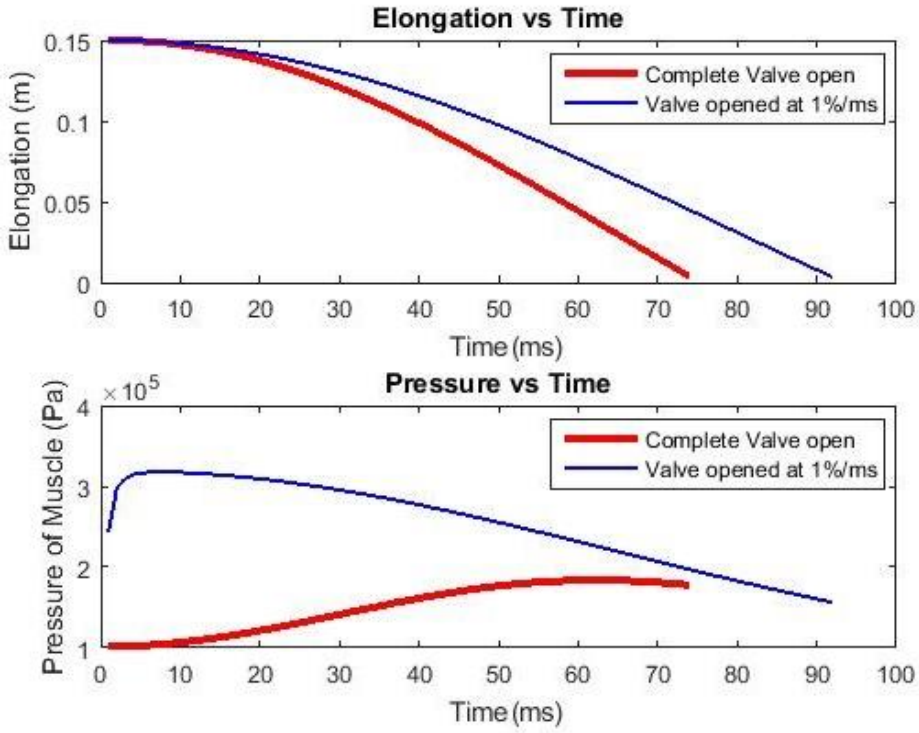


**Figure 14: Simulation of Hydro Muscle Dynamics. Displays Elongation of muscle and Pressure as a function of time.**

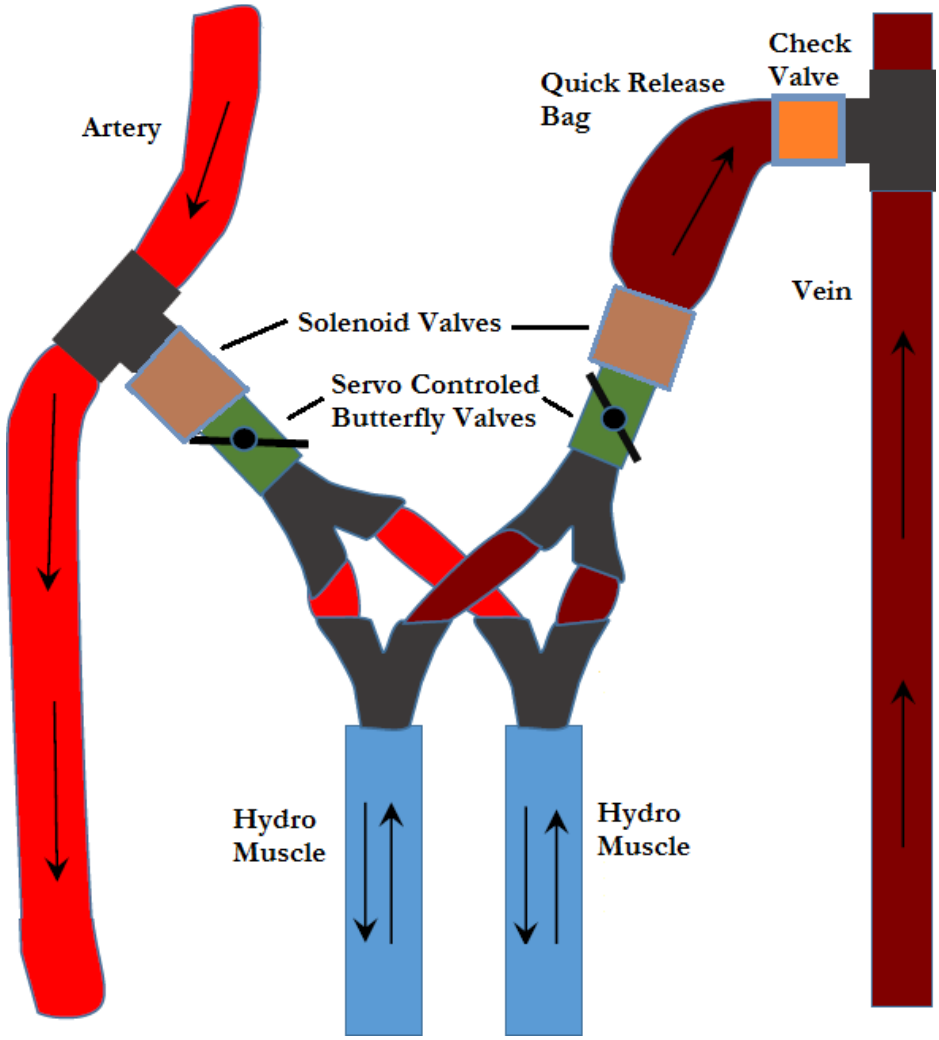


**Figure 15: Hydraulic Subsystem**

### 3.2.4 Joint System Support Architecture

In order to create the support for the Joint System a supporting structure was designed. The Joint System was built to achieve multiple low-level integral functions. These included similarity to human limb biomechanics and the ability to support and be actuated by Hydro Muscles and Coupler/Decoupler devices, while supporting the load of the actuation subsystem and in the case of the Legchair, a human operator.

From these specifications of this Joint System, the requirements of the joint structure were to be similar in size and actuation capability to the human leg system. This would allow for supporting the other components of the hydro muscle test leg system, creating a platform that previous biomechanics research could be applied to (e.g. muscle activity during locomotion and obstacle traversing), and propagating linear forces from the hydro muscles to rotational movement.

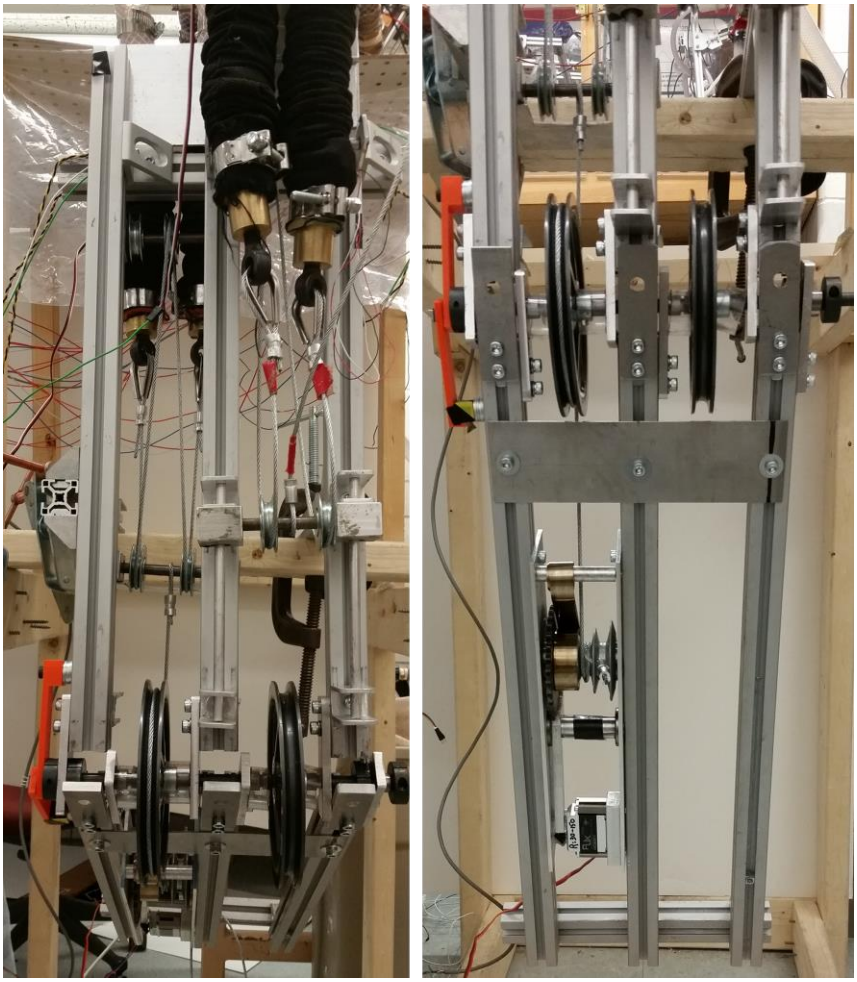

**Figure 16: Knee System Support Structure Left) Femur Right) Tibia**

From these functional requirements, the joint structure of Figure 16 was built. The leg skeletal structure, including the femur and tibia, was constructed with 80/20 T-slot 6105-T5 aluminum, comprised of two sets of three 60 cm by 3 *cm* by 3 *cm* lengths. This allowed for the strength and space to mount the other subsystems while being similar in proportion to a human leg for biomechanical research applicability. The rotational joint structure was constructed with aluminum plates with press fit bearings connecting the femur and tibia together through a steel axle. Damping and stopping mechanisms were implemented by attaching aluminum plates on the knee side of the tibia that collided with the rubber disks on the femur at the maximal 180° joint angle. The linear to rotational motion conversion was accomplished via a cable system that connected the hydro muscles on the femur to the Coupler/Decoupler device on the tibia.

### 3.2.5 Force Augmentation

The force provided by the Hydro Muscles contraction was augmented via two components, a Force Multiplier subsystem and a moment arm. The design consisted of a steel wire cable [78] connected between a pair of Hydro Muscles through a collection of pulleys as shown in Figure 17, then along a large diameter pulley and finally to the tibia of the Joint System. The Force Multiplier's sliding mechanism consisted of a pair of linear bearings housed inside aluminum metal blocks which each run over a hardened aluminum rod. This design augments the force provided by Hydro Muscles by a factor of two. The length of the sliding run was thus calculated to be half

the extension length of the Hydro Muscle. The large 7.1 *cm* diameter pulley at the knee of the system was used as a lever arm to convert the tension from the Force Multiplier to a moment about the system's knee joint.

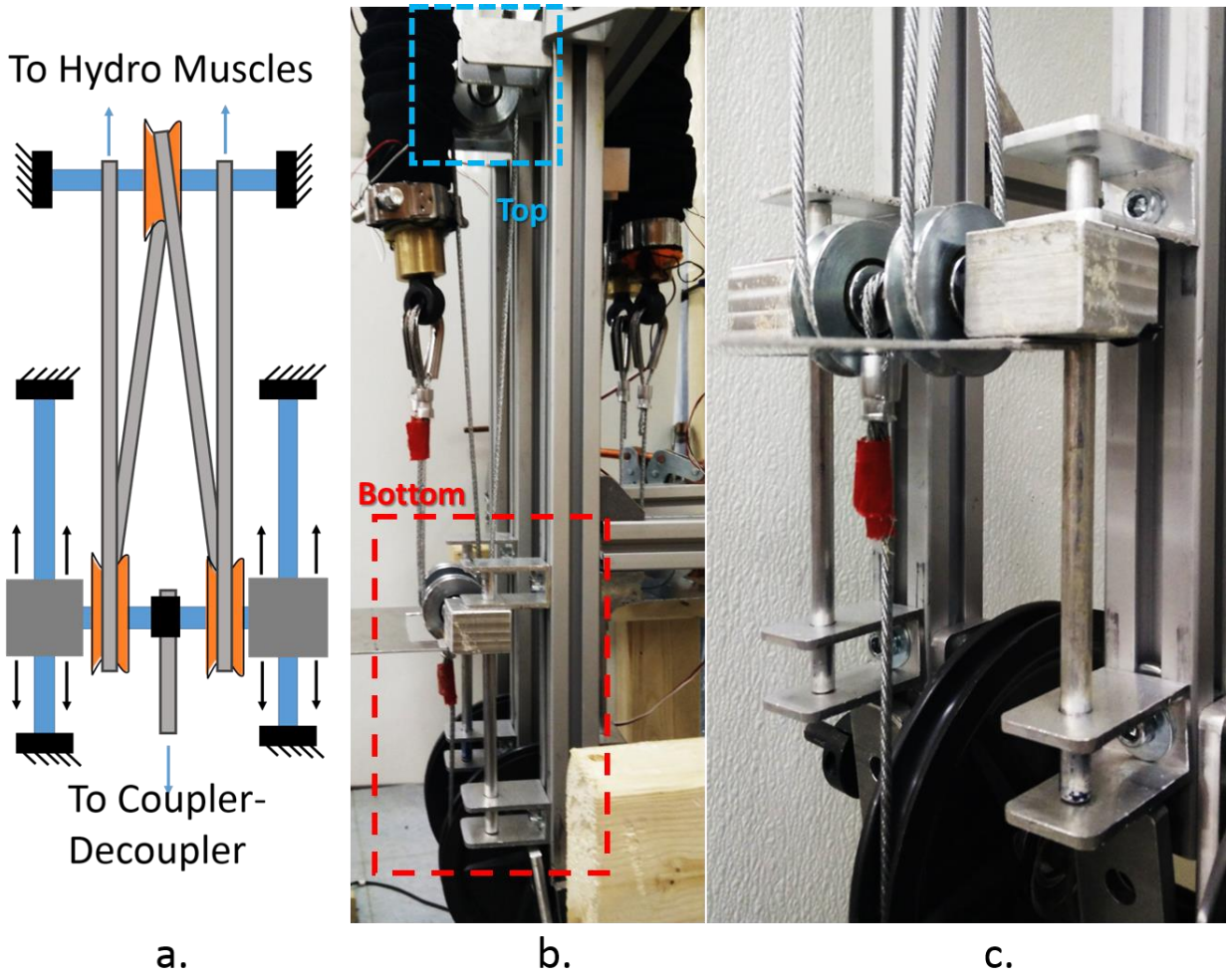


**Figure 17: Force Augmentation mechanisms. a) Complete assembly diagram**

Through the combined force augmentation components, the output moment of the Legchair Knee System was defined by Eq. 7.

$$M = 4rTm \quad (7)$$

Where M is the moment about the system's knee, Tm is the tension in one Hydro Muscle, and r is the radius of the knee pulley.

### 3.2.6 Coupler/Decoupler

The Coupler/Decoupler of the Joint System is a latching device seen in Figure 18 and Figure 19, is designed to allow for low complexity actuation and improved range of forces in systems actuated with synthetic muscle technology. The Coupler/Decoupler allows for controlled selective engagement of the Joint System, coupling or decoupling the tibia from its respective pair of Hydro Muscles (quadriceps or hamstring). The Joint System uses two Coupler/Decoupler devices placed on the tibia frame. Each Coupler/Decoupler is in line serially with the cabling and Force Multiplication subsystem connecting to one of the muscle pairs.

The Coupler/Decoupler provides key functionalities of the Joint System. Primarily, the selective engagement allows for the changes in length of the muscles to affect the change in joint angle only when actuation is desired. With this, muscle length is not tied to joint angle, allowing for any muscle length at any joint angle. Therefore, any muscle contraction induced moment can be exerted at any joint angle, without the act of charging affecting the state of the joint. The second major contribution of the Coupler/Decoupler is allowing for simple joint actuation, depending only on the fast and strong contraction action of a single muscle group. By decoupling only one muscle

group of the Joint System, the joint can be actuated without fighting or charging an antagonistic muscle group. Therefore, actuation efficiency and strength is not tied to the rate at which muscle groups can be charged.

By using a pair of Coupler/Decoupler devices with different states of engagement, the Joint System is capable of three distinct states of actuation ability. When both Coupler/Decoupler devices are decoupled, the Joint System is capable of free movement in both directions. This can be beneficial for both gravity assisted system dynamics and charging Hydro Muscles in preparation for multiple actuation trajectories. When only one Coupler/Decoupler is coupled the joint can travel and actuate in the pull direction of the engaged muscle group while freely charging the muscles to prepare for actuation in the disengaged direction. Finally, when both Coupler/Decoupler devices are coupled the joint can be held in place with a stiffness factor of Hydro Muscles group elasticity. Therefore, from an uncharged state, a joint actuation consists of the following steps. First the Coupler/Decoupler of the muscle group to be actuated is decoupled. Second this muscle set is charged to a length proportional to the desired actuation distance or moment. Third the Coupler/Decoupler of the charged muscles is coupled while the opposite muscles are decoupled from the Joint System tibia. Last the charged Hydro Muscle set is released, activating its stored elastic energy and actuating the Joint System.

The mechanical design of the Coupler/Decoupler consists of a sprocket, a large and small lever, a 2.2 *N* • *m* (1.6 *ft* • *lb*) High Voltage Digital Servo [79], and a stainless steel constant-force, 26.42 *N* (5.9 *lbs*), spring [80].

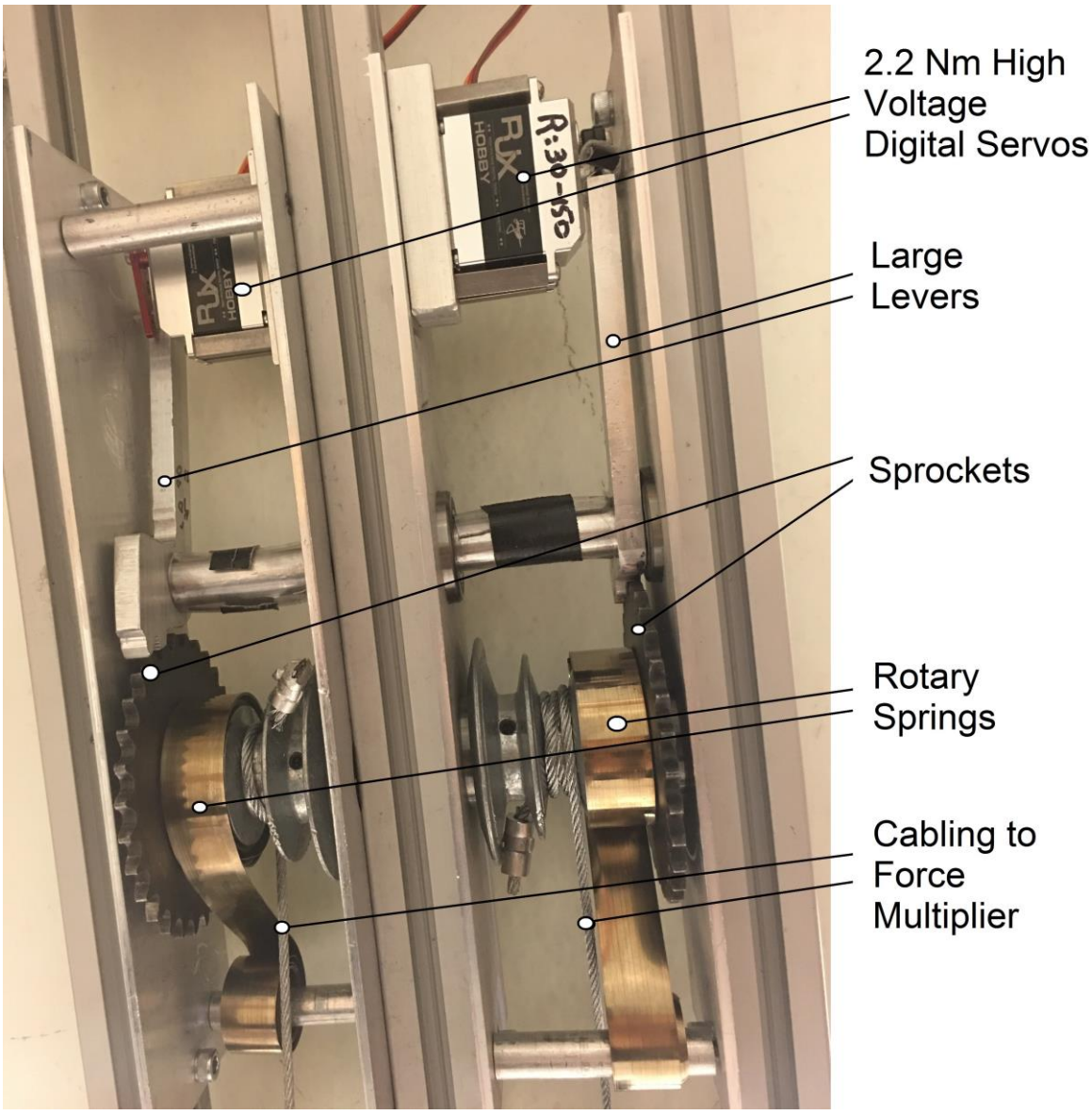


**Figure 18: Two Coupler/Decoupler devices side-by-side**

The servo and small lever control the state of the Coupler/Decoupler by engaging the large lever to the sprocket to maintain tension of the cabling during muscle contraction. Disengaging the sprocket permits rotation, which enables the spring to absorb any relaxed tension in the cabling during muscle expansion.

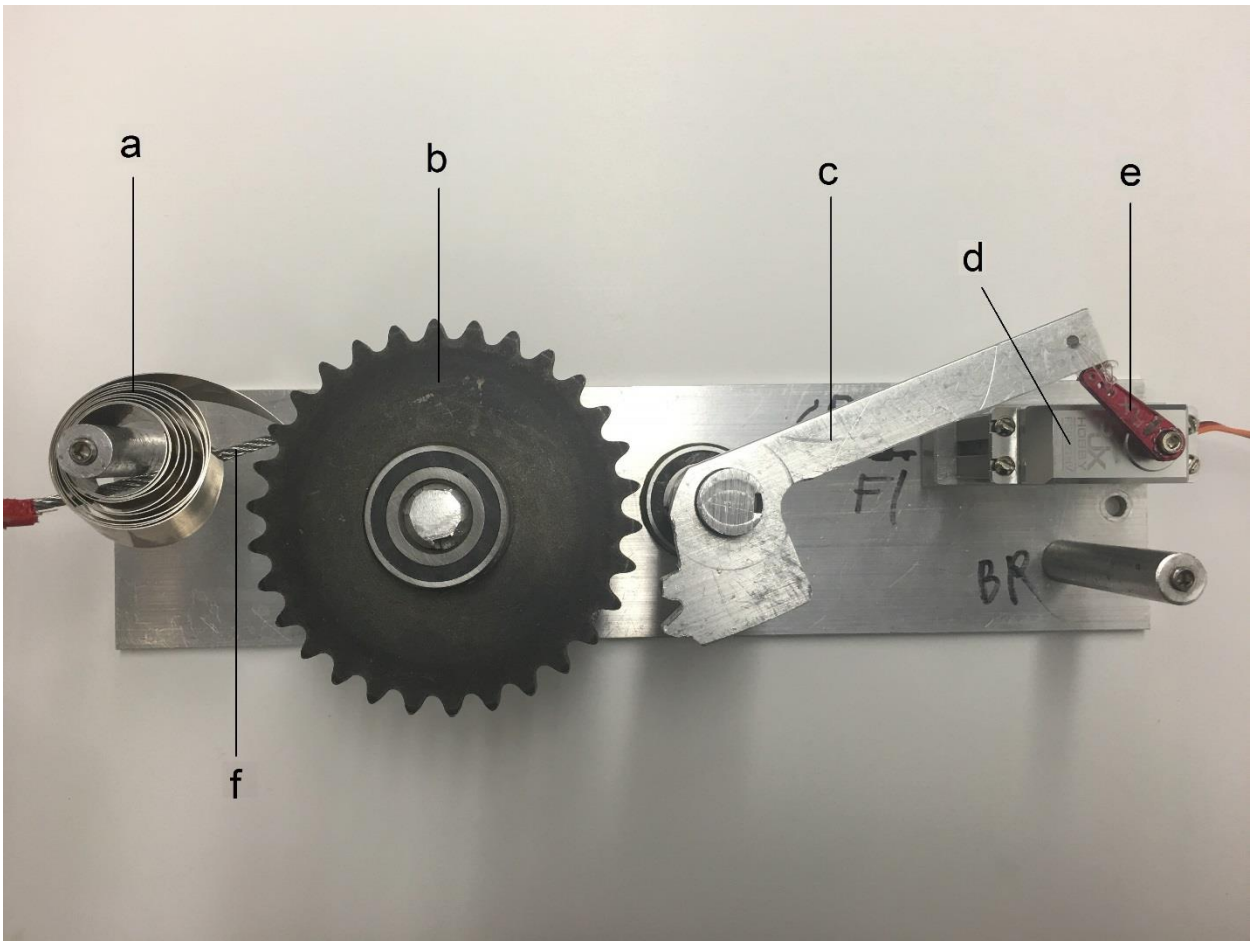


**Figure 19: Inside View of Coupler/Decoupler. a) Stainless steel constant-force spring. b) Sprocket. c) Large lever. d) 2.2 N m (1.6 ft lb) High Voltage Digital Servo. e) Small lever. f) Cabling connecting to the Force Multiplier**

The cabling is attached to a small pulley with a radius of $X_1 = 1.2cm$ (0.47 *in*), which is rigidly attached to the sprocket with teeth at a distance of $X_2 = 3.6cm$

(1.42 *in*) from the shared axis of rotation. The lever's teeth engage the sprocket at a distance of $X_3 = 2.5cm$ (0.98 *in*) from its axis of rotation. No active force is required to keep the lever engaged to the sprocket when tension is exerted on the cabling. However, active force is needed to disengage the lever from the sprocket. Friction is the only component against the force of the servo; for a greasy, lubricated contact static coefficient of friction is 0.3. In the opposite end of the lever, a small lever connected to the $\tau = 2.2N\ m$ (1.6 $ft \bullet lb$) servo engages the large lever at a contact point of $X_4 = 8.7cm$ (3.43 *in*) from the large lever axis of rotation, and $X_5 = 1.4cm$ (0.55 *in*) distance from the servo axis. Therefore, the latching ratchet inspired Coupler/Decoupler can withstand large cable forces of F=5.47 *kN* (1230 *lbs*) using Eq. 8.

$$F = \frac{X_1}{X_2} * \frac{1}{0.3} * \frac{X_4}{X_3} * \frac{\tau}{X_5} \tag{8}$$

### 3.2.7 Sensors

Several sensors were incorporated into the system to provide feedback for controls. The four properties that were measured are the knee joint angle, the elongation of the Hydro Muscle, the pump source pressure, and internal pressure of the Hydro Muscle.

The angle of the knee is determined through a rotary potentiometer attached at the axis of rotation on the knee joint. The elongation of the muscle is calculated using an IR sensor which measures the sliding movement of the aluminum blocks in the Force

Multiplier. Pump source pressure is measured through a digital pressure sensor located in front of the outflow of the pump; this sensor is used to monitor the water going into the hydraulic subsystem. The internal pressures of the muscles were measured through a load sensor placed between the latex and the nylon sheath. As the muscles expands the load sensor outputs a force reading that is mapped to pressure; this was done to keep the hydraulic subsystem as compact as possible.

### 3.2.8 Fine Flow Control and On/Off Solenoid Latching Valves

Two subsystems, each comprised of a one way magnetically latching solenoid valve [81] connected in series with a 21.3 *kg/cm* (119 *lb/in*) torque servo motor [79] controlled butterfly valve [82], are used to control the input and output flow rate of each Hydro Muscle. The servo motor provides an actuation speed of $0.05s/60^{\circ}$ at $8.4V$. The motorized butterfly valve provides finer control while the solenoid valve is used for switching the flow on and off. The valves are used in series because the butterfly valve cannot be fully closed over the gasket and the solenoid gives more control over the system because it is faster by comparison. Additionally, flow through the solenoid valve does not travel a completely straight path, resulting in energy losses.

### 3.2.9 Control

The goal of the control setup was to track and control the angular position of the Joint System. The angle of the joint was obtained as a function of the rotary

potentiometer's resistance and was actuated using a servo installed on a butterfly valve in series with a latching solenoid valve as stated above. A simple proportional controller was uploaded onto an Arduino Yun. The system was initialized by running water through the hydraulic subsystem until there was no air remaining and then expanding the back-muscle pair to its full length by closing the outflow valves. When given a set angle, the controller checks for the error based on the desired angle and then opens the outlet solenoid valve and tunes the butterfly valves position as a function of the error.

## 3.3 Experiments

The instance of the Joint System built for the Legchair knee was run through multiple experiments. Each experiment was in the testing configuration as seen in Figure 13.

### 3.3.1 Experiment I-Knee Joint Angle

This experiment shows the effect of the Coupler/Decoupler state on how the muscle length change effects the change in knee joint angle. For this experiment the muscle length was oscillated with the Coupler/Decoupler decoupled and then again with it coupled. The knee joint angles were measured as the muscles changed state. Results of the experiment are shown in Figure 20.

### 3.3.2 Experiment II- Torque test on Quadricep Muscles

This experiment measured the moment exerted by the Quadriceps at different muscle lengths. The Quadriceps were extended through pressurization while the Coupler/Decoupler was decoupled. To measure the force, a digital scale [83] was connected at the bottom of the leg's tibia via a steel cable at a 90° angle. Next to pressurize the muscles, the outlet was closed, the inlet was opened, and the pump was activated. After reaching a desired muscle extension, the inlet was closed again to maintain muscle state. The Coupler/Decoupler was then coupled and the outlet was closed to depressurize the Hydro Muscle and the force exerted at the foot was measured. Results of the experiments are shown in Figure 21.

### 3.3.3 Experiment III- Torque test on Hamstring muscles

This experiment measured the force exerted by the Hamstring muscles at different muscle lengths. For this experiment, the Hamstring muscles were extended by external pulling and the force exerted at the foot was measured with the digital scale. Results of the experiments are shown in Figure 21.

### 3.3.4 Experiment IV-Knee Joint Angle Control

The following experiment was designed to evaluate the performance of the knee joint angle proportional controller. A set angle of 25° was given to the controller and the parameters involved such as the desired angle, current angle, angle of the butterfly

valve and response time were recorded. Results of the experiments are shown in Figure 22.

### 3.4 Results

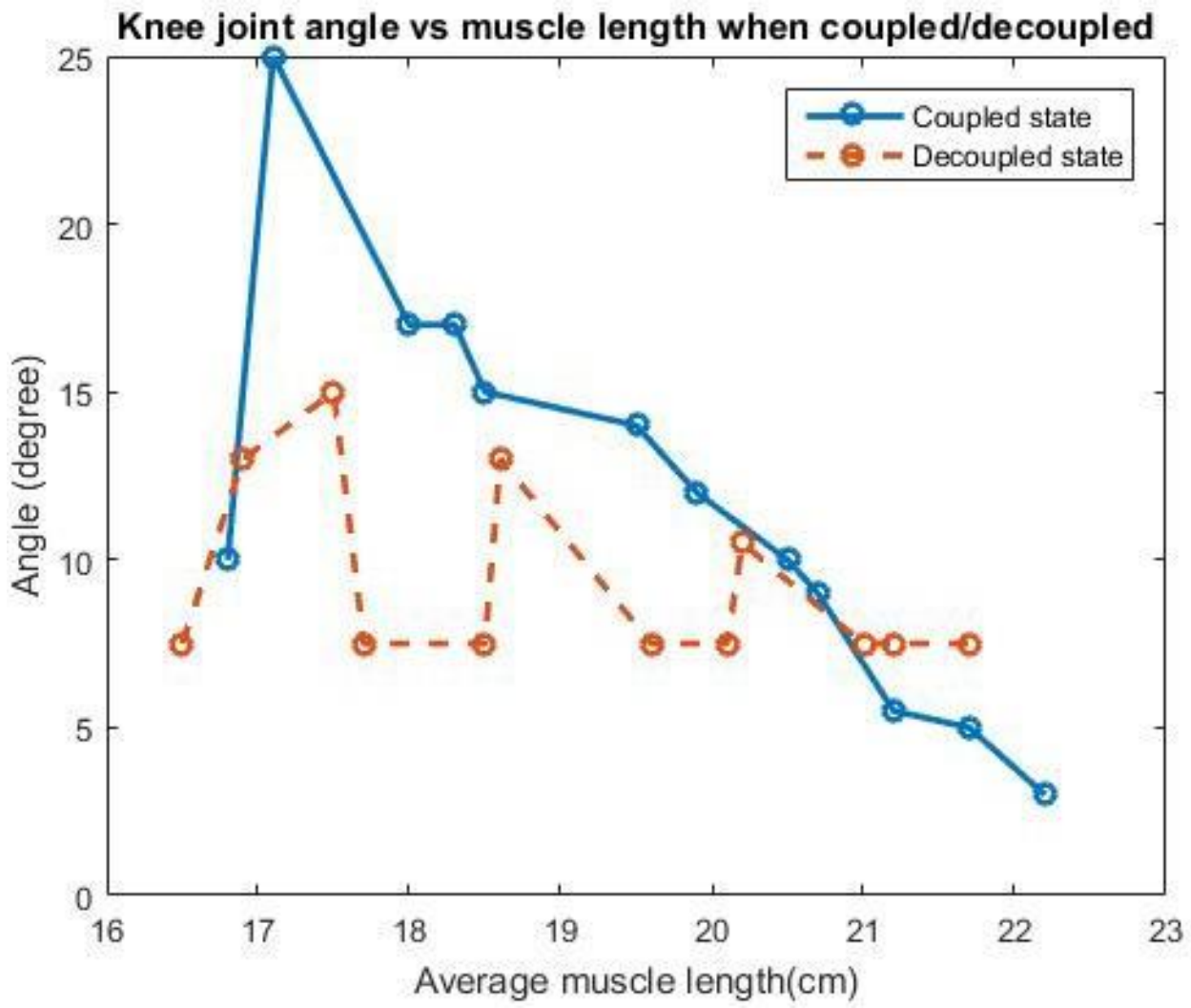


**Figure 20: Knee joint angle when coupled/decoupled vs muscle length**

The knee joint angle plot in Figure 20 also shows a near linear change with change in muscle length in coupled state. Fluctuations appear instead of a constant angle in decoupled state due to the friction between the steel cable and pulley surface.

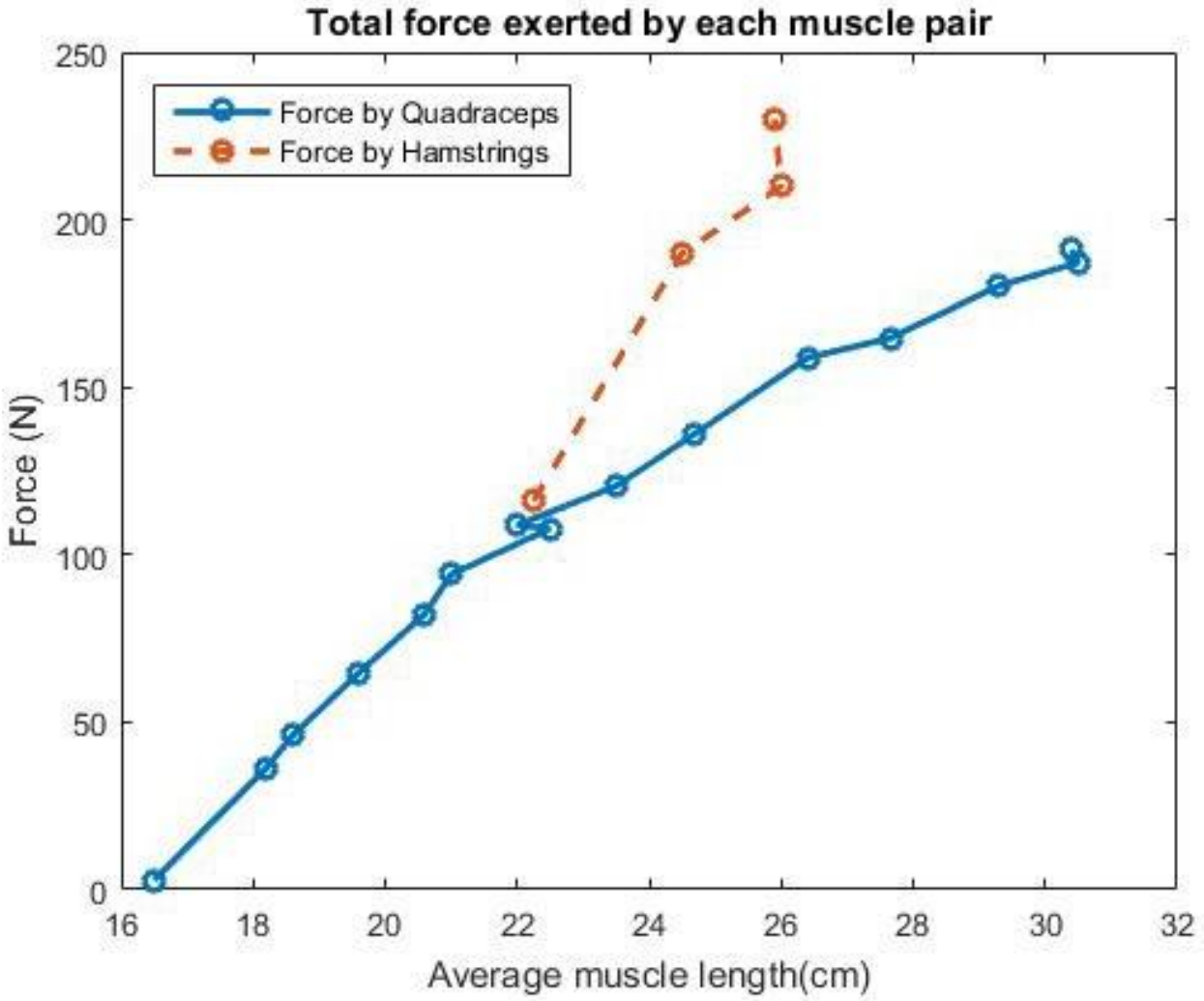


**Figure 21: Force exerted by Quadriceps and Hamstring muscles vs muscle length**

A near linear increase in force exerted by quadriceps is seen in Figure 21 with increase in quadriceps's length with maximum being 191.1 *N* (43 *lbs*) at extension of 30.4 *cm* (12 *in*). Since the force was measured at 0.61 *m* (24 *in*) from knee joint, the

maximum moment at 191.1 *N* (43 *lbs*) was calculated to be 116.571 *N* • *m* (86 ***ft*** • *lb*) A similar trend for force exerted can be seen for Hamstring muscles when pulled using external manual force. Since the force was measured at 0.61 *m* (24 *in*) from knee joint, the maximum torque at 230 *N* (51.7 *lbs*) was calculated to be 140.3 *N* • *m* (104 ***ft*** • *lb*)

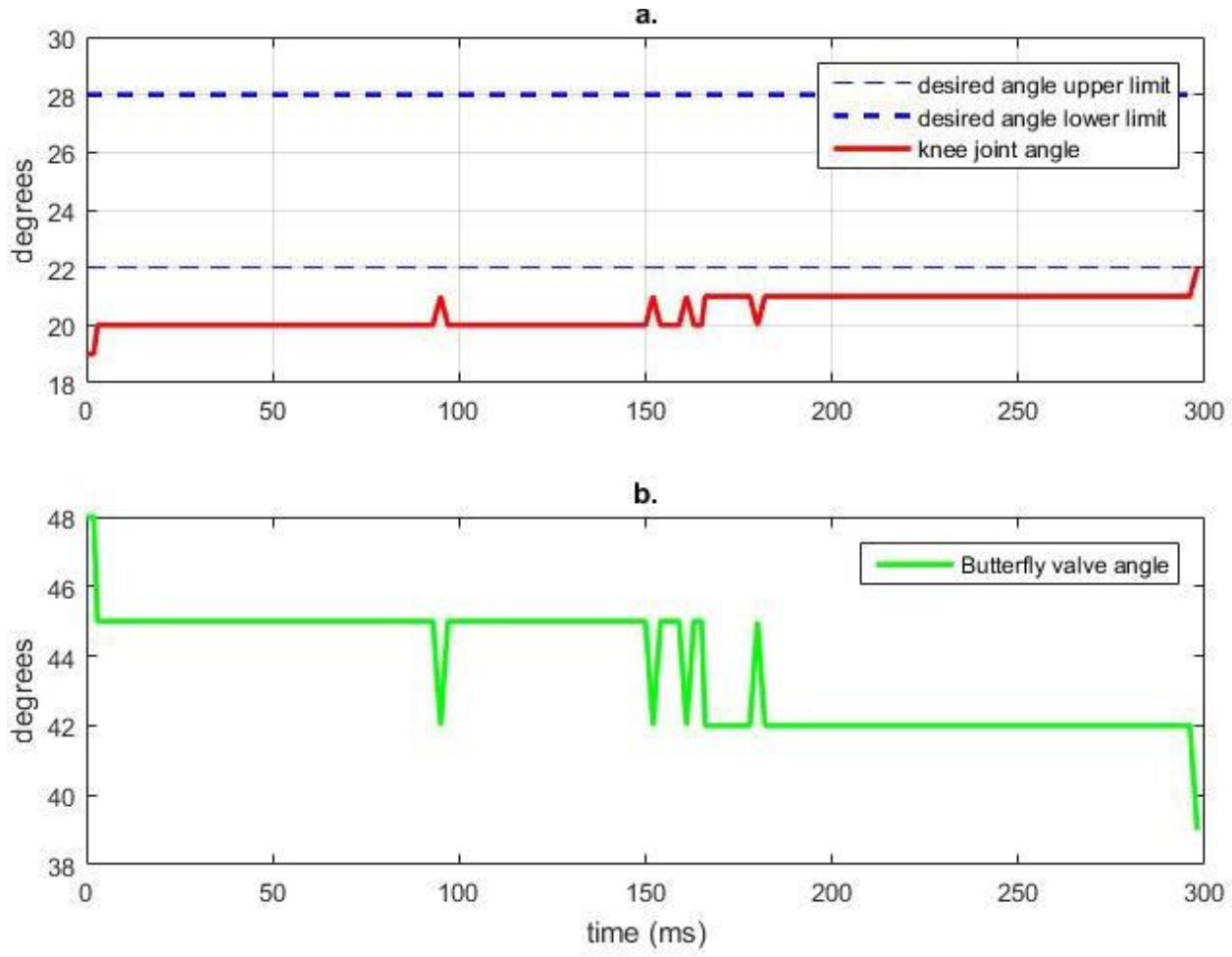


**Figure 22: a. Knee joint angle vs time. b. Butterfly valve angle vs time.**

Figure 22 shows the change in knee joint angle and butterfly valve angle compared to the desired angle as recorded through controller.

### 3.5 Discussion and Future Work

The Joint System hydraulic actuator with selective muscle engagement was designed and an instance of it was built to the specifications of a Legchair bipedal transportation device knee joint. This Legchair knee joint was tested to verify functionality of its sub-components along with joint torque magnitude and position control ability. Two pairs of selectively antagonistic Hydro Muscles actuate the knee with use of two Coupler/Decoupler devices. Hydro Muscles are inexpensive linear actuators similar to ordinary biological muscles in terms of active dynamic output, passive material properties and appearance. The force of each Hydro Muscle pair was doubled through the use of a cable pulley-based Force Multiplier. The selective engagement of the muscles was handled by the latching ratchet inspired Coupler/Decoupler that enforces binary muscle recruitment and allows for joint moment to be applied independent of joint angle and therefore maximal muscle force.

From the results of the Coupler/Decoupler experiment, the effect of its state on the system is shown. With variable connection between the Hydro Muscles and joint tibia, any moment of the leg can be performed at any joint angle. Thus, allowing for any muscle force to be applied at any joint angle, without affecting the joint angle before actuation.

Scaling human biomechanics data on stair ascent for the combined Legchair and user system suggests that a Legchair knee joint should be able to provide about 0.6 *N*

• *m/kg* (930 $in^2/s^2$) times the combined moment; e.g 150 *kg* (331 *lbm*) combined mass requires 90 *N* • *m* (66.4 *ft* • *lb* ). The peak moment estimated based on linear extrapolation on the muscle force tests was 200 ± 30 *N* • *m* (148 ± 22 *ft* • *lb*) suggesting a maximal mass of 333 *kg* for a Legchair and user system. Therefore, the design of the Joint System was strong enough to be able to meet the stair climbing needs of a human knee joint with enough overhead for a robust Legchair design.

It is noteworthy that the moment tests run by the system were consistently weaker than the same for the hand actuated tests. While the low forces are enough to meet the requirements of the Legchair knee, further work is needed to reduce energy loss through the subsystems of the Joint System and achieve the maximum theoretical moment through system actuation.

With the selective engagement, moment magnitude, and actuation of the Joint System illustrated the performance contributions of the Coupler/Decoupler can be seen. Without the use of an antagonistic muscles actuation method, the Joint System is capable of high enough joint moments to be suitable for a large-scale humanoid robot application, such as the Legchair. In addition, the Joint System is capable of this performance without being based on the level of hydraulic pump technology used in the system, therefore decoupling actuation speed and strength performance from the sophistication of the pump technology.

Future work will focus on functionality additions and design improvements for the Joint System. Of primary interest is variable stiffness capabilities. With this the Joint System could couple the joint with different levels of stiffness response, to emulate rigid and compliant interactions in humanoid tasks such as walking. Sensing of contact forces interactions is also of potential use. By utilizing muscle pressure and length the forces due to contacts with the environment could be deduced. The other area of focus is in design improvements of the Joint System. When multiple instances of the Joint System are used, such as in the joints of a leg, it becomes costly to distribute hydraulic hardware to each joint. A potential design could be to have all the synthetic muscle in one location with a Bowden cables system distributing their force to the joints of the system. Additionally, subsystems of the Joint System could be compacted for size and weight concerns. Planetary gear mechanism and other potential gearing mechanisms will be considered to compact the Force Multiplier, joint level arm, and Coupler/Decoupler.

# CHAPTER 4

# DESIGN AND TEST OF BIOLOGICALLY INSPIRED MULTI-FIBER HYDRO MUSCLE ACTUATED ANKLE

This chapter explores the concept of selective recruitment using groups of artificial muscles acting on the same joint. Each of these muscle fibers is controlled to produce movements, forces, and stiffnesses that are independent of each other. Additionally, a viscoelastic model is developed that helps us understand the Hydro Muscle better.

---

The material in this chapter is adopted from the self-authored publication: [84]
M. P. Bowers, C. V. Harmalkar, A. Agrawal, A. Kashyap, J. Tai, and M. Popovic (2017, March). "Design and test of biologically inspired multi-fiber Hydro Muscle actuated ankle," In *2017 IEEE Workshop on Advanced Robotics and its Social Impacts (ARSO)* (pp. 1-7). IEEE.

## 4.1 Introduction

A high level of biological realism in the context of prosthetic devices not only provides a more natural mechanical performance but also opens the door for more natural neural pathways that can be used for control. The human body is much more complex than any robotic system built so far. It has more than 600 skeletal muscles and each muscle has at least 100 (typically a lot more) motor units that are independently controlled. Conventional 20$^{th}$ century robots use motors to actuate each of the individual muscles. This makes the system heavy and bulky, reducing its mobility. Fortunately, pneumatic and hydraulic approaches could be useful to achieve the same degree of control that a human body has while not adding large amounts of excess weight to the assembly. Only one or two prime movers (e.g. pumps) would be the heavier components while the rest (e.g. valves) could be miniature devices. Additionally, hydraulics have

better energy efficiency than pneumatics due to the incompressibility of liquids like water. In this work, an experimental platform for studying a single degree of freedom joint controlled by multiple independently actuated Gastrocnemius and Soleus muscle fibers is proposed.

A planar leg with a one degree of freedom ankle is designed and prototyped to study the multi-fiber control of the ankle's properties. The Gastrocnemius and Soleus lower leg muscle groups have a multi-fiber composition allowing for active control of stiffness and force similar to recruitment in biological muscles [10]. Additionally, the Tibialis Anterior muscle is passively included. The inexpensive Hydro Muscle technology could be a candidate for efficient actuation. Utilized here as individual muscle fibers controlling the same single degree of freedom joint, Hydro Muscles are linear actuators resembling ordinary biological muscles in terms of active dynamic output, passive material properties, and appearance. The Hydro Muscle has a single fluid flow opening and is comprised of an inner and an outer structural element. The inner element is a smooth tubing made of an elastic material such as latex. The outer element is a non-stretchable sleeve made of a soft, inelastic material, such as polyester, to limit radial expansion while promoting lengthwise expansion when pressurized.

In contrast to the PAM McKibben artificial muscles [8], [9], Hydro Muscles elongate axially, stiffen radially, and do not bulge when pressurized. When depressurized, they contract axially, and soften radially. Hydro Muscles exhibit better efficiency than McKibben's muscles [25]. Substantial radial expansion and deflation of McKibben's

elastomer introduces substantial energy loss in transfer from the source to the actuated load. Furthermore, Hydro Muscles can easily reach strains of 3.0, while McKibben muscles typically have a maximum strain of about 0.4. Biological muscles have an average maximum strain of 1.0 [85].

In biological systems, the increased frequency of action potential for specific motor units result in an increased motor unit force until maximum tetanus contraction is achieved. Here, the depressurization of a Hydro Muscle increases the muscle force and maximum force is achieved when fluid pressure in the Hydro Muscle is approximately equal to the low hydraulic pressure (e.g. atmospheric pressure). Furthermore, in biological systems the increased synaptic activity results in a gradual increase of force corresponding to a gradual, likely similar order motor units recruitment within the muscle, often referred to as the size principle [86]. A similar muscle recruitment approach is addressed here with Hydro Muscle based multi-fiber architecture of the Gastrocnemius and Soleus muscle groups. Multi-fiber actuation has been investigated in the past [87], but they did not control the individual fibers.

The viscoelastic properties of the Hydro Muscle based muscle fibers were experimentally investigated. Test procedures and results are presented in Section 4.2. The physical realization of the multi-fiber Hydro muscle actuated ankle by synthetic Gastrocnemius and Soleus muscles, i.e., the experimental platform for the study of ankle action has been described in Section 4.3. Position, stiffness, and force control tests were performed to characterize the proposed musculoskeletal model; these experimental

procedures and test results are presented in Section 4.4. The results are discussed and compared to the performance of biological systems and future work is addressed in Section 4.5.

### 4.2 Viscoelastic Model

The viscoelastic model of the Hydro Muscle is a mathematical model designed to estimate the behavior of the muscle based on the extension, the rate of extension of the Hydro Muscle and the pressure of the hydraulic fluid actuating the Hydro Muscle. The model employs multivariate linear regression to develop a model which predicts the force exerted by the Hydro Muscle. The experiment involves the actuation of a single Hydro Muscle. The hydraulic pressure, tensile expansion of the Hydro Muscle and the force exerted by the Hydro Muscle are recorded and are utilized in developing the model.

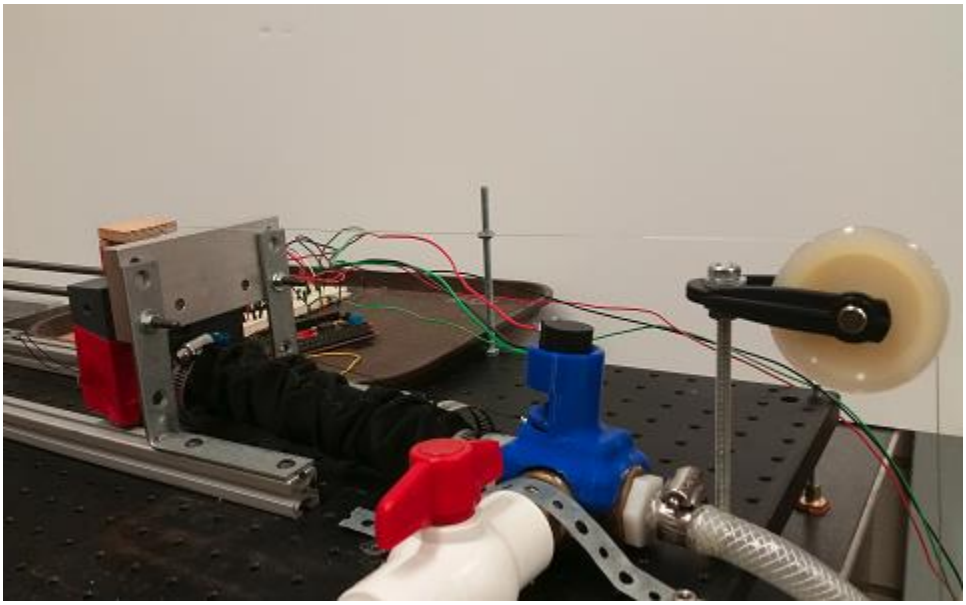

**Figure 23: Viscoelastic Modeling Test Setup**

The test is conducted on a single Hydro Muscle of length 0.02 *m* with the internal diameter of the latex tube 0.75 *inches* (0.019 *m*) and the outer diameter 1.125 *inches* (0.028 *m*). The muscle is actuated using an inlet of water capable of producing variable pressure. One end of the Hydro Muscle is clamped to a testbed. The free end is attached to a block placed on a sliding rail which is free to move in the direction of elongation of the muscle. This block has two load cells (range 0 – 50 *kg*) [88] attached in front of the muscle to measure the force exerted by the muscle. There is a mass suspended from the load cell to achieve a reaction force. The experimental setup is shown in Figure 23. The distance measuring sensor unit [89] is composed of an integrated combination of PSD (position sensitive detector), IRED (infrared emitting diode) and signal processing circuit. The sensor unit utilizes the triangulation method for distance measurement and is not influenced by the reflectivity of the object, the environmental temperature, and the operating duration. This device outputs the voltage which can be mapped to a corresponding distance based on the sensor model. The system has a pressure sensor [90] with the range of 1.2 *MPa*. A micro-controller is used to drive the sensors and collect data. The controller uses 12-bit analog-to-digital converters to convert the analog data from the sensors to comprehensible data in physical units. Based on the resolution of the sensors and the analog-to-digital converters, the sensors could detect a minimum change of 1171 *Pa* for pressure, 1 *mm* for length, and 0.01 *N* for force. The data is exported to MATLAB and the *fitlm* function is used to obtain the multivariate linear regression quadratic and cubic models for predicting the force exerted by the muscle as a function

of the elongation, (*x*), rate of elongation, (*v*), and the hydraulic pressure, (*P*), in the system.

### 4.2.1 Results

The data obtained is filtered using a moving average filter to reduce the spurious noise. The filtered values are used to evaluate a linear regression model for the force produced by the Hydro Muscle. The models obtained using the elongation, (*x*), and the rate of elongation, (*v*), as predictor variables proved to be fairly accurate. On addition of hydraulic pressure, (*P*), of the system as a predictor variable, the models presented an improvement over their previous versions as shown in Table 2.

**Table 2: Viscolelastic Model: Confidence of Fit**

| Model Specification | $R^2$ | Adjusted $R^2$ | RMSE |
|---|---|---|---|
| Quadratic without Pressure terms | 0.672 | 0.661 | 0.0366 |
| Cubic without Pressure terms | 0.816 | 0.807 | 0.0276 |
| Quadratic with Pressure terms | 0.819 | 0.808 | 0.0275 |
| Cubic with Pressure terms | 0.85 | 0.816 | 0.0256 |

The cubic polynomial model, involving pressure as a variable, produced results better than the other models developed. The model equation is as below with the physical quantities in their SI units -

$$\begin{aligned} F = {} & C_0 + C_1 x + C_2 v + C_3 P + C_4 x^2 + C_5 xv \\ & + C_6 v^2 + C_7 xP + C_8 vP + C_9 x^3 + C_{10} x^2 v \\ & + C_{11} xv^2 + C_{12} v^3 + C_{13} x^2 P + C_{14} xvP \\ & + C_{15} v^2 P \end{aligned} \tag{9}$$

The estimated co-efficients of the terms in the equation are shown in Table 3. The quadratic as well as the cubic linear regression models exhibit a high confidence of fit.

Figure 24 shows the prediction of the force exerted by the muscle using the model in Eq. 9 and the actual force measured by the load cell. The results demonstrate high fidelity of the model to the actual behavior of the Hydro Muscle.

**Table 3: Model Co-Efficient Estimates**

| $C_0(N)$ | $C_1(N/m)$ | $C_2(Ns/m)$ | $C_3(m^2)$ | $C_4(N/m^2)$ | $C_5(Ns/m^2)$ | $C_6(Ns^2/m^2)$ | $C_7(m^3)$ |
|---|---|---|---|---|---|---|---|
| -6.426 | 41.744 | -52.309 | 15.135 | -1586.5 | 2786 | -137.77 | -355.69 |
| $C_8(ms)$ | $C_9(N/m^3)$ | $C_{10}(Ns/m^3)$ | $C_{11}(Ns^2/m^3)$ | $C_{12}(Ns^3/m^3)$ | $C_{13}()$ | $C_{14}(s)$ | $C_{15}(s^2)$ |
| 73.913 | 23321 | -51458 | 6754.7 | 622.14 | 1567.8 | 914.38 | -58.823 |

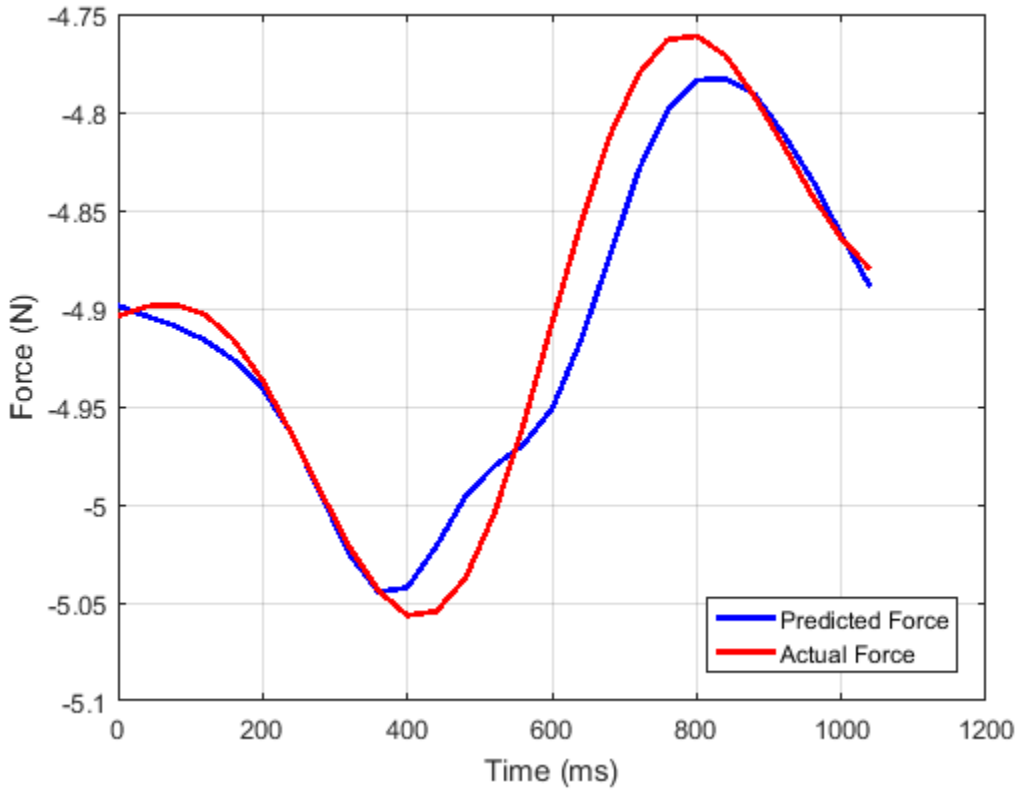


**Figure 24: Model Prediction of Hydro Muscle Force**

### 4.3 Multi-Fiber Musculoskeletal Model

The Musculoskeletal model was designed with biofidelity in mind. In particular, the dimensions [91], [92] and maximum forces [93] of a human leg walking were used as

design criteria. Additionally, in order to achieve the variable stiffness of human muscles, multiple independently actuated Hydro Muscles were used for the Soleus and Gastrocnemius muscle groups, while unactuated hydro muscles are used for a passive Tibialis Anterior. The Musculoskeletal model consists of the leg structure, Hydro Muscles, control hardware, and data collection hardware.

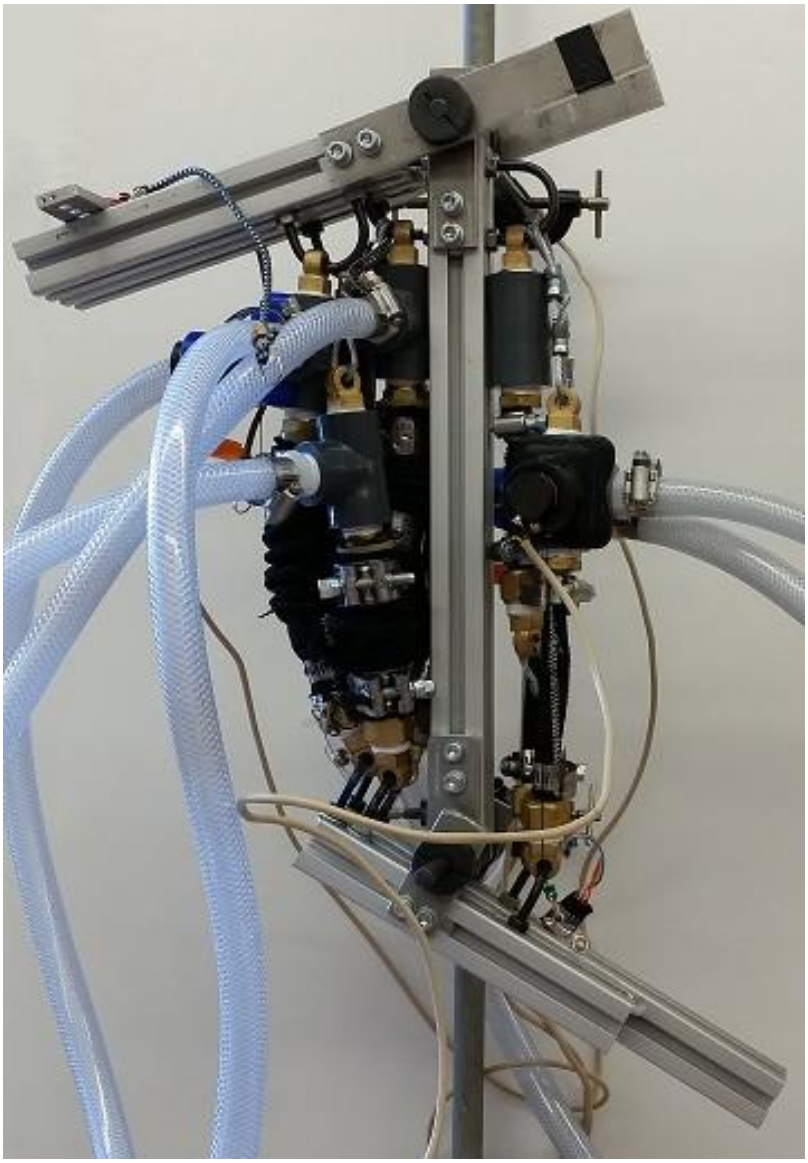

**Figure 25: Leg Structure**

The leg structure seen in Figure 25 consists of aluminum 80/20 extruded beams representing a foot and a Tibia, each of average male adult length, and a partial Femur. In addition, there is a single degree of freedom knee joint which is locked in place at 90° as well as a single degree of freedom ankle joint each consisting of an axle, rotational

bearings, attachment plates, and fasteners. Finally, there are Hydro Muscle fiber attachment points consisting of u-bolts and nuts placed in locations corresponding to its biological muscle's counterpart. The attachment points for the Soleus muscles were placed at the top of the foot behind the ankle and at the backside of the Tibia near the top. The first attachment point for the Gastrocnemius muscles was also placed at the top of the foot behind the ankle. The Gastrocnemius is a two-joint muscle; therefore, the other attachment point was placed on the backside of the Femur near the bottom. Finally, the attachment points for the Tibialis Anterior were placed at the top of the foot near the front of the ankle and on the front of the Tibia near the top.

The Hydro Muscles consist of natural latex rubber tubing encompassed by a sheathing made of nylon hydraulic sleeving. These are then super glued and clamped onto brass barbed to threaded plumbing components, completing the muscle. A threaded 1/2 inch PVC tee is attached to the upper part of the muscle, a barbed to threaded nylon adapter is connected to the side of the tee. Both the bottom of muscle and the top of the tee are connected to a brass garboard drain plug with loop. In some muscles the drain plug is directly connected to the u-bolts of the structure, while in others 1/8 inch steel cable is swaged between the plug and u-bolt to allow the proper length.

**Figure 26: Hydro Muscle based muscle fibers; from left to right the fibers are the Tibialis Anterior, the Gastrocnemius, and the Soleus**

There are eight Hydro Muscles; two for the Gastrocnemius, three for the Soleus, and three for the Tibialis Anterior. Examples of each type are shown in Figure 26. The dimensions of the muscles were designed to recreate the range of motion of the ankle and knee joints as well as being able to produce 40% of the maximum force of an average adult [25], with a maximum pressure less than 0.47 *MPa*. The maximum pressure of 0.47 *MPa* allowed the Hydro Muscles to achieve the forces desired, while maintaining a reasonable size and did not require the use of more specialized and expensive components. Based on resting lengths of 0.076 *m*, 0.024 *m*, and 0.023 *m*, with full elongation lengths of 0.19 *m*, 0.083 *m*, and 0.053 *m* for the Gastrocnemius, Soleus, and

Tiabialis Anterior muscle fibers respectively, these design metrics and resulting muscle dimensions and pressures are shown in Table 4.

**Table 4: Muscle Design**

| Muscles | 40% of Maximum Force (N) | Sheathing Diameter (m) | # of Hydro Muscles | Maximum Pressure (MPa) | Rubber Tubing Inside Diameter (inches) | Rubber Tubing Outside Diameter (inches) | Rubber Tubing Length (m) | Sheathing Length (m) |
|---|---|---|---|---|---|---|---|---|
| Gastrocnemius | 655.6 | 0.033 | 2 | 0.38 | 0.5 | 0.875 | 0.124 | 0.355 |
| Soleus | 1553.2 | 0.038 | 3 | 0.47 | 0.75 | 1.125 | 0.071 | 0.135 |
| Tibialis Anterior | 94.1 | 0.011 | 3 | 0.34 | 0.25 | 0.375 | 0.063 | 0.072 |

The control hardware consists of an entrance and exit solenoid (0 - 145 *PSI*, normally closed, EHCOTECH B21 V - 1/2-CC-12 *V*DC) for each Hydro Muscle. These valves have an opening delay of 60 - 80 *ms* and unfortunately a closing delay of approximately 1 *s*. They are powered by a switching power supply (12 *V* 20A SUPERNIGHT 6473493) and controlled by a microcontroller (Arduino MEGA 2560), connected to a basic MOSFET (IRF520) solenoid control circuit. In addition, there is a pump (6-roller Delavan 6900C-R) which is driven by a motor (BLDC 1000W 60V 3000RPM UUMotor). This motor is powered by a Variable Power Supply (60 V 30 A) that requires a step-up transformer, and the motor speed is controlled by the microcontroller. The valves are connected to the Hydro Muscle with braided nylon tubing. The exit paths are joined together from all of the muscles by a series of tubing and wye connectors, and the same is done for the entrance paths. The combined exit path flows into an open container that is used as a water reservoir. The combined entrance path is then connected to a series of three brass tees. The first tee has a water hammer arrestor on its side tee, the second has a digital pressure sensor (G1/4 inch 5 *V* 0-1.2 *MPa* Pressure Transducer Sensor Oil Fuel Diesel Gas Water Air DIGITEN PS-12) on its side tee, and the final tee

has a pressure relief valve on its side tee which then connects to the water reservoir through nylon tubing to control the maximum system pressure by allowing a path for excess flow. These tees are connected to each other and to the roller pump. The entrance to the pump is connected to the water reservoir. All male threaded pipe connections are wrapped in thread seal tape, all fasteners are secured with thread lock, and all barbed connections are clamped to nylon tubing with hose clamps.

(a) Linear Sensor Components (b) Assembled Linear Sensor

**Figure 27: Details of linear sensor**

The data collection hardware consists of the previously mentioned pressure sensor and the microcontroller as well as a three turn 10k potentiometer connected to the ankle joint. Three linear sensors were created with one connected to a muscle from each of the three muscle groups. The linear sensor consists of the same three turn linear potentiometer connected to the functional inner parts of a retractable key chain and then mounted to the PVC tee of the Hydro Muscle using two 3D printed plastic parts as shown in Figure 27.

### 4.4 Experiments and Results

#### 4.4.1 Maximum Force Test

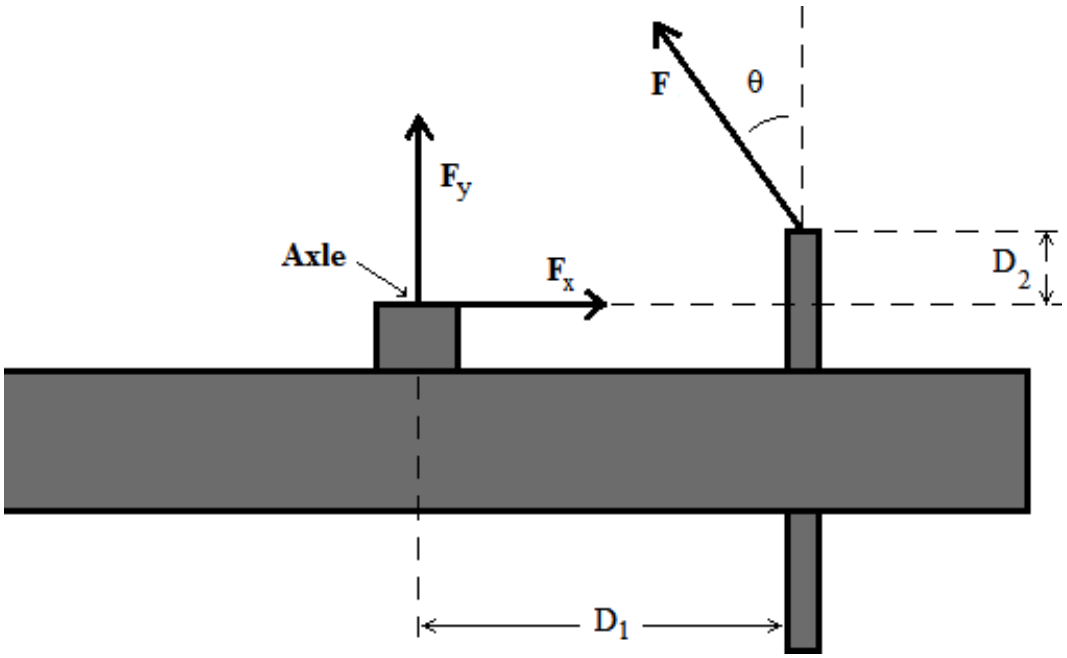


**Figure 28: Full Force Test Ankle Geometry**

In order to verify the design goal of producing 40% of the maximum force capable by an average male, a full force test was conducted on the maximum force attainable by a single Gastrocnemius muscle fiber as well as a single Soleus muscle fiber. The 40% threshold was chosen, in part, because it would produce the necessary torque per kg, 1.5 *Nm/kg*, for walking [94]. Using the test setup from the viscoelastic model tests, a single Hydro Muscle was fully elongated. A plate was then attached to the setup, which could restrict the movement of the muscle when pressure is released, with the force sensor resting against it. The muscles were then depressurized. In the depressurized state, the plate prevents the muscle from contracting and shrinking in length, causing the muscle to

exert its full force against the plate. For the Gastrocnemius muscle, the maximum force $F_g$ recorded was 307 N against a desired of 327 N, and for the Soleus muscle $F_s$ was 356 N against a target of 516 N. To calculate the torque, ($\tau$), applied by the extended muscles on the ankle joint, shown in Figure 28, the maximum forces of each muscle fiber were added together in

$$F = (3F_s) + (2F_g), \tag{10}$$

resulting in F = 1682 N. Which is then substituted in Eq. 11, with the horizontal distance between the axle and F is $D_1$ = 0.065 *m*, the vertical distance between the axle and the muscle attachment point is $D_2$ = 0.015 *m*, and $\theta = 0\, rad$. The calculation of

$$\tau = F(D_1 cos\theta + D_2 sin\theta) \tag{11}$$

results in a torque of 109 Nm. Because average adult has a mass of 62.0 *kg* [95], if the ankle was used as a prosthesis,

$$\tau/kg = \tau/m_{Avg} \tag{12}$$

would produce approximately 1.76 Nm/kg which is above the 1.5 Nm/kg threshold needed for walking [94].

### 4.4.2 Variable Stiffness

The ankle was tested under all rear muscle recruitment combinations to show the ability to vary the rotational stiffness of the ankle using the selective recruitment capabilities of the multi-fiber design. A weight of 9.1 kg (20 lbs) was hung on the back of

the ankle while only one or both Gastrocnemius muscles were recruited. 18.1 kg (40 lbs) was used for all other recruitment configurations. Muscle fibers were disengaged by elongating them more than the other fibers. The rotation of the ankle when the muscles were stretched by the added weight was measured with the aforementioned potentiometer rotational sensor in order to calculate the stiffness of the muscles when engaged. Each experiment started with the ankle fully in plantarflexion.

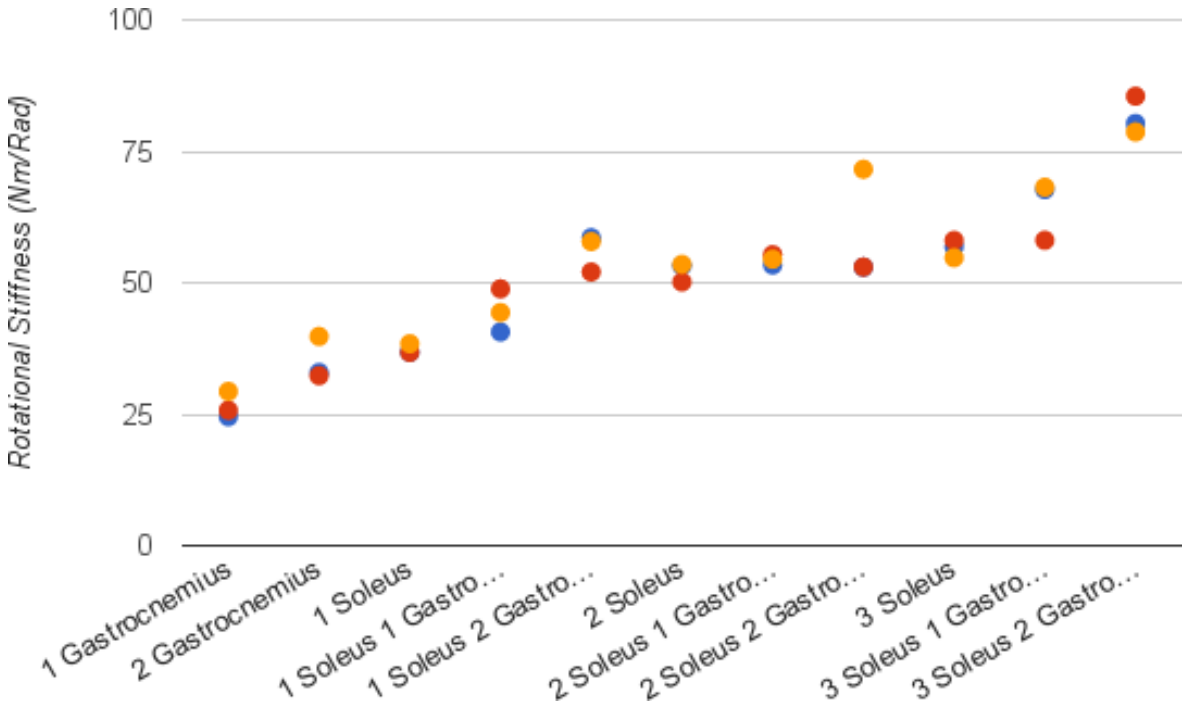


**Figure 29: Rotational Stiffness Results**

Eq. 13 is used to calculate the rotational stiffness of the ankle in its various recruitment combinations. While the weight was attached the ankle position, $\theta$, was used to calculate the normal force on the ankle. That force, (F), was multiplied by the distance, (d), of the weight attachment point from the ankle and then divided by the change in

rotation of the ankle joint, $\Delta\theta$. Figure 29 shows that selective recruitment of the muscles alters the joint stiffness, allowing the ankle to achieve the variable stiffness in a manner similar to recruitment in the muscles of humans. Three experiments were conducted for each configuration. The Rotational Stiffness, (k), calculated from

$$k = \frac{F\cos(\theta)d}{\Delta\theta} \tag{13}$$

ranged from about 25 Nm/rad when only one Gastrocnemius fiber was recruited to about 85 Nm/rad when all five fibers were recruited.

### 4.4.3 Position Control

In this section, the controllability of the ankle is tested, and the results are presented. The ankle is actuated by multiple muscle fibers and the length of each fiber determines the position of the ankle. The length of each of these muscle fibers changes depending upon the state of the entry and exit valves. If the entry valve is opened and the exit valve closed, the muscles extend causing dorsiflexion of the ankle, whereas if the entry valve is closed and exit valve opened, it produces a plantarflexion. Hence, the duration for which the entry or exit valves are to be kept open is determined, which is sufficient for the position control of the ankle.

The solenoid valves open very fast, but close slowly because of their spring mechanism. In addition, they have to compensate for the pressure of the system which further slows down the closing. These delays have a significant impact on the

controllability of the ankle and conventional methods such as PD control or pulse width modulation of the valves are rendered useless. Hence, an unconventional methodology that uses regression to calculate the duration for which the valves should be kept open is used.

The duration for which the valves are to be kept open (entry or exit depending on the direction of movement) is considered to be a function of the starting current state of the ankle and the target position. To determine this function, data was collected by running a number of experiments sampling various starting positions and times. An important point to be noted here, for the constant motor speed and source pressure implemented, the muscles contract faster than they expand. This is because of the slow closing of the exit valves and the high pressure created inside an extended muscle fiber. Hence, a different regression model for the two directions is needed. The regression analysis resulted in the equations,

$$\begin{aligned} T_{entry} = &- 0.081\theta_c^3 + 0.18\theta_t^3 + 0.16\theta_c^2\theta_t \\ &-0.27\theta_t^2\theta_c - 2.09\theta_c^2 + 0.44\theta_t^2 \\ &+1.77\theta_t\theta_c - 28.71\theta_c + 37.16\theta_t \\ &+48.75 \end{aligned} \tag{14}$$

and

$$T_{exit} = 3.34\theta_c - 3.98\theta_t + 45.64, \tag{15}$$

where $T_{entry}$ is the duration the entry valves have to be kept open for during dorsiflexion from the starting current position $\theta_c$ to target position $\theta_t$, and $T_{exit}$ is the same but during plantarflexion.

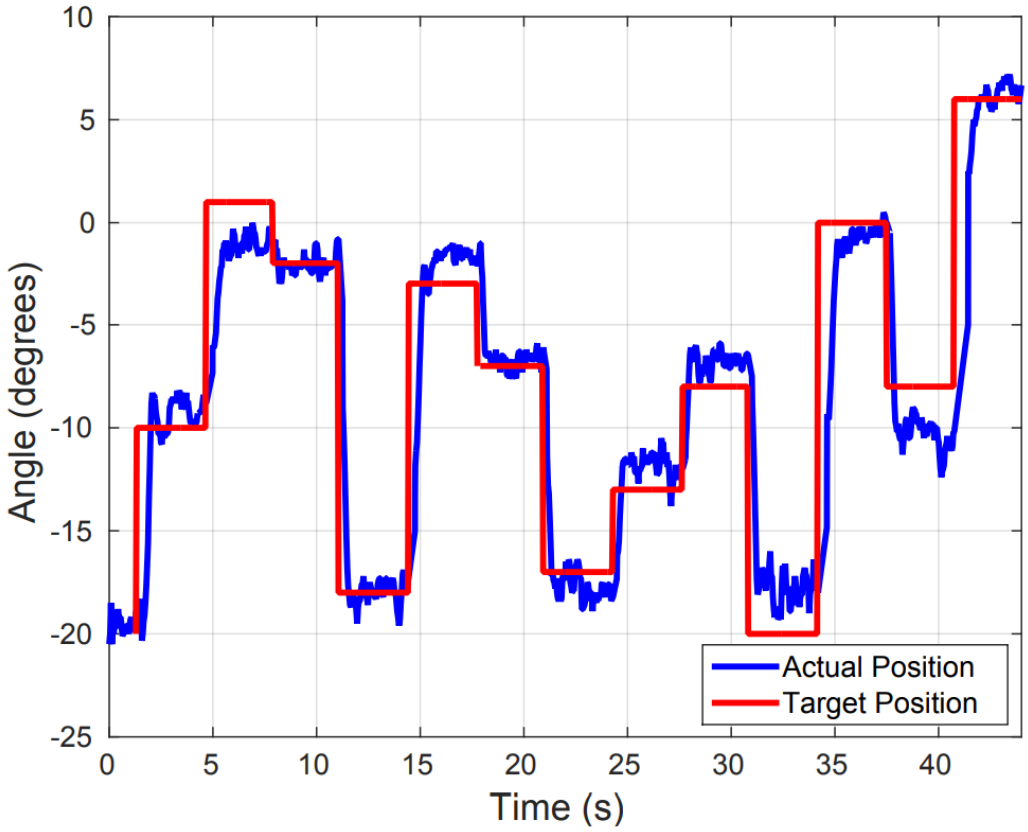


**Figure 30: Results of the position control experiment showing the target positions and the actual positions**

The regressions for the two directions resulted in a cubic equation for dorsiflexion and in a linear equation for plantarflexion and the result of the position control test using these is shown in Figure 30. The graph shows the different target points selected for both the directions and the algorithm achieving those targets within acceptable precision when compared with human ankle precision [95]. The position displayed is a running average of the five most recent sensor readings. It can be seen from the graphs that the time taken for roughly the same amount of angle is different while moving in different directions and is also dependent on the starting position.

### 4.4.4 Variable Force Using Multi-Fiber Hydro Muscle

The human ankle is capable of delivering varied force at a given position. Here, it is shown that the multi-fiber Hydro Muscles can mimic this variation of force. The actuation of each fiber provides differing forces delivered through the ankle. While the maximum force delivered at the toe is coupled to the position, the force can range in value for a particular position utilizing multi-fiber actuation.

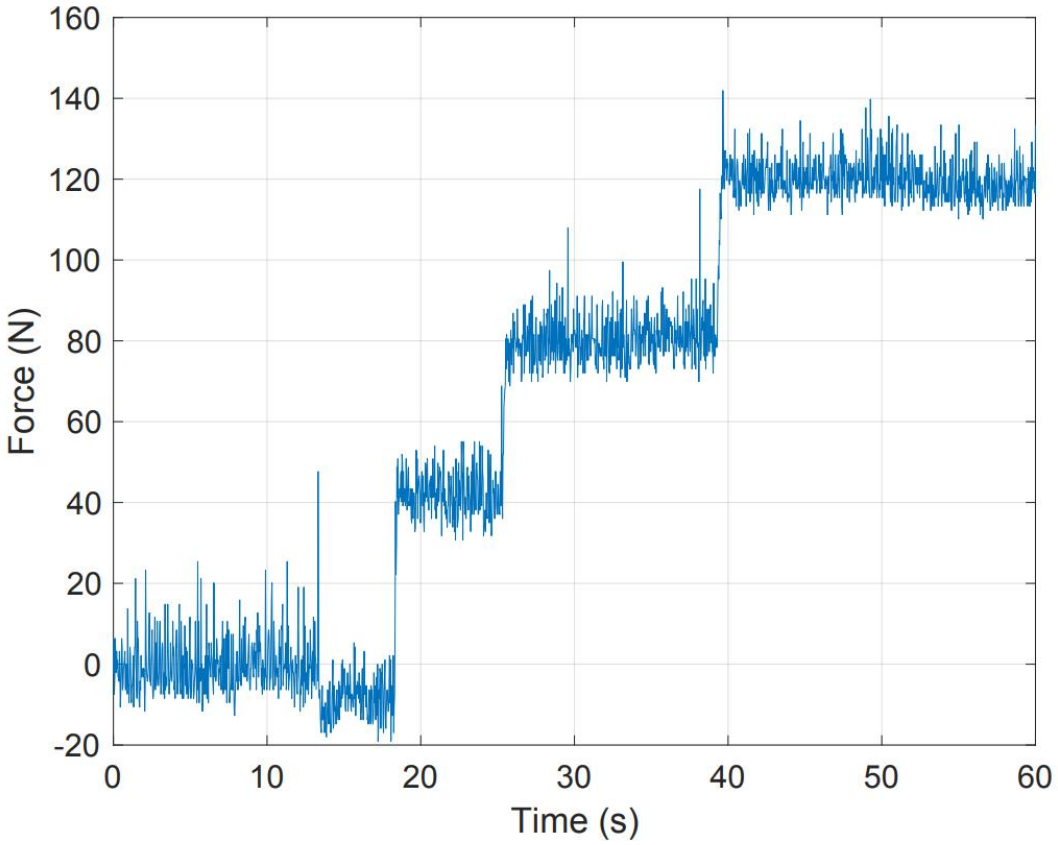


**Figure 31: Modular Force Results**

In the test performed, the foot was made to come in contact with a wedge and register the force on a force sensor. The wedge was placed such that the ankle was in plantarflexion of 15° when the foot made contact with the sensor. The force registered

was 40 N as the foot hit the wedge. Next, the Gastrocnemius fibers were deflated, increasing the force to 80 N. Then, the Soleus fibers were similarly deflated, and the force readings increased to 120 N. This verifies that the independent multi-fiber actuation of the same degree of freedom can vary the forces delivered at a given position. Figure 31 shows the results of this experiment, with noise from the sensor.

### 4.5 Discussion and Future Work

The current system is still too bulky and has too large of delays to be used for locomotion. Several developments, including smaller efficient valves need to be completed to realize efficient locomotion tasks. A model for the viscoelastic hydro muscle was presented, which can be further advanced by using a COMSOL like simulation software. A further study modeling the biomechanics of ligaments, bones, etc. should be carried out to gain a better understanding of the potential of a multi-fiber muscle approach.

The current approach of using multiple Hydro Muscles to actuate the same single degree of freedom joint is similar to how our body recruits different muscle fibers for different tasks. The multi-fiber Hydro Muscles were successfully demonstrated to provide variable stiffness. This variation was achieved by altering the level of engagement or disengagement of each of the muscle fiber. Moreover, a peak stiffness of approximately 85 Nm/rad was achieved, which is comparable to the requirements of human walking [97]. In addition, the full force tests show the system is robust enough to withstand an average adult walking. Moreover, position control tests conclude that this system, despite

its complexities can be controlled using only on/off electrical signals. Furthermore, it can deliver various forces for the same position of the ankle replicating the selective recruitment in human muscles. Moreover, these actuators are relatively inexpensive. Hence, overall, it seems to be the ideal candidate to be incorporated in leg prosthesis and in fact all legged robots.

# CHAPTER 5

# HYDRO MUSCLE VARIABLE STIFFNESS 2DOF LEG DESIGN FOR SOFT LANDING IN LOW GRAVITY ENVIRONMENT

This chapter explores further research into the multi-fiber approach to implementing Hydro Muscles. The ability to create different and time varying stiffnesses is explored with a testing apparatus that simulates a low gravity environment. A novel, low cost, and small hydraulic servo pump is developed to provide fine control of the individual muscles.

## 5.1 Novel Servo Pump Design

After dozens of iterations, a working servo pump was created. The servo pump consists of the fingertip of a rubber glove which has been superglued to a 1/8 inch NPT nut as seen in Figure 32. That piece is then glued into one end of a fabric tube which has been hand sewn to the proper geometry for the valve. The other side of the tube is plugged by a 3d printed plastic piece. This can also be seen in Figure 32.

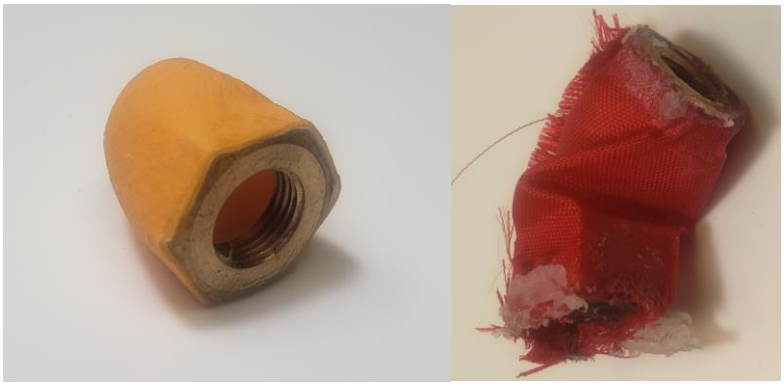

**Figure 32: Rubber Reservoir Left) without sleeve Right) with sleeve**

The plastic end of the reservoir is attached to a 3D printed paddle which is attached to the gear of the servo. The other end is attached to the nonmoving 3D printed part, the wall, that is attached to the housing of the servo. A quick connect tube tee adaptor is screwed into the nut from the other side of the wall. All 3D printed parts have been coated with steel reinforced epoxy to help them handle the forces and pressures involved. The paddle, the servo, and the wall can all be seen in Figure 33.


**Figure 33: Paddle, Servo, and Wall (from left to right)**

The plastic end of the sleeve is attached to the paddle with screws and the paddle is attached to servos horns on top and bottom for additional strength. A bolt is put through a bearing which has been set in the top of the wall then it goes through the paddle coming out the bottom of the servo horn. This assembly can be seen in Figure 34, and the assembly with the quick connect and servo can be seen in Figure 35.

**Figure 34: Paddle Wall Assembly**

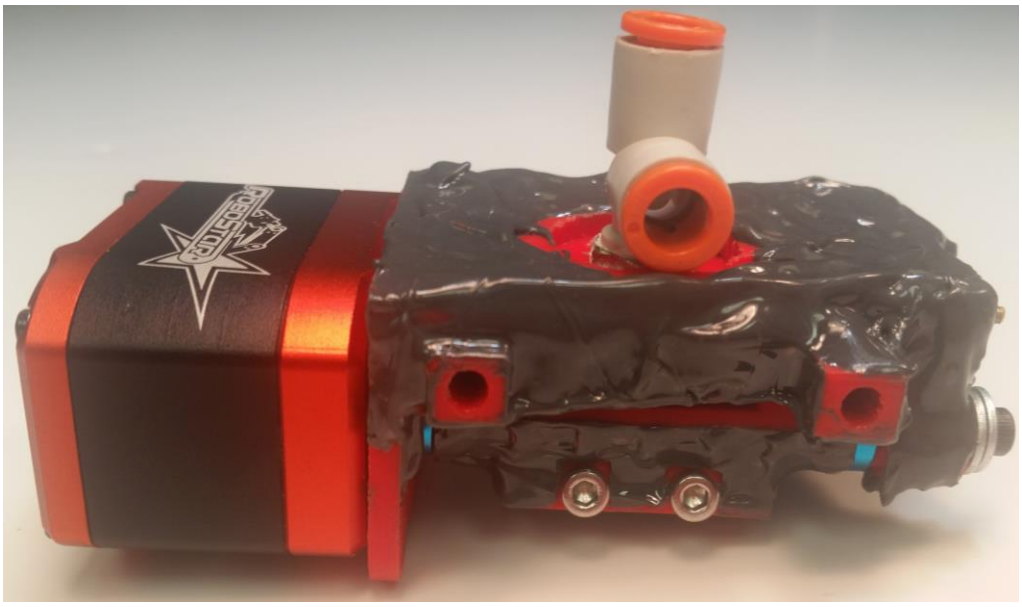

**Figure 35: Assembled Pump**

In Figure 36 you can see a CAD (computer aided design) image of the servo pump. It has the Hydro Muscle attached but is missing the rubber reservoir and sleeve. The servo controls the blue servo horns, causing the pump to swing open and closed like a door.

You can see the pump in the open and closed positions in Figure 37. When the reservoir is attached, the closing motion squeezes the water into the Hydro Muscle, causing it to expand. When the servo is reversed, there is then room in the reservoir for the water, and the muscle squeezes the water back into the reservoir while decreasing in length.

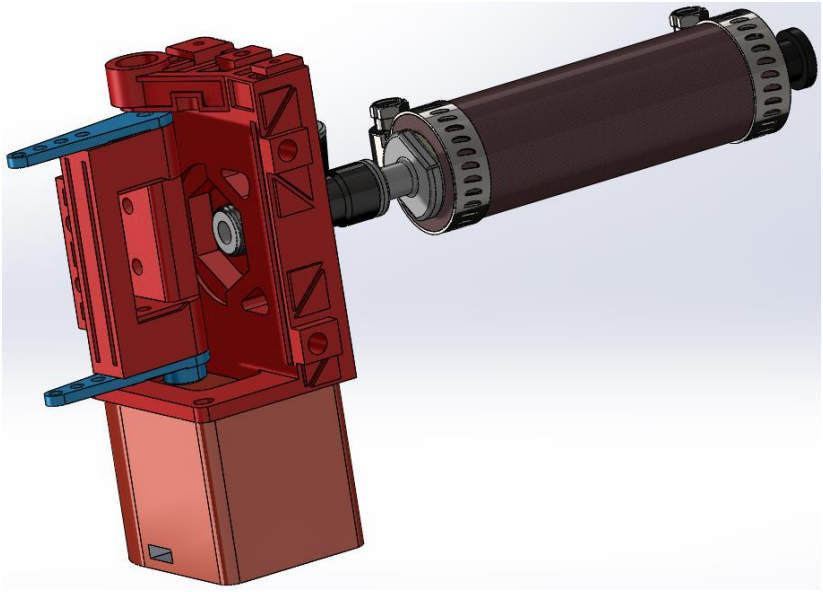

**Figure 36: CAD of Servo Pump with Hydro Muscle Attached**

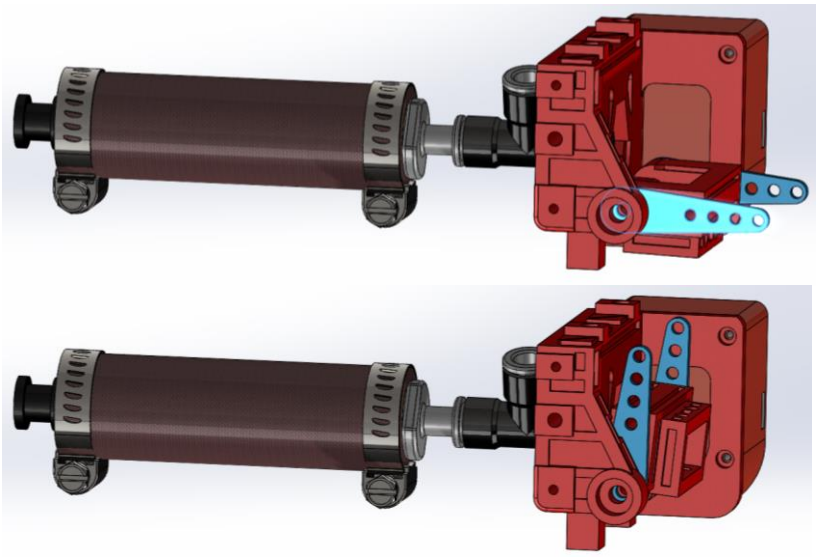

**Figure 37: Servo Pump: Top) Open Bottom) Closed**

## 5.2 Leg Design

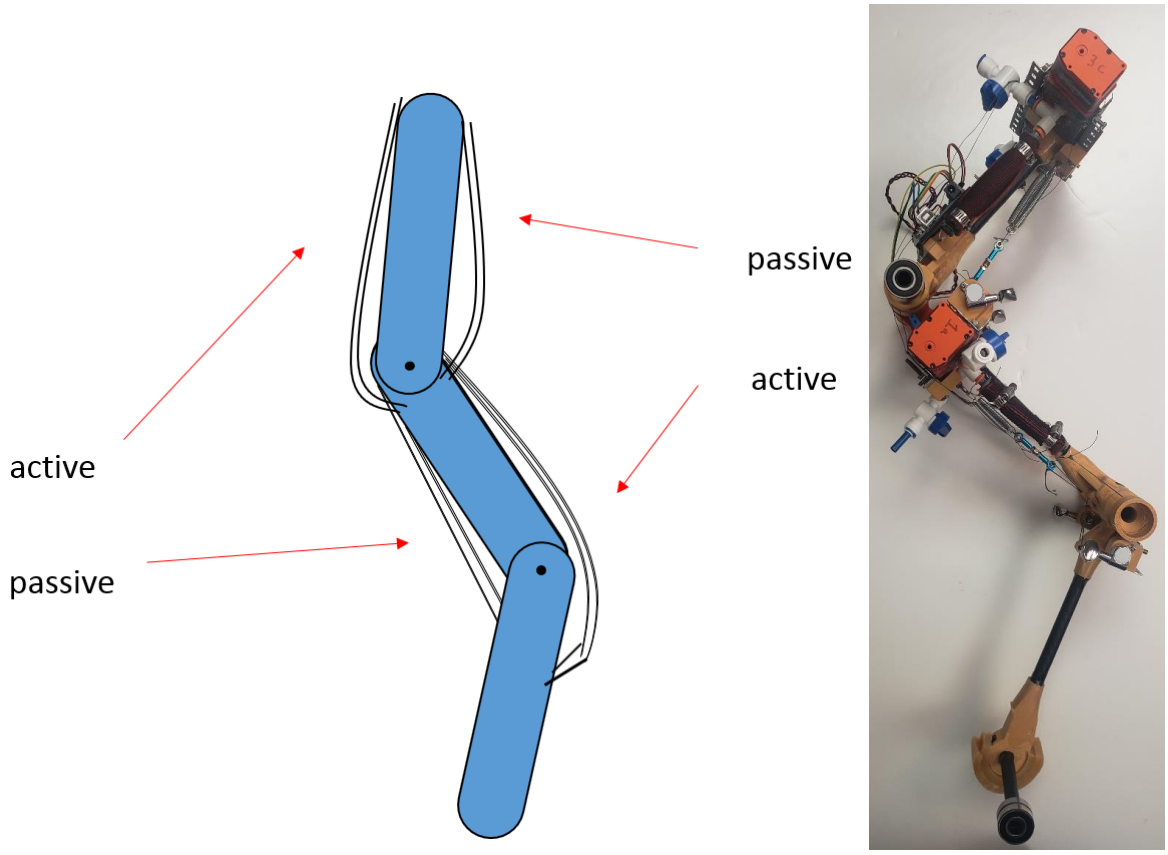


**Figure 38: Leg: Left) Simple Design Right) Final Construction**

The leg was designed to be have two planar degrees of freedom with one side of hip and knee active while the other side is passive. This can be seen in where it shows both the simplistic model of the leg and the final version. It was designed to attach to a testbed at both the foot and the hip. Both attachment points can rotate freely. The “foot” is a rounded end to the lower leg with a Latex outer layer. This can be seen in Figure 39.

**Figure 39: Lower Leg and Foot with Test Bed Attachment**

The leg is made of PLA 3D printed parts and carbon fiber tubes. The carbon fiber tubes are used for both connecting the printed parts and for the rotational joints. There are bearings inside the hip and knee as well as where the foot and hip attach to the testbed. The servo pumps are attached to a metal scaffolding, seen in Figure 40, that is attached just below the hip and at the top of a waste section. The Hydro Muscle is attached to the servo pumps on one end and then a string is attached to the other end, guided over the joint below it and then attach to a guitar tuning peg for tuning/tensioning. Springs are attached opposite to the Hydro Muscles in the antagonistic position because

actuated rotation in that direction was determined to be unneeded for these experiments. The partially assembled leg can be seen in Figure 41.

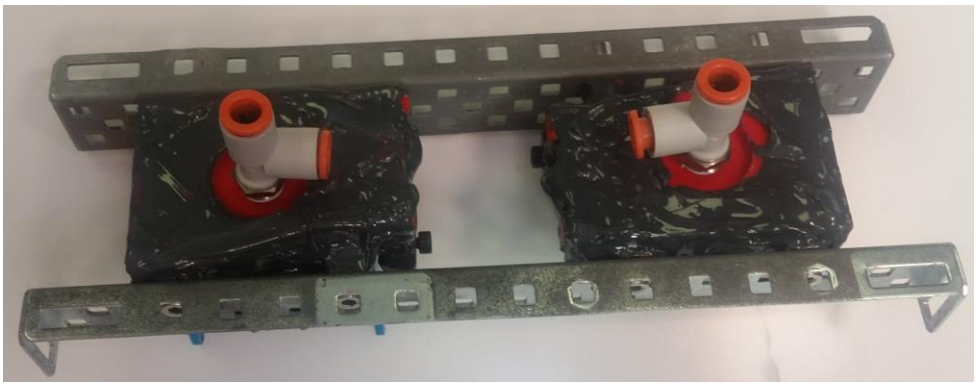

**Figure 40: Servo Pump Scaffolding Assembly**

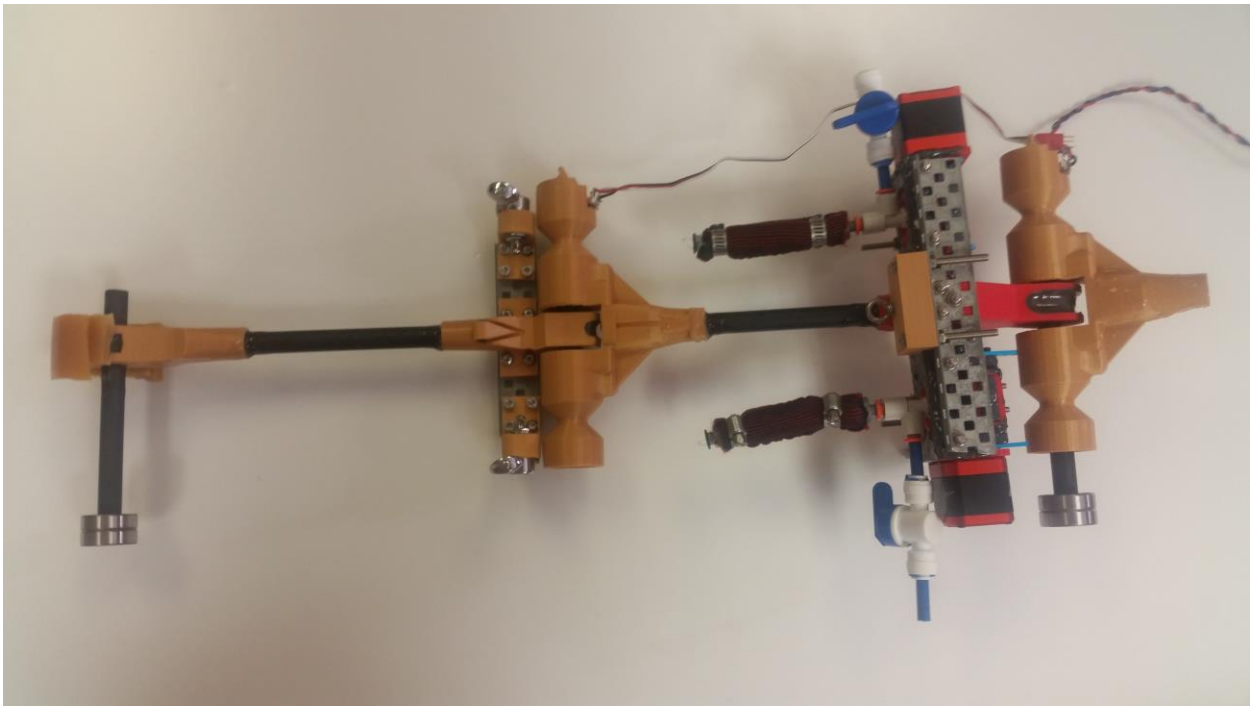

**Figure 41: Partial Leg Assembly**

The leg has an Arduino Uno, two Potentiometers (one for the knee and one for the hip), it also has an IMU which was not used for this series of experiments. The hip section

with attached electronics can be seen in Figure 42. While the fully assembled leg on the testbed can be seen in Figure 43.

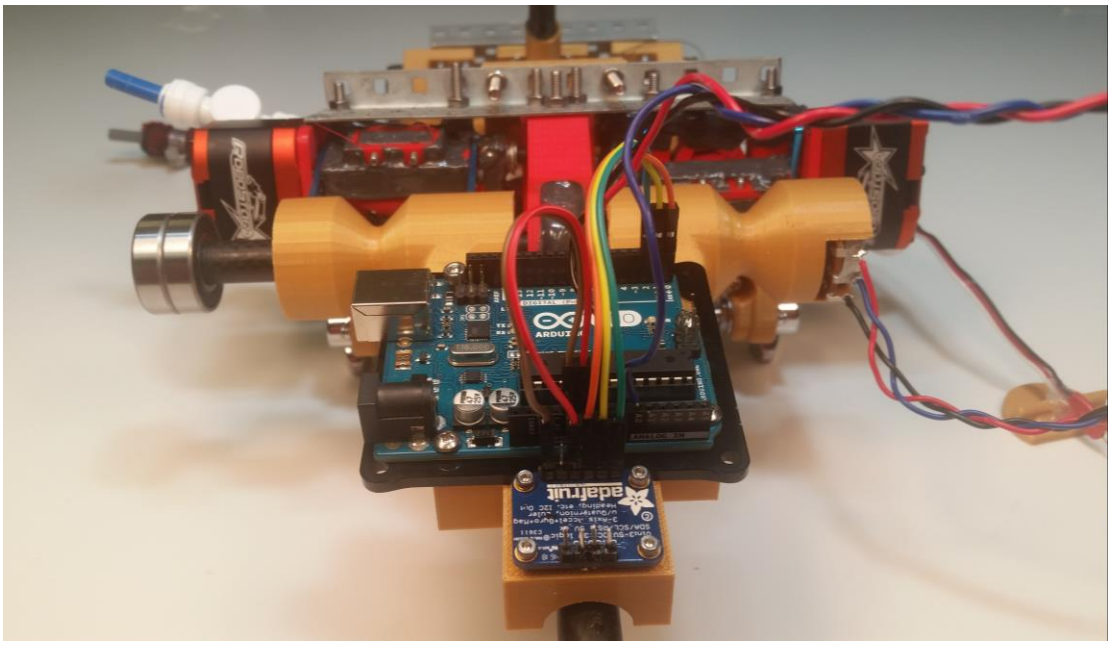

**Figure 42: Electronics**

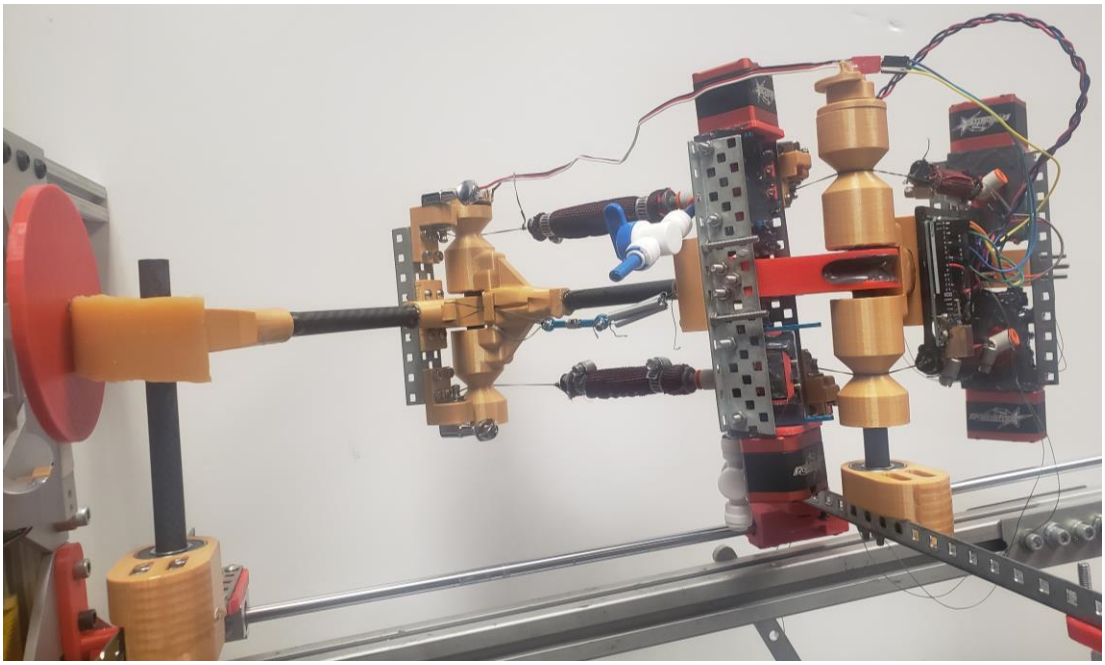

**Figure 43: Assembled Leg**

### 5.3 Testing Platform Design

The Testbed seen in Figure 44 is mainly made of 80/20 with two linear rails and two crossbeam sliders that attach to the foot and hip of the leg. The angle of the rails can be adjusted. The force is measured by a load cell with a red circular plate which can be seen on the left in Figure 44. This sensor is attached to an Arduino Uno which has a shield for high speed analog data logging. This allows the Arduino to take a force reading every 0.2 ms.

**Figure 44: Testbed**

### 5.4 Experiments and Results

I tested the rotational stiffness of the knee and the rotational stiffness of the hip. While they have the same geometry and Hydro Muscle dimensions the hip results were approximately six times greater than the knee results. This is because for the knee I tested the rotational stiffness with only the Hydro Muscles attached and not the antagonistic

springs, while with the hip I had the springs attached as seen in Figure 45. The knee measurements give a simple rotational stiffness that is due to the elasticity of the latex when there is no antagonistic engagement. However, the hip number is much greater because the increase in load on the joint caused a rotation that decreased the length of the antagonistic spring which reduced the internal torque. Basically, an increase in external torque on a passive antagonistic joint causes a decrease in the internal torque. You can see this relationship in the measured stiffnesses for the given cases which is shown in Table 5.

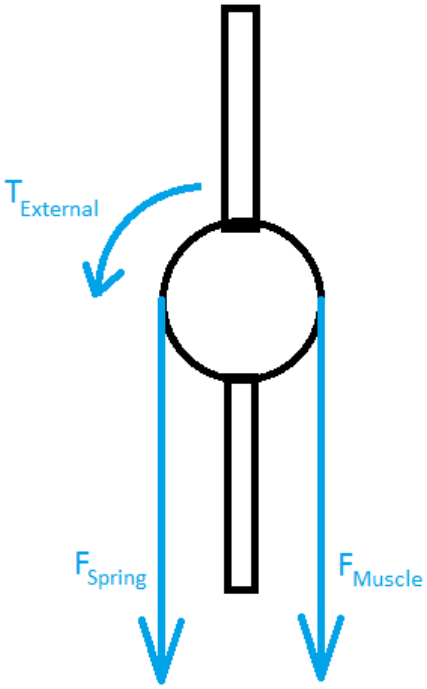


**Figure 45: Joint Stiffness**

**Table 5: Joint Rotational Stiffness (N•m/rad)**

| Uncoupled | | | Coupled | | |
|---|---|---|---|---|---|
| Knee A | Knee B | Knee Both | Hip C | Hip D | Hip Both |
| 0.36 | 0.37 | 0.79 | 2.42 | 2.12 | 4.15 |

This result shows that you could alter the stiffness of a joint in a given direction by engaging and disengaging Hydro Muscles on both sides of the joint, which would allow for more combinations of engagement, resulting in a greater variety of stiffness values.

The test bed was set to an angle of 12° which translates to a gravity of about 0.208 that of Earth. Additionally, there is some friction even with lubricated linear rails and linear bearings, which causes a slight reduction in acceleration during drop tests. The leg was raised so that the foot was 25 cm above the force plate every experiment. Several different muscle engagements were tested with 3 drops each. While all are shown below, I focused on four representative cases, no muscles engaged, all muscles engaged, one hip and one knee muscle engaged, and the case where varying stiffness is implemented. Here, one hip and one knee muscle are engaged at the beginning of contact and the other two muscles start to engage during contact. This causes a varying stiffness during the landing. The outcome of varying stiffness was a much better landing than the other configurations.

As seen in Figure 46, the drops with no muscles engaged had a spike of around 60 N when the foot made initial contact with the ground, then almost immediately it had a large spike of almost 100 N when the upper leg collapsed into the bottom, This caused it

to bounce up and had subsequently smaller events. Also, these bounces lasted well over a second before coming to an oscillating rest.

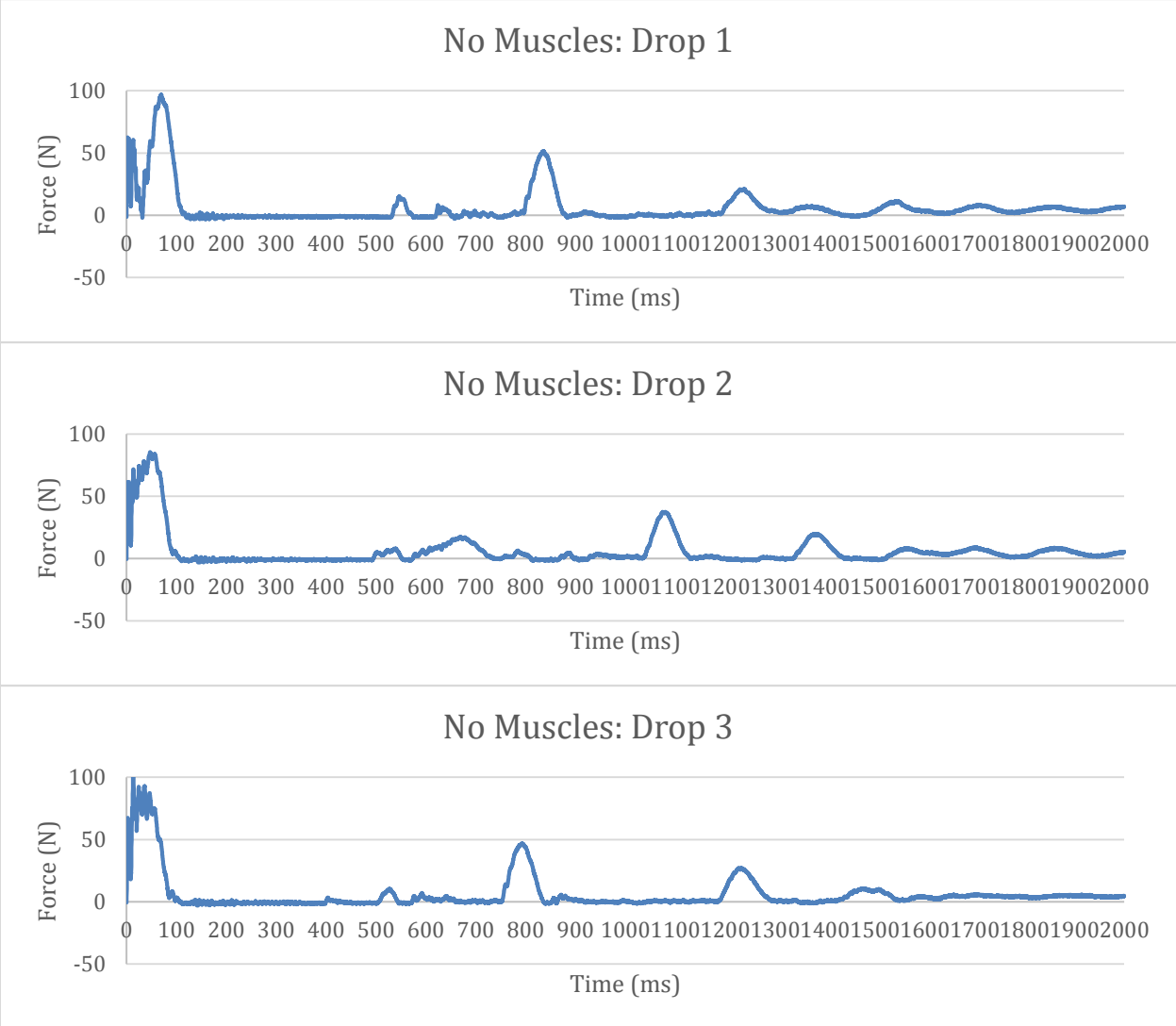


**Figure 46: No Muscles Engaged**

The one hip one knee engaged configuration also lasts more than a second. However, the large spike from the upper leg collapsing is both delayed by almost 100 ms and lessoned to only about 90 N as seen in Figure 47.

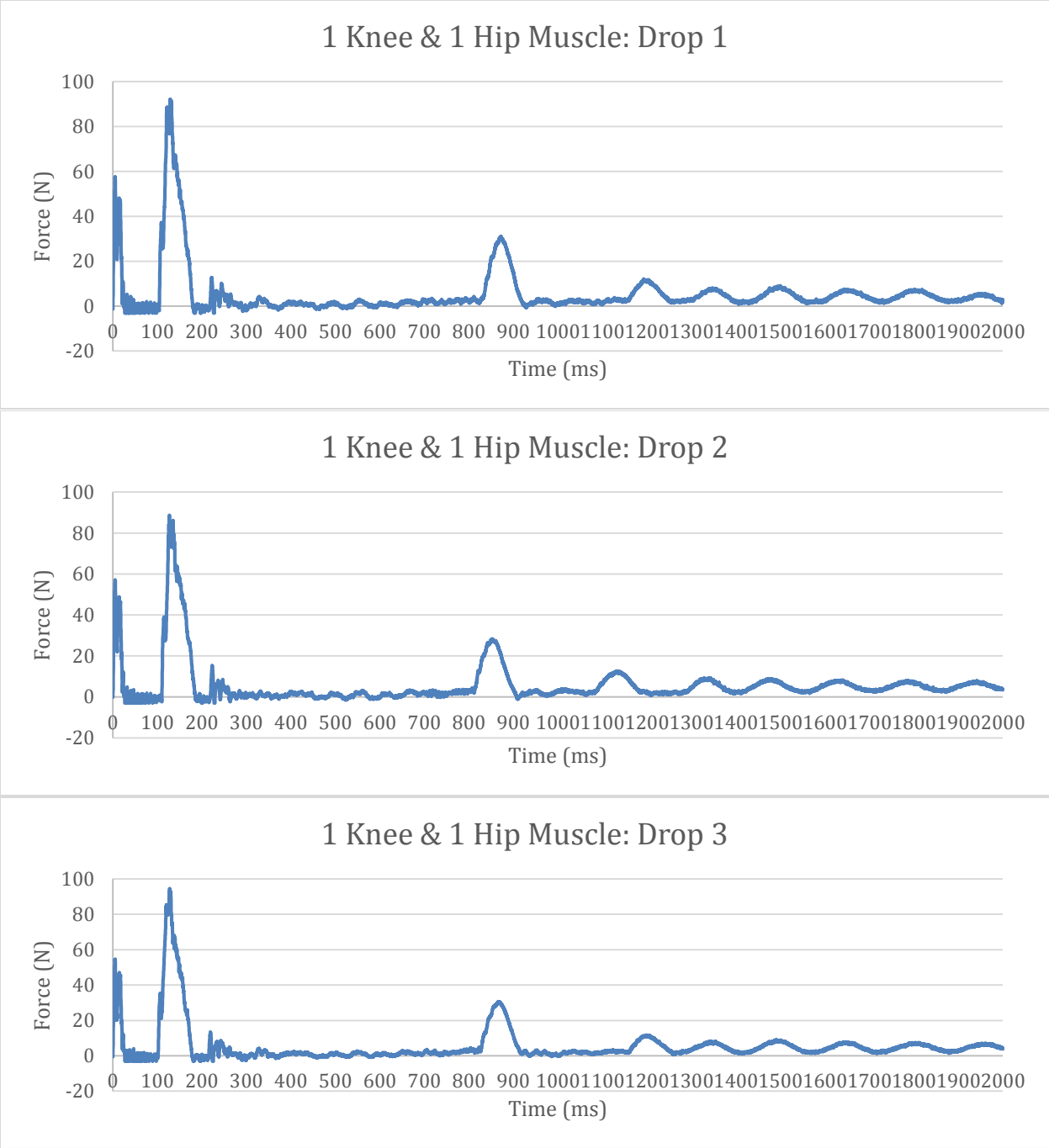


**Figure 47: 1 Knee and 1 Hip Engaged**

As you can see in Figure 48, having all four muscles engaged improved the landing quite a bit as the initial impact was still around 60 N, but the secondary impact from the

upper leg collapsing was spread out over two smaller spikes with a peak value just over 80 N. Additionally, the impact had no other major bounces and it was finished moving in less than 0.5 s.

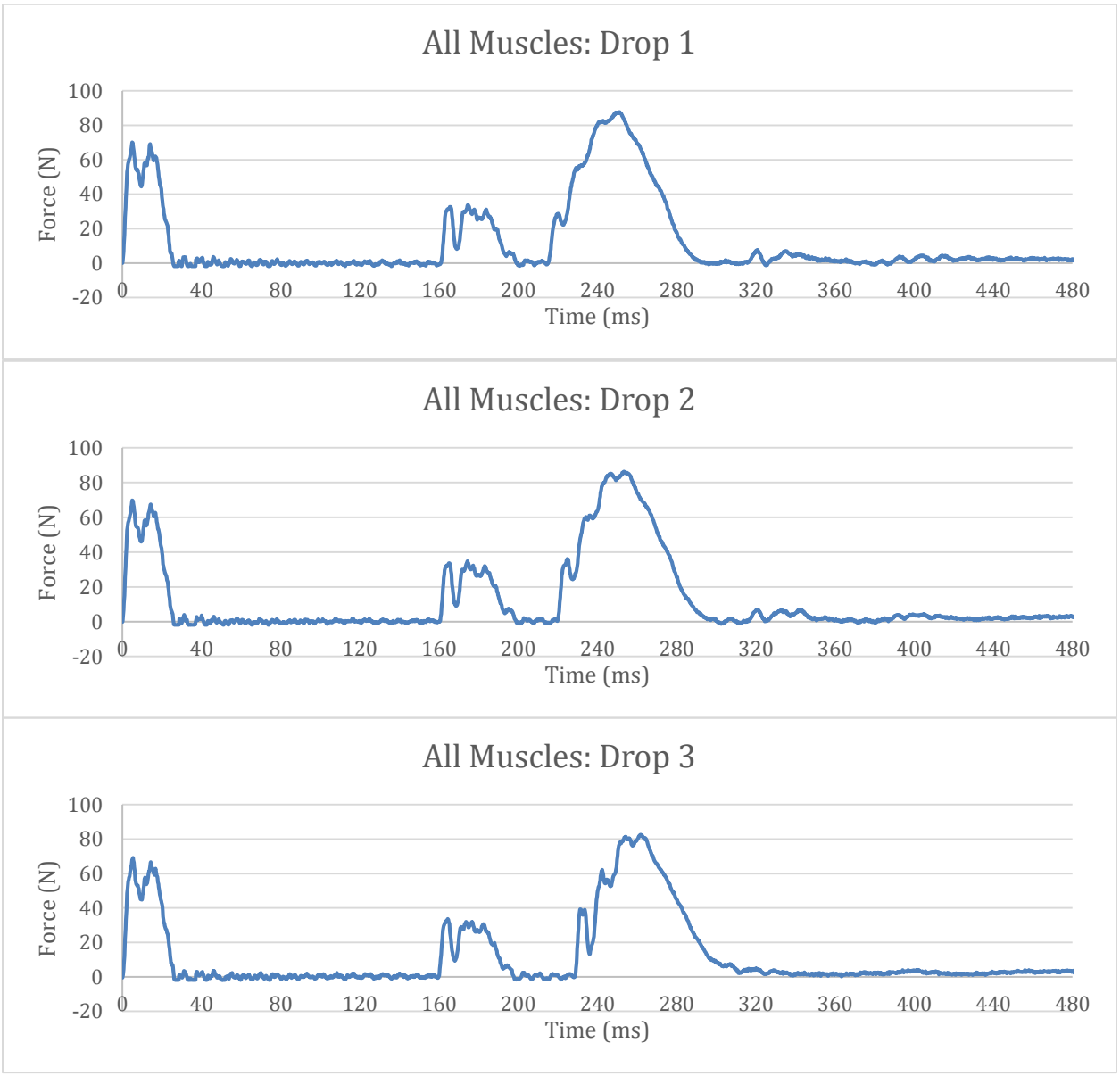


**Figure 48: All Muscles Engaged**

By far the best results were for the drops where the stiffness increased during the impact. As you can see in Figure 49, the initial impact from the foot was the same as previous scenarios with a peak of around 60 N. It also came to a rest in less than 0.5 s, but the spikes after the initial impact were all smaller. This is expected because the work discussed in section 1.2.4 showed that not only is there an ideal stiffness for landing this stiffness should change over time.

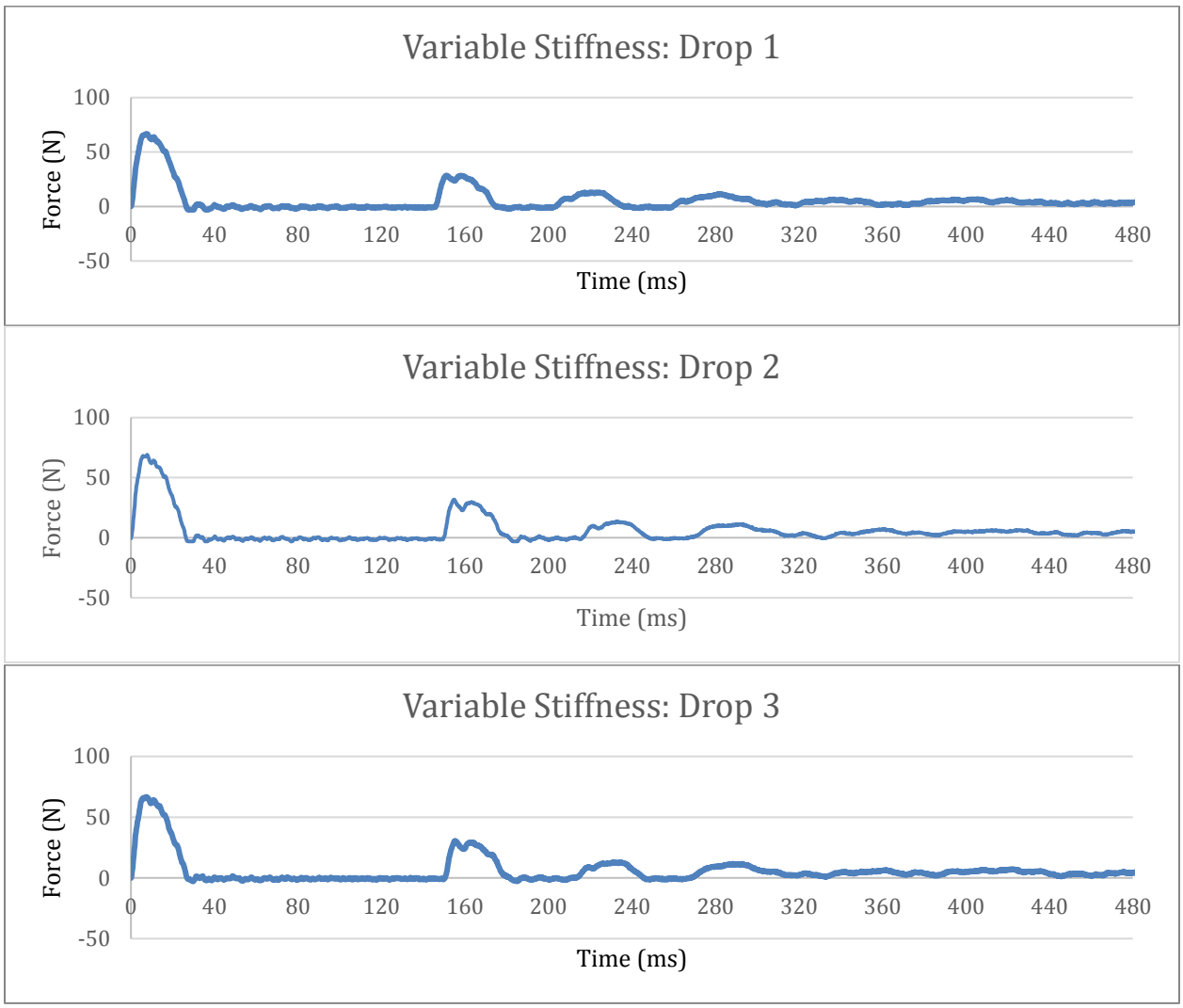


**Figure 49: Variable Stiffness**

The other engagement configurations had similar results to the previous cases. They can be seen in Figure 50 and Figure 51.

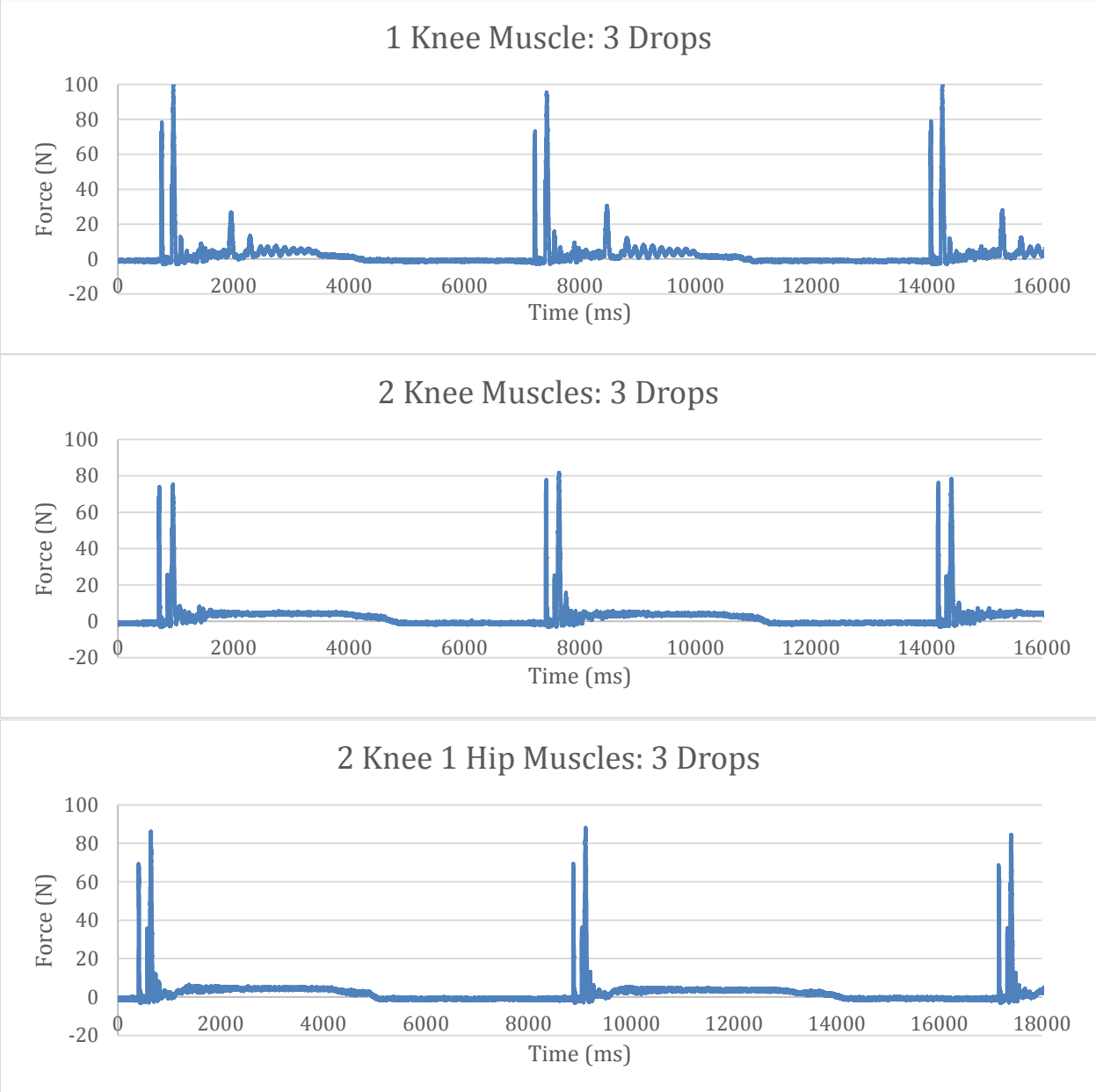


**Figure 50: Various Drop Configurations Part 1**

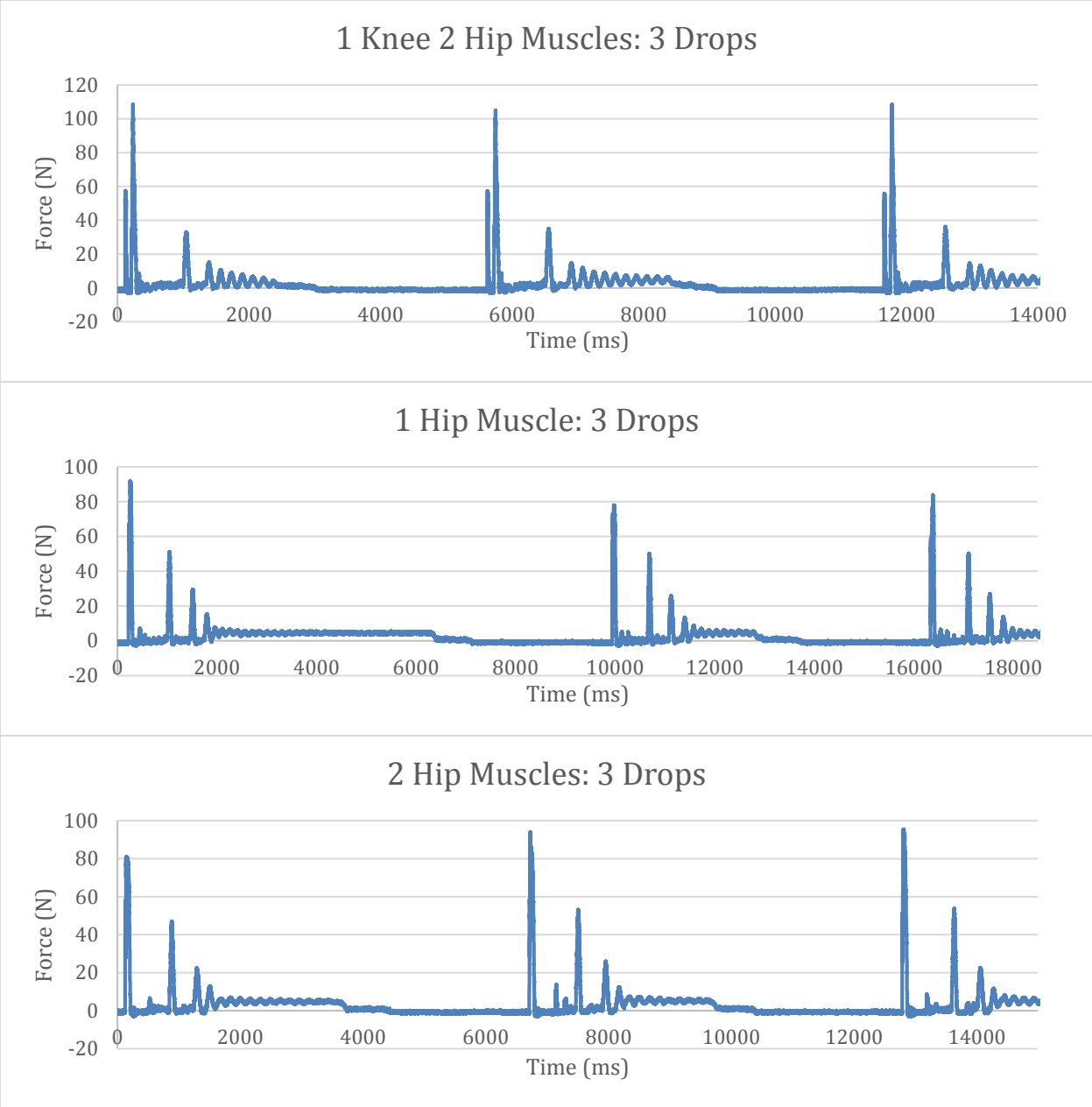


**Figure 51: Various Drop Configurations Part 2**

### 5.5 Discussions and Future Work

The leg is capable of providing a softer landing by actively altering the engagement of different Hydro Muscles during landing. The compact lightweight servo pumps were able to actuate each muscle and while the results were promising there is much more that can be done. Unfortunately, time and low-quality servos did not allow us to explore this further and develop the ideal landing control. Further work modeling this ideal stiffness profile and developing a control method with improved servos would be the next step in this research. The servos could be greatly improved to allow for higher speed operation and more complex actuation profiles. Also, the use of controlled antagonistic muscles would allow us to alter the stiffness even better. The ideal stiffness pattern could be explored both mathematically and practically. Many improvements can be made to the servo pump design to make it smaller and lighter.

Earlier work on coupling/decoupling could also be revisited to see if there is a more compact and reliable method to achieve that capability. Because even though the multi-fiber approach allows us to alter our force at various positions, the maximum force is still only achievable when the muscle is fully elongated.

Overall, the Hydro Muscle has proven to be one of the best options for compliant actuation and further research would be of great benefit to the field of robotics.

# REFERENCES


[1] G. McCarthy, D. Effraimidis, B. Jennings, N. Corso, C. D. Onal, and M. B. Popovic (2014). "Hydraulically Actuated Muscle (HAM) Exo-Musculature," in "Robot Makers: The future of digital rapid design and fabrication of robots" (RoMa) Workshop, the 2014 Robotics: Science and Systems Conference (RSS) July 12, 2014 Berkeley,USA. [http://users.wpi.edu/~mpopovic/media/pubs/HAMproceedingSubmitted1.pdf]

[2] D. Effraimidis, B. Jennings, G. McCarthy, N. Corso. "Hydro Artificial Muscle Exo-Musculature," A Major Qualifying Project, Primary Adviser: Marko B. Popovic. Worcester Polytechnic Institute May 1, 2014. [https://www.wpi.edu/Pubs/E-project/Available/E-project-050114-143641/unrestricted/Exo-Musculature_MQP_Report.pdf]

[3] A. Barth, J. Sorrells, S. Ueda, J. Wu. "Hydro Muscle Control System," A Major Qualifying Project, Primary Adviser: Marko B. Popovic. Worcester Polytechnic Institute April 15, 2015. [https://www.wpi.edu/Pubs/E-project/Available/E-project-043015-122552/unrestricted/MQPaper.pdf]

[4] T. Noritsugu, H. Yamamoto, D. Sasaki, M. Takaiwa. "Wearable power assist device for hand grasping using pneumatic artificial rubber muscle," SICE Annual Conference in Sapporo, Avgust 4-6, 2004. pp 420

[5] T. Noritsugu, et al. "Wearable Power Assist Device for Standing up Motion Using Pneumatic Rubber Artificial Muscles," Journal of Robotics and Mechatronics, Vol.19, No.6, pp.6 19-628, 2007.

[6] R. Deimel, O. Brock. "A compliant hand based on a novel pneumatic actuator," 2013 IEEE International Conference on Robotics and Automation, ICRA, 2013, pp. 2047–2053.

[7] K. C. Galloway, P. Polygerinos, C. J. Walsh, and R. J. Wood, "Mechanically programmable bend radius for fiber-reinforced soft actuators," in Advanced Robotics (ICAR), 2013 16th International Conference on, Montevideo, Uruguay, 2013, pp. 1-6.

[8] C. P. Chou, and B. Hannaford (1992). "Measurement and Modeling of McKibben Pneumatic Artificial Muscle," University of Washington, Department of Electrical Engineering, Seattle.

[9] G. K. Klute, J. M. Czerniecki, and B. Hannaford. "McKibben artificial muscles: Pneumatic actuators with biomechanical intelligence," in Proc. IEEE/ASME Int. Conf. Adv. Intell. Mechatron., 1999.

[10] M. B. Popovic. "Biomechanics and Robotics," book 364 pages, Copyright © 2014 Pan Stanford Publishing Pte. Ltd., Singapore, ISBN 978-981-4411-37-0 (Hardcover), 978-981-4411-38-7 (eBook). [www.panstanford.com]

[11] C. P. Chou and B. Hannaford. "Measurement and modeling of McKibben pneumatic artificial muscles," IEEE Trans. Robot. Automat., vol. 12, pp. 90–102, Feb. 1996.]

[12] I. Galiana, F. L. Hammond, R. D. Howe and M. B. Popovic (2012). "Wearable Soft Robotic Device for Post-Stroke Shoulder Rehabilitation: Identifying Misalignments," 2012 IEEE/RSJ International Conference on Intelligent Robots and Systems, October 7-12, 2012. Vilamoura, Algarve, Portugal. [http://users.wpi.edu/~mpopovic/media/pubs/IROS2012_Galiana.pdf]

[13] S. B. Kesner, L. Jentoft, F. L. Hammond, R. D. Howe and M. B. Popovic (2011). "Design Considerations for an Active Soft Orthotic System for Shoulder Rehabilitation," 33rd Annual International IEEE EMBS Conference, August 30 - September 02, 2011, Boston, USA. [http://users.wpi.edu/~mpopovic/media/pubs/Kesner_EMBC2011_SoftOrthotics.pdf]

[14] M. H. Raibert, and I. E. Sutherland. "Machines That Walk," Scientific American Vol. 248 Issue 1, pp. 44-53, 1983.

[15] I. E. Sutherland, and M. K. Ullner. "Footprints in the Asphalt," The International Journal of Robotics Research, vol. 3 no. 2 29-36, 1984.

[16] L. F. Sang, H. B. Wang, D. F. Zhang, Z. H. Tian, F. H. Deng, and D. L. Fang. "Application of parallel mechanism in varistructured quadruped/biped human-carrying walking chair robot," International Journal of Automation and Computing 10, no. 5 (2013): 447-454.

[17] T. Kamada. "My Agent: A Practical Personal Assistant," Proc. of the JSME ROBOMEC 94, pp. 1107-1112, Kobe, Japan, 1994 (in Japanese)

[18] Y. Takeda, M. Higuchi, and H. Funabashi. "Development of a walking chair (Fundamental investigations for realizing a practical walking chair)," Proc. of the CLAWAR2001, pp. 1037-1044, Karlsruhe, Germany, September 2001.

[19] Y. Wu, H. Nakamura, Y. Takeda, M. Higuchi, and K. Sugimoto. "Development of a power assist system of a walking chair based on human arm characteristics," In Intelligent Robots and Systems, 2006 IEEE/RSJ International Conference on, pp. 4328-4335. IEEE, 2006.

[20] J. Y. Kim, J. Lee, and J. H. Oh. "Experimental Realization of Dynamic Walking for a Human-Riding Biped Robot, HUBO FX-1," Advanced Robotics, vol. 21, no. 3-4, pp. 461-484, 2007.

[21] "Robot Overview" Toyota Motor Corp., 2003. [http://www.toyota.co.jp/en/news/04/12031d.html]

[22] Y. Sugahara, T. Hosobata, Y. Mikuriya, H. Sunazuka, H. O. Lim, and A. Takanishi. "Realization of dynamic human-carrying walking by a biped locomotor," In Robotics and Automation, 2004. Proceedings. ICRA'04. 2004 IEEE International Conference on, vol. 3, pp. 3055-3060. IEEE, 2004.

[23] Y. Sugahara, A. Ohta, K. Hashimoto, H. Sunazuka, M. Kawase, C. Tanaka, H. O. Lim, and A. Takanishi. "Walking up and down stairs carrying a human by a biped locomotor with parallel mechanism," In Intelligent Robots and Systems, 2005. (IROS 2005). 2005 IEEE/RSJ International Conference on, pp. 1489-1494. IEEE, 2005.

[24] M. B. Popovic, C. Onal, G. McCarthy, N. Corso, D. Effraimidis, and B. Jennings (2014) Hydro Artificial Muscles. United States Patent and Trademark Office, Assignee Worcester Polytechnic Institute. Serial No.: 62/011,830. Filed: June 13, 2014.

[25] S. Sridar, C. J. Majeika, P. Schaffer, M. P. Bowers, S. Ueda, A. J. Barth, J. L. Sorrells, J. T. Wu, T. R. Hunt, and M. Popovic. “Hydro Muscle - a novel soft fluidic actuator,” IEEE International Conference on Robotics and Automation (ICRA), pp. 4014-4021. IEEE, 2016.
[26] S. Feng, et al. “Optimization based controller design and implementation for the Atlas robot in the DARPA Robotics Challenge Finals,” Humanoid Robots (Humanoids), 2015 IEEE-RAS 15th International Conference on. IEEE, 2015.
[27] N. A. Radford, et al. “Valkyrie: NASA’s first bipedal humanoid robot,” Journal of Field Robotics 32.3 (2015): 397-419.
[28] S. Sung, and Y. Youm (2007). “Landing motion control of articulated hopping robot,” International Journal of Advanced Robotic Systems, 4(3), 33.
[29] J. Lei, J. Zhu, P. Xie, and M. O. Tokhi (2017). “Joint variable stiffness of musculoskeletal leg mechanism for quadruped robot,” Advances in Mechanical Engineering, 9(4), 1687814017690342.
[30] K. Tsujita, T. Inoura, T. Kobayashi, et al. “A study on locomotion stability by controlling joint stiffness of biped robot with pneumatic actuators,” In: Proceeding of the 9th international conference on motion and vibration control, Munich, Germany, 15–18 September 2008, pp.305–314. Kluwer Academic Publishers. 16.
[31] J. M. Calderón, W. Moreno, and A. Weitzenfeld. “Fuzzy variable stiffness in landing phase for jumping robot,” Innovations in bio-inspired computing and applications. Berlin: Springer, 2016, pp.511–522. 15.
[32] Dual Range Force Sensor, Vernier, Sarasota Florida, USA
“Teaching Science with Technology,” Vernier Software & Technology. N.p., n.d. Web. 6 Feb. 2015. [http://www.vernier.com/]
[33] P. H. Mott, and C. M. Roland. “Limits to Poisson’s ratio in isotropic materials,” Physical Review B 80.13 (2009): 132104.
[34] J. A. Rinde. “Poisson's ratio for rigid plastic foams,” J. Applied Polymer Science, 14, 1913-1926, 1970.
[35] G. N. Greaves, et al. “Poisson's ratio and modern materials,” Nature materials 10.11 (2011): 823-837.
[36] “Natural Rubber.” MatBase. N.p., n.d. Web. 7 Feb.2015.
[37] “Leading the Way in Materials Testing.” Instron: Materials Testing Machines for Tensile, Fatigue, Impact, Rheology and Structural Testing. N.p., n.d. Web. 27 Feb. 2015. [http://www.instron.com/en-us]
[38] D. A. Winter. “Biomechanics and motor control of human movement,” John Wiley & Sons, 2009.
[39] H. Schiessel, et al. “Generalized viscoelastic models: their fractional equations with solutions,” Journal of physics A: Mathematical and General 28.23 (1995): 65-67.
[40] A. V. Hill. “The heat of shortening and the dynamic constants of muscle,” Proceedings of the Royal Society of London B: Biological Sciences 126.843 (1938): 136-195.
[41] H. M. John, and D. F. Kurtis. “Numerical methods using MATLAB,” (2004).
[42] H. A. Haxton. “Absolute Muscle Force in the Ankle Flexors of Man,” J. Physiol. 103:267–273, 1944.
[43] C. N. Maganaris. “Force–length characteristics of in vivo human skeletal muscle,” Acta Physiologica Scandinavica 172.4 (2001): 279-285.
[44] X-HOSE - the Original Kink Free Lightweight Expandable Garden Hose. (n.d.). Retrieved April 2014, from XHOSE - the Original Kink Free Lightweight Expandable Garden Hose.
[45] G. D. Ragner, and R. deRochemont (2001). Patent No. US 20030098084 A1. United States of America.
[46] G. D. Ragner (2003). Patent No. US 7617762 B1. USA
[47] G. D. Ragner, and R. D. deRochemont Jr. “Pressure-actuated linearly retractable and extendible hose,” U.S. Patent 6,948,527, issued September 27, 2005.
[48] C. Degen, A. Gregorian, and R. Siber (2007). Patent No. US 20100300569 A1. United States of America.
[49] G. D. Ragner. “Flexible hydraulic muscle,” U.S. Patent 7,617,762, issued November 17, 2009.
[50] M. Berardi (2011). Patent No. US 20130087205 A1. United States of America.
[51] M. Berardi. “Expandable garden hose,” US patent office publication number US 20130087205 A1, Application number US 13/690,670, Filing date Nov. 30, 2012.
[52] R. A. Lia. “Borescope or endoscope with fluid dynamic muscle,” U.S. Patent No. 4,794,912. 3 Jan. 1989.
[53] Super Soft Latex Rubber Tubing 3/8” ID, ½” OD, 1/16” Wall, Semi-Clear Amber, McMaster-Carr, Robbinsville, New Jersey, USA
[54] Nylon Tubular Webbing, XHose, Norwalk, Connecticut, USA
[55] NBPDANN150PAUNV Pressure Sensor, Honeywell Sensing and Control, Friction Materials LLC, Green Island, New York, USA
[56] Conductive Rubber Cord Stretch Sensor, Adafruit, New York, New York, USA
[57] KY-040 Rotary Encoder Module, Shenzhen KEYES DIY Robot Co. Ltd., Shen Zhen, China
[58] Arduino Uno R3, Arduino, manufactured in Italy
[59] 2W-025-08 12V DC ¼” Solenoid Valve, Hiwell, manufactured in Zhejiang, China
[60] 6380490 PVC Ball Valve, The Specialty MFG Co., Saint Paul, Minnesota, USA
[61] S3305 Standard HT Servo, Futaba, Chiba Prefecture, Japan.
[62] R. Pelrine, R. Kornbluh, Q. Pei, and J. Joseph. “High-speed electrically actuated elastomers with strain greater than 100%,” Science, vol. 287, pp. 836-839, 2000.
[63] H. Wang, C. Wang and T. Yuan. “On the energy conversion and efficiency of a dielectric electroactive polymer generator,” Appl. Phys. Lett. 101, 033904 (2012); http://dx.doi.org/10.1063/1.4737439
[64] A. Canga, M. Delia, A. Hyman, A. Nagelin. “Fluidic Muscle Ornithopter,” A Major Qualifying Project, Primary Adviser: Marko B. Popovic. Worcester Polytechnic Institute March 27, 2015.
[https://www.wpi.edu/Pubs/E-project/Available/E-project-032715-150348/unrestricted/Fluidic_Muscle_Ornithopter.pdf]
[65] D. P. Coffey, P. Starek. “Legged Robot Using Hydro-Muscles,” A Major Qualifying Project, Primary Adviser: Marko B. Popovic. Worcester Polytechnic Institute August 25, 2015. [https://www.wpi.edu/Pubs/E-project/Available/E-project-082515-084953/unrestricted/Legged_Robot_Using_Hydromuscles_MQP.pdf]

[66] D. Fitzgerald, T. Hunt, A. Leiro. "HydroDog: A Quadruped Robot Actuated by Soft Fluidic Muscles," A Major Qualifying Project, Primary Adviser: Marko B. Popovic. Worcester Polytechnic Institute April 30, 2015. [https://www.wpi.edu/Pubs/E-project/Available/E-project-043015-154626/unrestricted/MQP_Report__Final.pdf]
[67] "How many People use assistive devices?" National Institute of Child Health and Human Development, Nov 30, 2012. [https://www.nichd.nih.gov/health/topics/rehabtech/conditioninfo/Pages/people.aspx]
[68] http://www.newdisability.com/wheelchairstatistics.htm
[69] "Fact sheet on wheelchairs" World Health Organization, Oct 2010. [http://www.searo.who.int/entity/disabilities injury rehabilitation/wheel_chair_factsheet.pdf]
[70] "iBot" Deka Research and Development Corp., 2009. [http://www.dekaresearch.com/ibot.shtml]
[71] E. Henneman reference; see www.ncbi.nlm.nih.gov/books/NBK11021/
[72] A. Protopapadaki, W. I. Drechsler, M. C. Cramp, F. J. Coutts, O. M. Scott. "Hip, knee, ankle kinematics and kinetics during stair ascent and descent in healthy young individuals," Clinical Biomechanics 22 (2007) 203210.
[73] S. M. Reid, S. K. Lynn, R. P. Musselman, and P. A. Costigan 2007. "Knee biomechanics of alternate stair ambulation patterns," Medicine and science in sports and exercise, 39(11), p.2005.
[74] B. R. Umberger, and P. E. Martin. "Mechanical power and efficiency of level walking with different stride rates," Journal of Experimental Biology 210.18 (2007): 3255-3265. Web.01 Mar. 2016.
[75] D. J. Farris, G. S. Sawicki. "The mechanics and energetics of human walking and running: a joint level perspective," Journal of the Royal Society Interface. 2012;9(66):110-118. doi:10.1098/rsif.2011.0182.
[76] 300 PSI 19.6 GPM 6 Roller Pump [http://www.pwmall.com/p-133879- 6900c r-6-roller-pump-delavan-300-psi-196-gpm-ci-cw.aspx]
[77] 1000 W BLDC Motor [http://www.uumotor.com/shop/electric- tricycle-motor/1000w-electric-tricycle-gear-motor-air-cooling]
[78] Everbilt 1/8 in. Stainless Steel Uncoated Wire Rope [http://www.homedepot.com/]
[79] RJX FS-0521HV Metal Gear Digital Servo Ultra High Speed and Torque 21.3kg / 0.05sec / 68g [http://www.hobbyking.com/]
[80] Stainless Steel Constant-Force Spring / 5.94 LBS [http://www.mcmaster.com/]
[81] 1" NPT Magnetically Latching Solenoid Valve 4.5 to 9 VDC for Water[http://www.ebay.com/]
[82] NPT Threaded Bronze Butterfly Valve, 1" Pipe Size, Manual Lever [http://www.mcmaster.com/]
[83] Digital Hanging Scale 300 Kg / 600 LBS Ocs-l Industrial Crane Scale [http://www.amazon.com/]
[84] M. P. Bowers, C. V. Harmalkar, A. Agrawal, A. Kashyap, J. Tai, and M. Popovic (2017, March). "Design and test of biologically inspired multi-fiber Hydro Muscle actuated ankle," In 2017 IEEE Workshop on Advanced Robotics and its Social Impacts (ARSO) (pp. 1-7). IEEE.
[85] D. B. Bertoti, P. A. Houglum, R. J. Houglum. "Brunnstrom's Clinical Kinesiology 6th revised edition," Davis Company, F. A. 2011.
[86] D. Purves, G. J. Augustine, D. Fitzpatrick, et al., editors. "Neuroscience 2nd edition," Sunderland (MA): Sinauer Associates; 2001. The Regulation of Muscle Force. Available from: http://www.ncbi.nlm.nih.gov/books/NBK11021/
[87] S. Wakimoto, K. Suzumori, and J. Takeda. "Flexible artificial muscle by bundle of McKibben fiber actuators," Advanced Intelligent Mechatronics (AIM), 2011 IEEE/ASME International Conference on. IEEE, 2011.
[88] Phidget, 3136 0 - Button Load Cell (0-50kg) - CZL204E. [www.phidgets.com/products.php?category=34&product id=31360]
[89] Sharp, Distance Measuring Sensor Unit Measuring distance: 4 to 30 cm Analog output type, GP2Y0A41SK0F datasheet, Apr. 2005.
[90] Digiten, "G 1/4" inch 5V 0-1.2 MPa Pressure Transducer Sensor". [https://www.amazon.com/DIGITEN-Pressure-Transducer-Sensor- Diesel/dp/B00YPA6V9U]
[91] A. Hrdlicka (1898). "Study of the normal Tibia," American Anthropologist, A11: 307312. doi:10.1525/aa.1898.11.10.02a00010
[92] "Average body statistics, height and weight charts and other interesting facts," in Average Foot. (n.d.). [Online]. Available: http://www.theaveragebody.com/average foot.php. Accessed: Sep. 16, 2016.
[93] E. C. Hardin, A. Su, and A. J. van den Bogert, 2004. "Foot and Ankle Forces during an Automobile Collision: The Influence of Muscles," Journal of Biomechanics, 37(5) pp. 637-644.
[94] S. Au, M. Berniker, and H. Herr. "Powered ankle-foot pros- thesis to assist level-ground and stair-descent gaits," Neural Networks 21.4 (2008): 654-666.
[95] S. C. Walpole, et al. "The weight of nations: an estimation of adult human biomass," BMC public health 12.1 (2012): 439.
[96] N. Forestier, N. Teasdale, and V. Nougier. "Alteration of the position sense at the ankle induced by muscular fatigue in humans," Medicine and science in sports and exercise 34.1 (2002): 117-122.
[97] M. Palmer. "Sagittal plane characterization of normal human ankle function across a range of walking gait speeds," Master's Thesis, Massachusetts Institute of Technology, 2002.